THESIS

SIMULATION OF HYDRODYNAMICS IN A DOWNFLOW FLUIDIZED BED REACTOR

ARCHWIT AIMDILOKWONG

**A Thesis Submitted in Partial Fulfillment of
the Requirements for the Degree of
Master of Engineering (Chemical Engineering)
Graduate School, Kasetsart University
2006**

ISBN 974-16-2673-8

Archwit Aimdilokwong 2006: Simulation of Hydrodynamics in a Downflow Fluidized Bed Reactor. Master of Engineering (Chemical Engineering), Major Field: Chemical Engineering, Department of Chemical Engineering. Thesis Advisor: Associate Professor Sunun Limtrakul, D.Sc. 123 pages.
ISBN 974-16-2673-8

A downflow circulating fluidized bed (downer) is important in gas-solid reaction processes. Apart from the conventional upflow circulating fluidized bed (riser), a downer has a special flow characteristic. The flow of gas and solids in a downer resembles that of the ideal plug flow. This makes the residence time distribution in a downer narrower compared with a riser. Hence a downer gives higher selectivity for many multiple reactions and becomes an important reactor in the chemical and petroleum industries. However, there is still inadequate data regarding the hydrodynamics in a downer. In this work, a 2-D full-components downer reactor model was designed and then simulated with Fluent software to study the hydrodynamics. The model components consist of a 9.3 m high and 0.1 m wide downer column, a riser, two gas-solid separators, and two storage tanks. The gas-solid separator used in this work was compared with the simple settling tank. The gas-solid separator designed in this work shows the outstanding abilities to separate particles and deal with high flow rate. The effect of the number of solid distributing tubes was also studied. The radial profiles of solid holdup and solid velocity shows that more particle distributing tubes provide more uniform radial solid holdup profile, thus enhancing the downer reactor performance. The axial and radial profiles of solid holdup and solid velocity were used to characterize the hydrodynamics in a downer in addition to the solid holdup contour and solid velocity plot. The flow in the downer column is separated into core and annulus zones with solid holdup peak near the wall. The axial solid velocity profile in the downer is divided in 3 zones; the first acceleration zone where particles are accelerated enormously by both gas momentum and gravity until their velocities equal, the second acceleration zone where particles are accelerated slowly by only gravity, and the constant particle velocity zone. More over, the effect of solid circulation rate (G_s) was studied. The cross-sectional averaged solid holdup increases linearly with the increasing solid circulation rate (G_s). The drag-back force of the gas phase has less effect upon the particle phase at high solid circulation rate in the second acceleration zone. Therefore the particle velocity with higher G_s can increase more. The simulation results of this work were compared with the experimental results of Zhang *et al*. (1999, 2000) and Yasemin *et al*. (2003). Both simulation and experimental results agree that hydrodynamics in a downer separates into core and annulus zones with solid holdup peak near the wall but the solid holdup peak of the experimental results disappeared at the end of the downer column. The hydrodynamics results obtained by this work can be used to design a proper circulating fluidized bed downer for industrial uses.

Student's signature Thesis Advisor's signature ____ / ____ / ____

ACKNOWLEDGEMENTS

First, I would like to thank my advisor, Associate Professor Sunun Limtrakul, for her directions to approach a research problem and her advices that guided me through this thesis. I also appreciate the help and valuable suggestions of my thesis committees, Assistant Professor Terdthai Vatanatham and Associate Professor Varangrat Juntasaro.

Thanks for financial supports from Shell Centenary Scholarship, the Thailand Research Fund (TRF) under Research Career Development Project, the Kasetsart University Research and Development Institute (KURDI), CHE-ADB Graduate Research and Education Development Program in Chemical Engineering at Kasetsart University.

Lastly, I thank my family for their supports during these years. A special thanks to my mother for the transportation between home and Kasetsart University. Without them, this thesis would be less enjoyable.

Archwit Aimdilokwong
August 2006

TABLE OF CONTENTS

TABLE OF CONTENTS (Cont'd)

LIST OF TABLES

LIST OF FIGURES

LIST OF FIGURES (cont'd)

Figure **Page**

LIST OF FIGURES (cont'd)

Figure **Page**

LIST OF FIGURES (cont'd)

Figure **Page**

Appendix Figure

LIST OF ABBREVIATIONS

ρ_i	Density of phase i
ε_i	Volume fraction of phase i
$\vec{u}_i$	Velocity vector of phase i
$\vec{g}$	Gravity Force
P	Pressure
τ_i	Stress tensor of phase i
μ_i	Viscosity of phase i
β	Interphase drag coefficient
R_j	Rate of occurrence of species j
H_i	Enthalpy of phase i
h	Interphase heat transfer coefficient
Re_s	Particle Reynolds number
Nu_s	Particle Knudselt number
Pr_f	Fluid Prandtl number
Θ_s	Granular temperature
τ_s	Solid phase stress
k_s	Diffusion coefficient of granular temperature
γ_s	Collisional dissipation of granular temperature
S_s	Deformation rate
P_s	Solid phase pressure
g_0	Radial distribution function
μ_s	Solid phase shear viscosity
$\mu_{s,dil}$	Solid phase dilute viscosity
μ_b	Solid bulk viscosity
d_p	Particle diameter
e	Particle–particle restitution coefficient
G_s	Solid circulation rate
K_i	Turbulence kinetic energy of phase i
E_i	Turbulence dissipation rate of phase i
$\mu_{t,i}$	Turbulence viscosity of phase i
G_i	The production of turbulence kinetic energy of phase i
t_s	Particulate relaxation time
$t_{F,ki}$	The characteristic particle relaxation time connected with inertial effects acting on a dispersed phase

$t_{t,ki}$	The Lagrangian integral time scale calculated along particle trajectories
$t_{t,i}$	The characteristic time of the energetic turbulent eddies
$\vec{R}$	Particle position
$\vec{r}_o$	Particle position of the former time step
$\vec{v}_p$	Particle velocity;
$\vec{v}_{po}$	Particle velocity of the former time step;
$\vec{a}_p$	Particle acceleration rate;
$\vec{a}_{po}$	Particle acceleration rate of the former time step;
$\vec{\omega}_p$	Particle angular velocity;
$\vec{\omega}_{po}$	Particle angular velocity of the former time step;
$\vec{\alpha}_p$	Particle angular acceleration rate;
$\vec{\alpha}_{po}$	Particle angular acceleration rate of the former time step;
dt	Time interval

SIMULATION OF HYDRODYNAMICS IN A DOWNFLOW FLUIDIZED BED REACTOR

INTRODUCTION

In a fluidized bed, solid particles are fluidized by fluid (either gas or liquid) and behave themselves like a fluid when the fluidizing fluid velocity reaches an exact amount called minimum fluidized velocity or U_{mf}. A fluidized bed is used as a reactor in which a fluid reactant is injected into the bed for fluidizing solid particles. The advantages of a fluidized bed are enhancing gas-solid contacting and heat and mass transfer rate. In addition, a fluidized bed containing small particles has lower pressure drop than a fixed bed reactor. The solid particles can be catalysts or solid reactants depending on the application. Fluidized bed reactors are important for chemical process industries, mineral processing, pharmaceutical production, fluid catalytic cracking, and solid catalyzed reaction.

Circulating fluidized bed (CFB) reactors are operated with higher superficial gas velocity compared to conventional fluidized bed reactors. By using high superficial gas velocity, particles can be circulated through circulating line. After particles leave the reactor, they are separated by one or more cyclones and can be re-generated or cooled down before they re-enter the CFB reactor section again.

CFBs can be separated to two types by considering the flow of gas phase and particle phase, i.e. co-current flow and counter-current flow. The co-current flow reactor has the same flow directions of particles and fluid while the counter-current flow has the opposite flow directions of particles and fluid.

CFBs can also be specified by the flow direction of the particle phase. CFB reactors with the up flow of solids are called risers while CFB reactors with down flow of solids are called downers.

The hydrodynamics in CFB is very important for the reactor performance because it affects both mass and energy transport phenomena in reactors. The studies of hydrodynamic behavior in CFB can be carried out by experiment and numerical simulation.

CFB is operated at higher superficial gas velocity than conventional bubbling fluidized beds (BFB). In this operating regime, the flow behavior enhances the performances of the reactors by increasing gas-solid contacting efficiency, eliminating gas bubbles, decreasing back-mixing, and also allows catalyst to be regenerated. The velocity profiles of both gas and solid phases inside CFB are closer to that of plug flow while the flow behavior of BFB is more like mixed flow. This improving flow pattern of CFB makes it easier to control the selectivity of desired products for reactions that have multiple products. Fluid Catalytic Cracking (FCC) is one of those examples.

Fluid Catalytic Cracking (FCC) is the first application of fine-powder fluidization. FCC catalysts are micro spheres usually produced by spray drying and characterized as Geldart Group A powder. Over the past 50 years, FCC catalysts are improved and product yields are increased by 50 %. Feed resident time is decreased to a much shorter time of only a few seconds. Therefore dense-bed crackers were not needed and were replaced by CFB. FCC is used to crack heavy petroleum fractions into lighter products. Normally, FCC units process about 38% of the crude run in the refinery. Some useful products of FCC process are gasoline and olefin. Hydrodynamics, heat and mass transfer in CFB is important to the design and operation of the FCC. The capabilities of CFB including high heat transfer rate and catalyst re-generated availability make it popular for the fluid cracking reaction. The performance of FCC units was gradually improved from the performance of the first model because of new catalysts and hardware improvements. The improvements of FCC units lead to a reduction in size of the unit hence reduce the construction and operating cost. FCC units were developed over decades. There are modern FCC units involved with new designs. The new design riser reactor is completely vertical. This will promote a uniform radial profiles through the riser section which is useful to acquire higher product selectivity. The feed stream is injected through several radial nozzles. These nozzles are designed to atomize feed stream into small droplets to enhance the contact between oil vapor and solids throughout the riser.

Fluid catalytic cracking is used conventionally in CFBs at this time but mostly in risers. The fact that hydrodynamics in downers gives higher performance than conventional CFB risers due to more plug flow behavior of particles is discovered and being interested. The flow in a downer has a particular uniform resident time distribution. Both gas and solids flow behaviors in a downer almost resemble the ideal plug flow. These advantages are particularly beneficial to processes that need short but uniform contact times between gas and solids such as fluid catalytic cracking.

A hydrodynamics modeling in downers is complicated because of the interaction between gas and solid phases. The experiments for several conditions of the downer reactors for design purpose are not possible because of high expenses and time-consuming processes. Computer simulation is then considered to be a good choice to study hydrodynamics behavior in the downer reactors. In the last decades, computer efficiency is much improved. Hence, they are available for the complicate simulation of the downer reactors that requires high computational performances. Numerical computation can be carried out by either self-programming or using commercial programs. There are several commercial computational fluid dynamic (CFD) software available lately and Fluent software from Fluent Inc. is one of the famous software for hydrodynamics simulation. Fluent has several models for turbulent models and numerical differencing schemes for individual's desires. Two models available in Fluent for a fluidized bed are the two-fluid model (TFM) and the dispersed phase model (DPM). The dispersed phase model uses Lagrangian approach for the particles and is the simple model that has the weakness for dense flow and the solid phase volume fraction is limited to 10 percents. On the other hand, the two-fluid model uses Eulerian approach for the particle phase and treats the particles as the other fluid phase.

In this work, hydrodynamics in a downer reactor will be investigated by using Fluent software. Fluid catalytic cracking particles are used in a downer reactor. Effects of designs and operating conditions such as solid circulation rate on the hydrodynamics will be studied. The simulation results from this work will be compared with the experimental results.

Objectives

1. Design the circulating fluidized bed (CFB) downer reactor model geometry, which includes each downer reactor components such as storage tanks, a downer column, a riser column, gas-solid separators.

2. Simulate the downer model by Fluent software to achieve hydrodynamics data in a CFB downer and study hydrodynamics behavior on each parts of the downer reactor model and the performance of the downer reactor.

3. Investigate effects of component designs and operating condition such as solid circulation rate on hydrodynamics behavior.

4. Compare simulation results with the experimental results available in literatures.

Scopes

1. Study hydrodynamics behavior in a CFB downer by using a 2-D geometry with axisymmetric assumption.

2. Simulate the downer reactor model by Fluent software using the Two-fluid model.

3. Use air properties for the gas phase with the assumption of Newtonian and incompressible fluid while using the properties of fluid catalytic cracking (FCC) particles for the solid phase.

4. Study hydrodynamics behavior in all components especially in the downer column and the effect of solid circulation rate on the hydrodynamics behavior in a downer column.

Benefits

1. Simulation can save time and expenses in predicting the hydrodynamics behavior in a CFB downer at varied conditions, which can be very expensive and time-consuming tasks.

2. The complete simulation data in every parts of the downer reactor domain can be achieved and used to efficiently improve and design a CFB downer model for the best performances.

3. This work can be used to develop Chemical and Petrochemical processes in the future.

LITERATURE REVIEWS

A gas-solid two phases flow system in CFBs can be operated in 3 modes consisting of co-current up flow, co-current down flow and counter current flow. The circulating fluidized bed reactor (CFB) can be operated by using any of these flow patterns.

In earlier times when fluidized bed was first invented, the gas flow is supposed to support the particles weight as in the co-current up flow CFB. The co-current down flow system that does not clearly represent the concept of fluidized bed is used in a CFB reactor because of its specific characteristics. The co-current down flow CFB being called shortly as ‘ downer ’ has a particular uniform resident time distribution and the flow of gas and particles inside almost resembles the ideal plug flow. Hence it is properly used with reactions such as fluid catalytic cracking (FCC) that need a small deviation of both gas and solids resident time. FCC reactions can be explained as multiple reactions and selectivity of products is one of the main interests. To control selectivity of desired products, the CFB with uniform RTD is needed. Risers with more back mixing hydrodynamics might not work well with such reactions.

A CFB downer has many advantages over a riser as stated by many researchers (Yang, Jin, Yu, Wang and Bai, 1991; Bai, Jin, Yu and Gan, 1991; Wang, Bai and Jin, 1992; Zhu, Yu, Jin, Grace and Issangya, 1995; Wei and Zhu, 1996; Zhu and Wei, 1996). For downers, the particles resident times are small because the gas flow and the gravity force are in the same directions. Solids circulation rate in downers is faster than that in risers. Hence downers are better for quick reactions that use up catalyst quickly. Solids concentration in a downer is more uniform across the reactor section compared with a riser and leads to uniform reaction time.

CFB reactors are in the conditions between the low-velocity fluidized bed like bubbling reactors and the dilute phase transport. Lately, the CFB reactors have been developed by optimizing the effects of each parameters such as the mixing characteristic, gas-solid contacting schemes, residence time, and heat transfer properties to fit any particular applications.

1. Regimes of Fluidization

Gas-solids contacting regimes of fluidized beds depend on several factors such as superficial gas velocity, particles properties, and reactor geometry. These regimes range from fixed bed, bubbling fluidized bed, turbulent fluidized bed, and fast fluidized bed with increasing superficial gas velocity. The contacting regimes of gas and solids have been studied by Kunii and Levenspeil (1997) and was presented by Figure 1. The solid distributions of each regime are also described by Kunii and Levenspeil (Levenspeil, 1997) in Figure 2. Regimes with high superficial velocity have lower solid concentration along bed height because solids are blown off the top of reactors.

Particles properties are also important to classify fluidization regimes. Geldart (Geldart, 1973) and Geldart and Abrahamson (Geldart and Abrahamson, 1978) had studied the effects of solids characteristic on fluidization pattern and came up with the following simple classification of solids which is called Geldart's particle classification of type A, B, C, D nowadays. This classification is shown in Figure 3.

Once the gas superficial velocity is raised to a value called the minimum fluidized bed velocity (U_{mf}), all of the solid particles in the bed will be suspended with the fluid. U_{mf} is determined when the pressure drop stop increasing with increasing superficial gas velocity. One of the useful equations for minimum fluidizing velocity condition developed by Wen and Yu (Wen and Yu, 1966) and being modified by Grace (Grace, 1982) is shown below.

$$Re_{mf} = \sqrt{27.2^2+0.0408Ar} - 27.2$$

where $Re_{mf} = \rho_g U_{mf}\, d_p/\mu_g$; U_{mf} is minimum fluidized bed velocity; d_p is particle diameter.

Ar is Archimedes number and written as $Ar = \rho_g(\rho_p - \rho_g)\, d_p^3\, g/\mu_g^2$

When the gas superficial velocity is increased from U_{mf}, the fluidized bed starts to enter the bubbling fluidized bed regime (BFB). The minimum bubbling fluidized bed (U_{mb}) velocity is described by Geldart and Abrahamsen in 1978.

$$U_{mb} = 33d_p(\rho_g/\mu_g)^{0.1} \quad \text{in SI unit}$$

With the increasing superficial gas velocity, the size of the bubbles keep growing and slugging will occur. This condition is found when the size of bubbles is comparable to the column diameter. The regime of slugging will occur when the gas superficial velocity reach the slugging velocity (U_{ms}) as derived by Stewart and Davidson (Stewart and Davidson, 1967).

$$U_{ms} = U_{mf} + 0.07\sqrt{gD}$$

where D is the bed diameter.

The turbulent and fast fluidized regimes use higher superficial velocity. The situation to separate the turbulent regimes from bubbling fluidized bed regime is when the pressure fluctuation reaches maximum. Bi and Grace (Bi and Grace, 1995) derived the equation for the turbulent fluidized bed in the following equation.

$$Re_c = 1.24\ Ar^{0.45} \quad (2<Ar<10^8)$$

where $Re_c = \rho_g U_c\, d_p/\mu_g$; U_c is the superficial gas velocity when the standard deviation of the pressure reaches maximum value.

The fast fluidized regime occurs when the significant numbers of particles are carried out of the top of the column (Yerushalmi, 1981) and the gas velocity at that state is called the transport velocity (U_{tr}). A sudden change of pressure drop with increasing solids flow rate disappears when the superficial gas velocity exceeds U_{tr}.

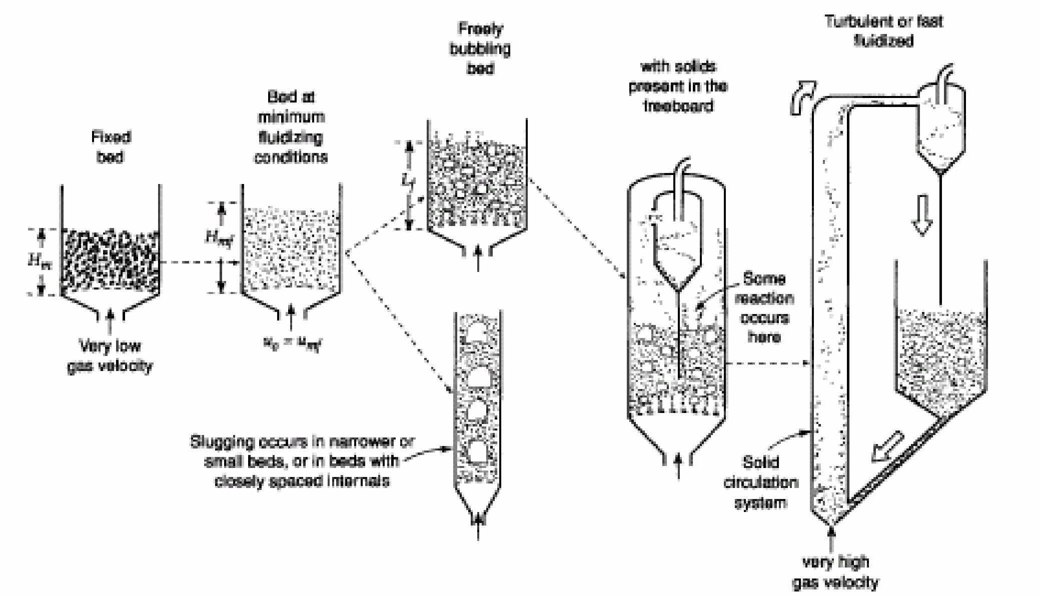

Figure 1 Gas/solid contacting regimes
Source: Kunii and Levenspeil (1997)

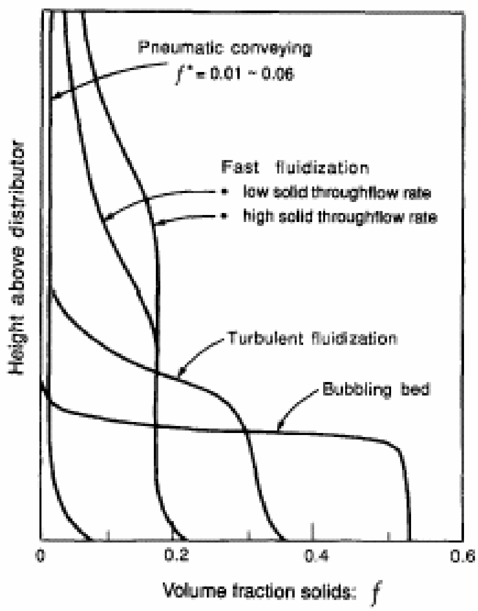

Figure 2 Solid distribution in each regime
Source: Kunii and Levenspeil (1997)

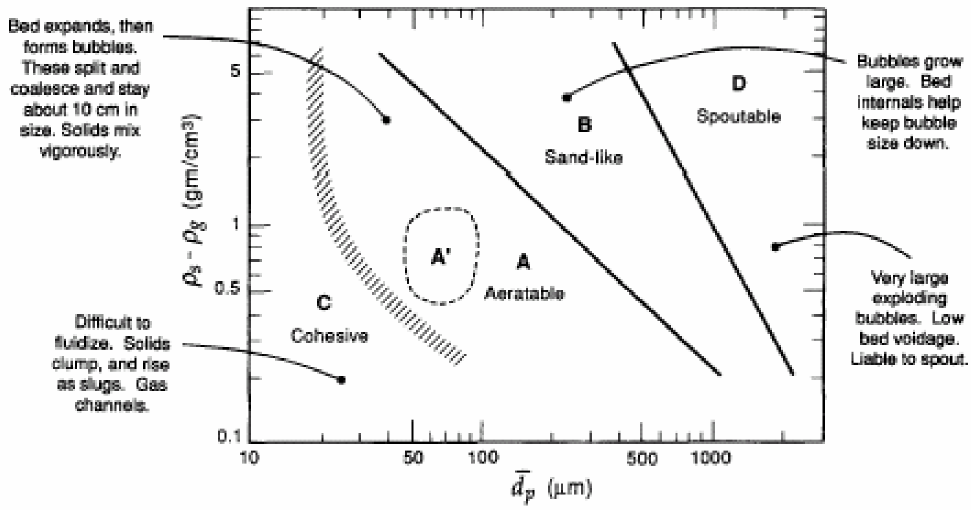

Figure 3 Geldart's classification of solids in BFB
Source: Kunii and Levenspeil (1997)

2. Physical Appearances of CFB

The CFB reactors are better than the bubbling fluidized bed reactors and the turbulent fluidized bed reactors in the view of increasing the contacting efficiency, decreasing the back mixing and a smaller variation of residence time distribution. The voidage in CFB reactors is in the range of 0.7-0.999. The absence of bubbles in CFB reactors creates more space for the solid particles. CFB reactors also have the lower clustering of particles (Zhu *et al*. 1995, Lim *et al*. 1995) especially in the down flow CFB or downers. These advantages make CFB reactors popular in industrial uses (Grace *et al*. 1997).

However, back-mixing can still occur near the wall region of risers depending on the reactor configuration in risers. This makes the contacting for gas and solid not occurring uniformly inside the reactor (Grace *et al*. 1997). By using CFB downers, this problem can be prevented. In a downer, solids weight is not supported by gas flow, hence there is no counter flow of gas and solid. The flows of gas and solids in a downer are almost the same as plug flow and prevent back-mixing that occur in risers.

One of the important applications of CFB reactors is the fluid catalytic cracking (FCC) process. This process needs the uniform residence time of both gas and solids, hence the CFB reactor needs to be designed to control back-mixing. Downers are then employed to this process because of its uniform residence time distribution. The reactor configuration designs normally involve designing of gas distributor nozzle and devices at the particles entrance and exit to help distribute particles efficiently.

The conventional CFB reactor is consisted of the reactor column, the circulating chamber, the cyclone to separate solid particles and gas, the gas nozzles, and the exit and entrance devices that link the main reactor and the circulating chamber. Picture of up flow CFBs (riser) collected by Levenspeil is shown in Figure

4. The components of a downer and a riser are much alike, but the flow directions in the reactor's column and circulating chamber are opposite. A picture of a downer is shown in Figure 5.

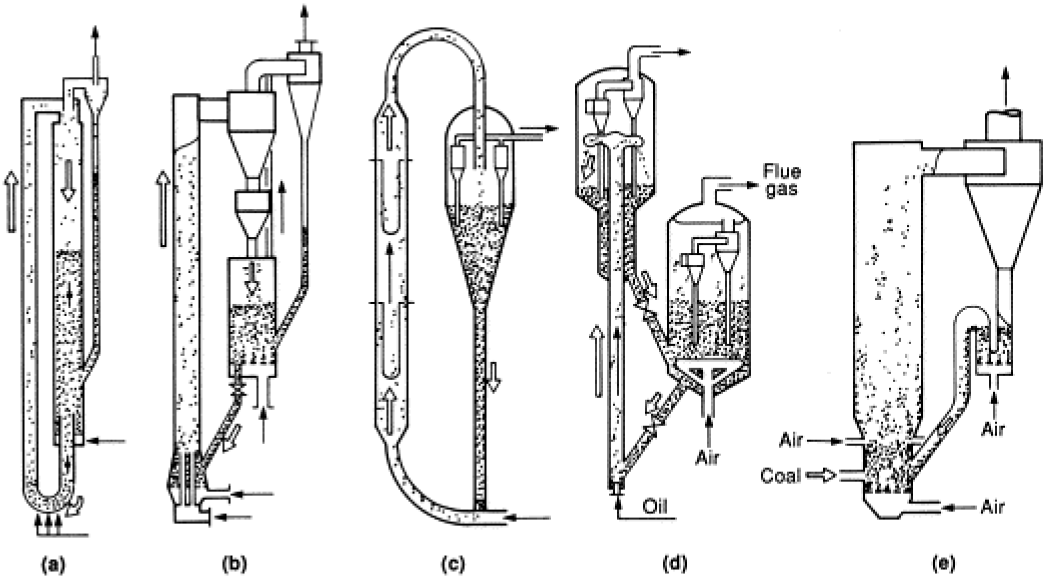

Figure 4 CFB risers
Source: Levenspeil (2001)

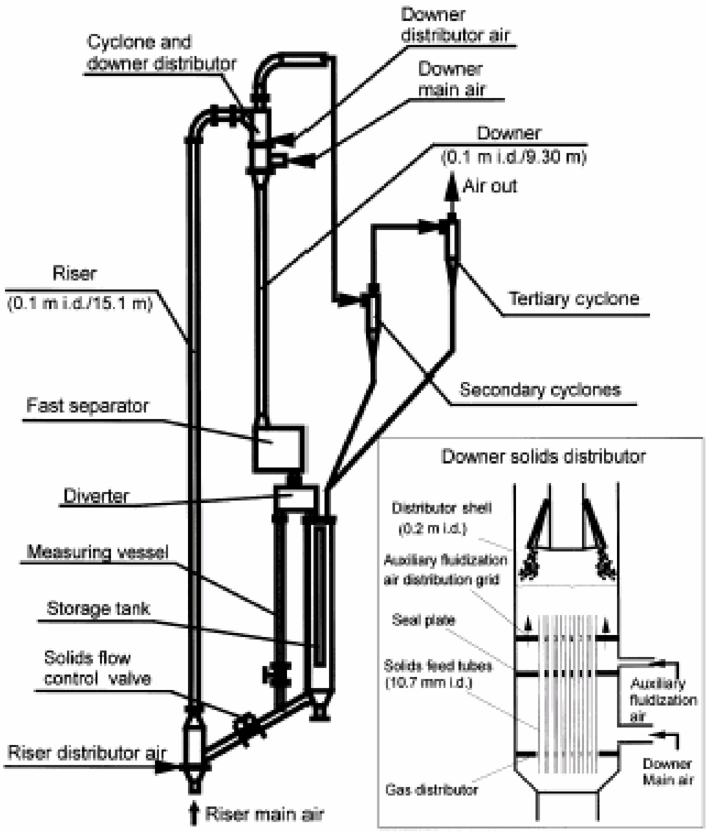

Figure 5 CFB downer
Source: Zhang *et al.* (2000)

3. Effect of Design and Operating Variables

CFB was first developed to replace a bubbling fluidized bed and was first introduced as a riser. Riser configurations and parameters have been studied so far and there is enough literature describing the effects of these configurations and parameters. These data were collected and reported in the book of "circulating fluidized bed" by J.R. Grace, A.A. Avidan, and T.M. Knowlton (1997). On the contrary, there is not much data regarding effects of dower geometry on the reactor performance. Only information for a riser can be shown here.

3.1 Riser Diameter

The effect of column diameter on radial gas dispersion coefficient might be more than linear for small tubes, approximately linear for medium size columns and less than linear for large columns (Yerushalmi and Avidan, 1985). These observations appear to agree with results of change in turbulent intensity as a function of particle diameter/length of turbulent eddies (d_p/l_e), under the assumption of constant length of turbulent eddies/riser diameter (l_e/D) (Gore and Crowe, 1989).

3.2 Riser Wall Geometry

The roughness of the riser wall surface could affect the flow structure, hence influencing the gas-solid contact efficiency and the conversion of reactants. Particles can be stripped off walls with smooth surface better than membrane surface (Wu *et al*., 1991). The ring-type baffles added to the wall surface can enhance the lateral radial mixing of gas and particles by increasing the particle exchange beween the core and wall regions (Jiang *et al*., 1991).

4. Exit Configuration

The geometry of riser exit can greatly affect the performance of CFBs by influencing pressure and voidage profiles, not only at region close to the roof, but also at the significant distance down the riser (Senior and Brereton, 1992; Brereton and Grace, 1993; Zheng and Zhang, 1993). Considering two main types of exit for CFB, the abrupt exits and the smooth exits.

With the abrupt exits, the riser roof is higher than the top of the exit. Heavy particles (too heavy to immediately change the direction) will be trapped at the roof and reflected back down the column, hence influencing the hydrodynamics of the CFBs.

The smooth exit has a radius pipe connected to the top of the riser. The dense zone at the roof then disappears. The volume fraction profile of solid particles is gradually decreased through the top of the riser and the greater portion of solids (than the abrupt exit's one) case will leave at the exit. The studies of effects of exits types showed that, with an equivalent of solids hold up, the smooth exits provide an increasing in axial gas dispersion than the abrupt exits (Brereton *et al*., 1988)

5. Effects of Particle Properties

The density and size of the particles has an effect on hydrodynamics and flow pattern of gas and solid in the riser. Increasing of particle density and size will enhance the radial mixing of gas phase (Zheng, 1994). The studies show that particles of different sizes could enhance or suppress turbulent intensity and therefore increase or reduce radial gas dispersion.

6. Effects of Solid Loading

With different amount of solid loading in to CFB reactors at constant superficial gas velocity, there are different data of solid distribution along the risers. These data was shown in Figure 6 (Levenspeil, 2001).

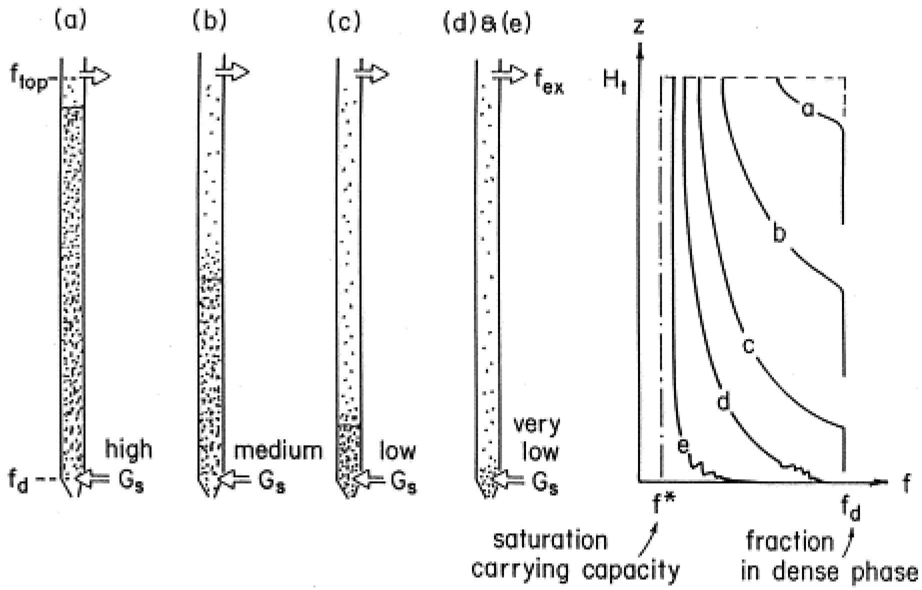

Figure 6 The CFB at various flow rates of solids with fixed gas flow rate
Source: Levenspiel (2001)

7. Hydrodynamics

Hydrodynamics can be seen in two points of view, one with the dynamic of the gas-solid suspensions over a solid fraction range, the other with the hydrodynamics characteristics of gas-solid contacting devices.

From the experiments, the clustering of dilute suspensions, which was first detected from the large gas-solid slip velocity (relative velocity) but it is also a result from the reactor design such as reactor diameter, wall shape, gas distributor design, exit structure, recycling devices, as well as operating conditions.

FCC is the first fluidized reactor that was studied by Davidson (1961) using hydrodynamics approach. The bypassing and interchanging gas were explained with the comprehensive theory. Before this time, the hydrodynamics of fluidized bed were analyzed based on the essence of bubbles only.

In 1980, the experimental study of a CFB riser dynamics show the S-shape of the axial voidage distribution (Li and Kwauk, 1980) with a transition from dense to dilute phase as the position move higher in the column which is an evident to clearly separate the fast fluidized regime from the turbulent fluidized regime and the pneumatic conveying regime.

In a riser, the radial profile of solids holdup separates into the core and the annulus zone (Ambler *et al*., 1990; Pugsley and Berruti, 1995) whereas the radial mixing occurs when the rising particles in the core zone contact with the descending particles in the annulus zone. In the dilute core zone, particles distribution is more uniform compared with the dense annulus zone (Berruti *et al*., 1995). This phenomenon induces the mass transfer from annulus to core.

For a downer, the flow structure is separated into 3 sections. Wang *et al*. (1992) studied the axial flow structure by means of pressure measurements. From the axial distributions of pressure gradient, they proposed a three-section axial flow structure in the downer. The first and second acceleration sections and the constant velocity section were found. Liu *et al*. (2001) used the axial pressure drop to propose a two-section flow structure: the acceleration zone and the fully develop zone. Johnston and Zhu (1999a) reported axial solids hold up and velocity profiles but limited to the entrance section which was used to characterize distributor designs.

7.1 Solid Holdup Profile in a Downer

Solids distribution is important to the performance of fluidized bed and plays important roles in hydrodynamics, heat and mass transfers. As seen in Figure 7, axial solids fraction drops dramatically at the top of a downer because particle velocity increases quickly in this zone. Then becomes constant in the lower section of a dower since particles velocity stops increasing (Zhang *et al*., 1999). The decreasing section of solids fraction occurs in the first and second acceleration zone (Wang *et al*., 1992; Zhu *et al*., 1995).

At the top entrance of a downer, radial solids holdup is not uniform due to the distributor effect. Along with further distance from the downer top, radial distribution of solids holdup becomes more uniform. Solid holdup has the uniform flat core where r/R is lower than a value between 0.7 and 0.94 and also has a maximum value in this region. Then the solid holdup decreases at the wall region (Zhang *et al*., 1999; Wei *et al*., 1996; Herbert *et al*., 1994; Wang *et al*., 1992; Bai *et al*., 1991). This r/R value varies from the size of a downer.

The superficial gas velocity and solids mass flux also have effects on solids holdup. With more solid mass flux, solid holdup is higher. In the opposite way, increasing superficial gas velocity will decrease solids holdup (Kim *et al*., 1996; Zhang *et al*., 1999; Liu *et al*., 2001).

7.2 Solid Velocity Profile in a Downer

Like solid holdup profile, a distributor effect on solid velocity can be seen at the top of a downer where the particle velocity fluctuates up and down in the radial direction. At some small distance away from the entrance, the particle velocity decreases with increasing radial distance and the highest velocity occurs at the column center. With increasing distance from the top entrance, the radial profile of particle velocity further develops and nearly reaches the fully developed state. After fully developed the solids velocity profile remains constant in the core and decreases toward the wall. Solids velocity profile is shown in Figure 8.

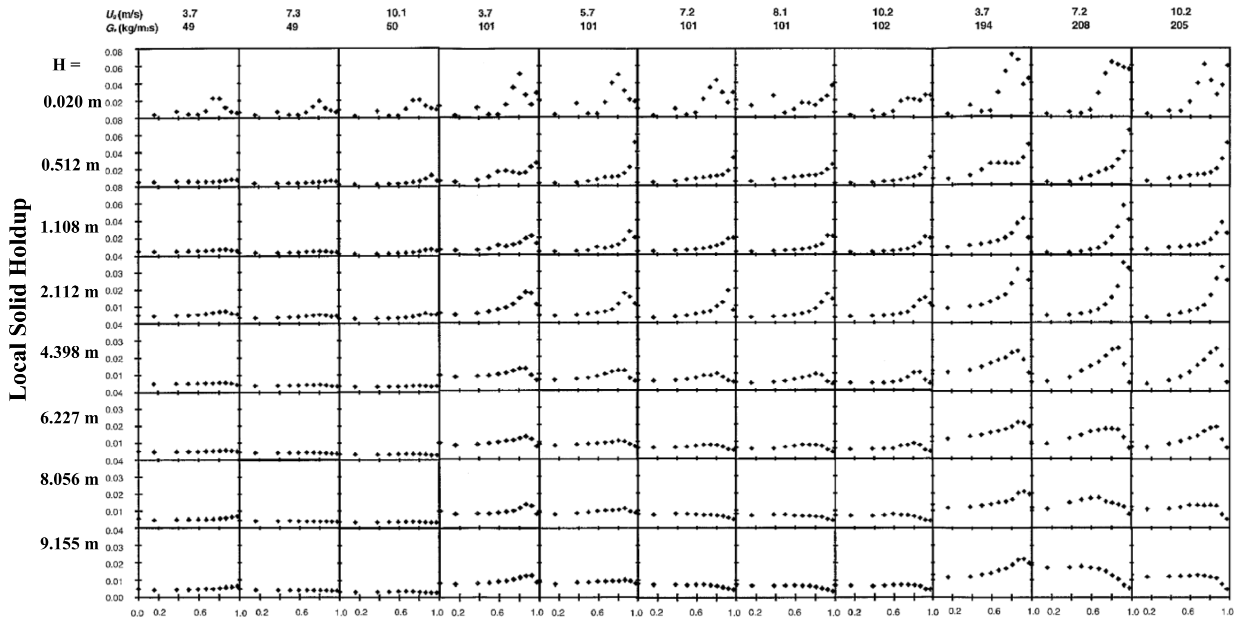

Normalized radial distance from the downer center, r/R

Figure 7 Radial profiles of solid holdup along the downer under different operating conditions

Source: Zhang *et al*. (1999)

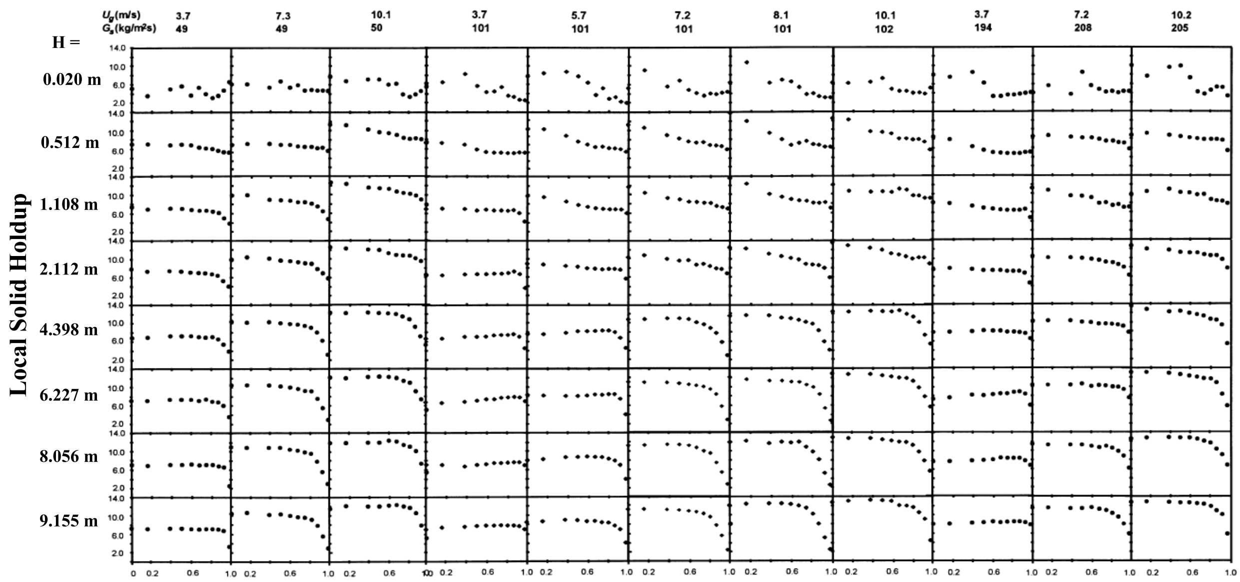

Normalized radial distance from the downer center, r/R

Figure 8 Radial profiles of particle velocity along the downer under different operating conditions

Source: Zhang *et al*. (2000)

8. Heat Transfer in CFB

Heat transfer in CFB is considered important especially when reactor temperature need to be controlled. Particle combustions and exothermic reactions require heat to be removed. However, endothermic reactions like pyrolysis or catalytic cracking need heat sources. Particles in fluidized bed are either combustion material, catalysts, or heat carrier in case of pyrolysis reaction. Heat transfer in or out of the bed will help keeping the designed temperature in reactor.

Heat can be transferred between bed and reactor wall by several ways. In case of heat removal from bed, hot particles in bed core move to the wall and transfer their heat to the wall across a thin layer of gas. This process is called particle convection. Particle convection is important in the dense region of the wall. Gas motion is important for heat transfer in the dilute region of the wall. Heat in the reactor core of fluidized bed can transfer to the wall using gas as carrier. This process is called gas convection. The other way to transport heat is radiation. At high temperature, heat transport by radiation is significant and cannot be neglected. Heat radiation can occur on both uncovered wall surface and surface covered by particles clusters.

Normally, particle convection is the primary heat transfer mechanism because high heat capacities of particles but gas convection may become important where gas velocity is high and solids holdup is low.

Many of reactions operated within CFB require heat transfer during the process. A clear understanding of heat transfer behaviors in CFB will help control the operating temperature and increase performances of CFB. There are many studies concerning heat transfer in risers. Many researchers have presented their reports on this subject (Grace, 1986, 1990; Glicksman, 1988; Leckner, 1991; Basu and Nag, 1996).

After downers were presented as an alternative to risers, many advantages of downers over risers have been notified e.g. narrow residence time distribution, uniform solids distribution. Though many researches have been carried out (Zhu *et al*., 1995; Zhu and Wei, 1996), there is very little information about heat transfer in downers reported.

Previous reports indicated that heat transfer in risers is controlled by the hydrodynamics near heat transfer surface (Wu *et al*., 1990; Bi *et al*., 1989; Basu and Nag, 1987; Gelperin *et al*., 1971). Gas convection is not very important in risers due to relatively high solids holdup in risers. The rate of heat transfer in risers also changes significantly along radial position because of increasing solids holdup. In downers, the heat transfer behavior is different due to different hydrodynamics. The average heat transfer coefficient decreases with decreasing solids mass flux due to decreased solids holdup (Ma and Zhu, 1999) as seen in Figure 9. The heat transfer coefficient does not always decrease with increasing superficial gas velocity, which results in lower solids holdup. Gas convective heat transfer at high gas velocity in downers can be significant and compensate with decreasing particle convective heat transfer as presented in Figure 10 and 11 (Ma and Zhu, 1999).

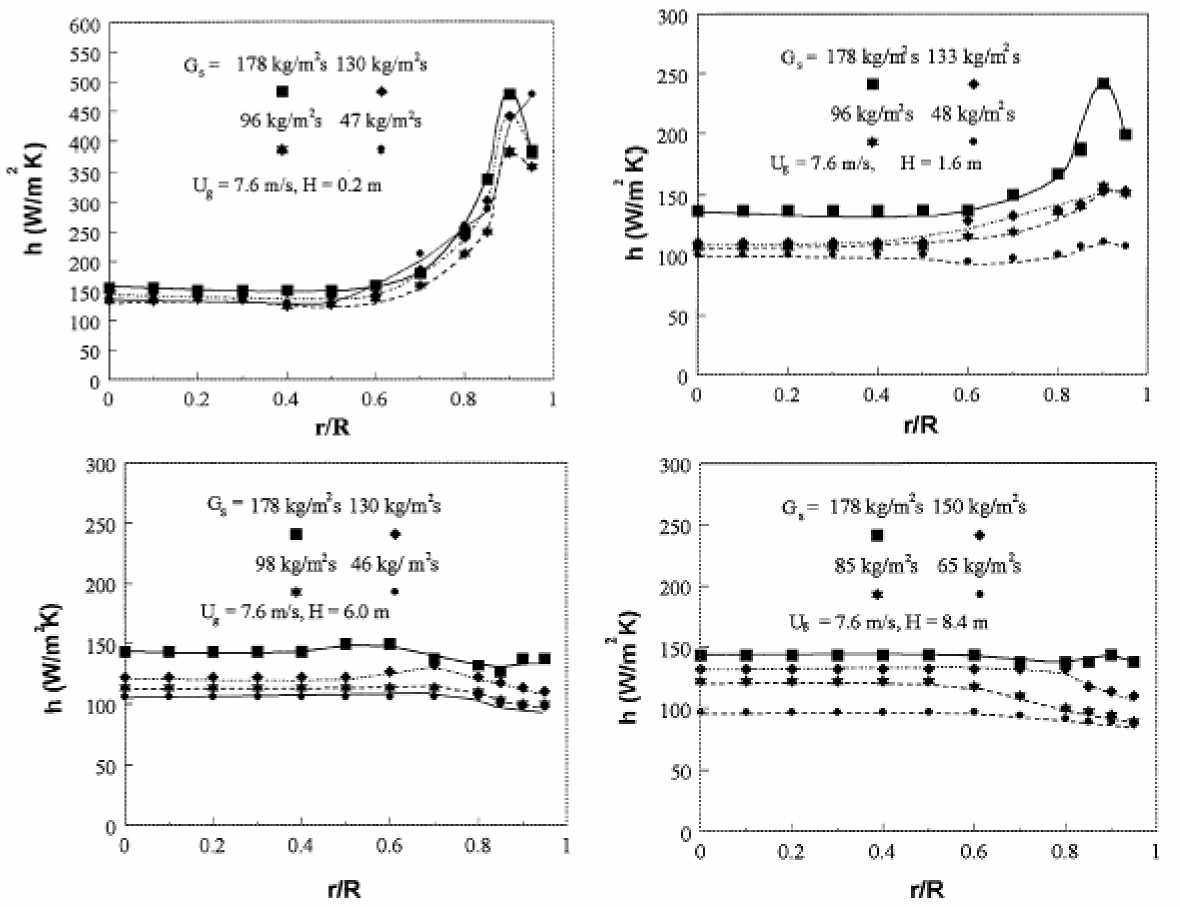

Figure 9 Effect of solids mass flux on the radial distribution of the heat transfer coefficient along downer column

Source: Ma and Zhu (1999)

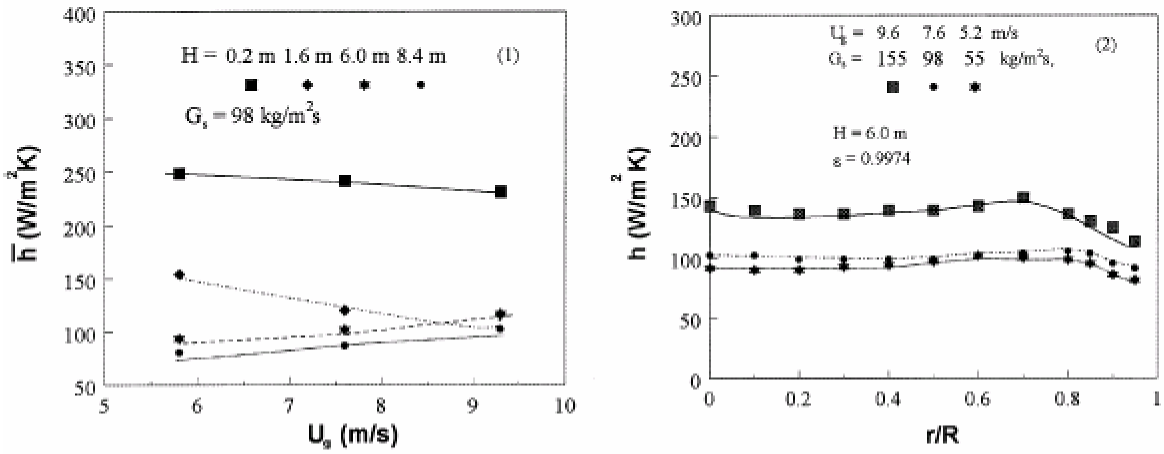

Figure 10 Effect of superficial gas velocity on the heat transfer coefficient
Source: Ma and Zhu (1999)

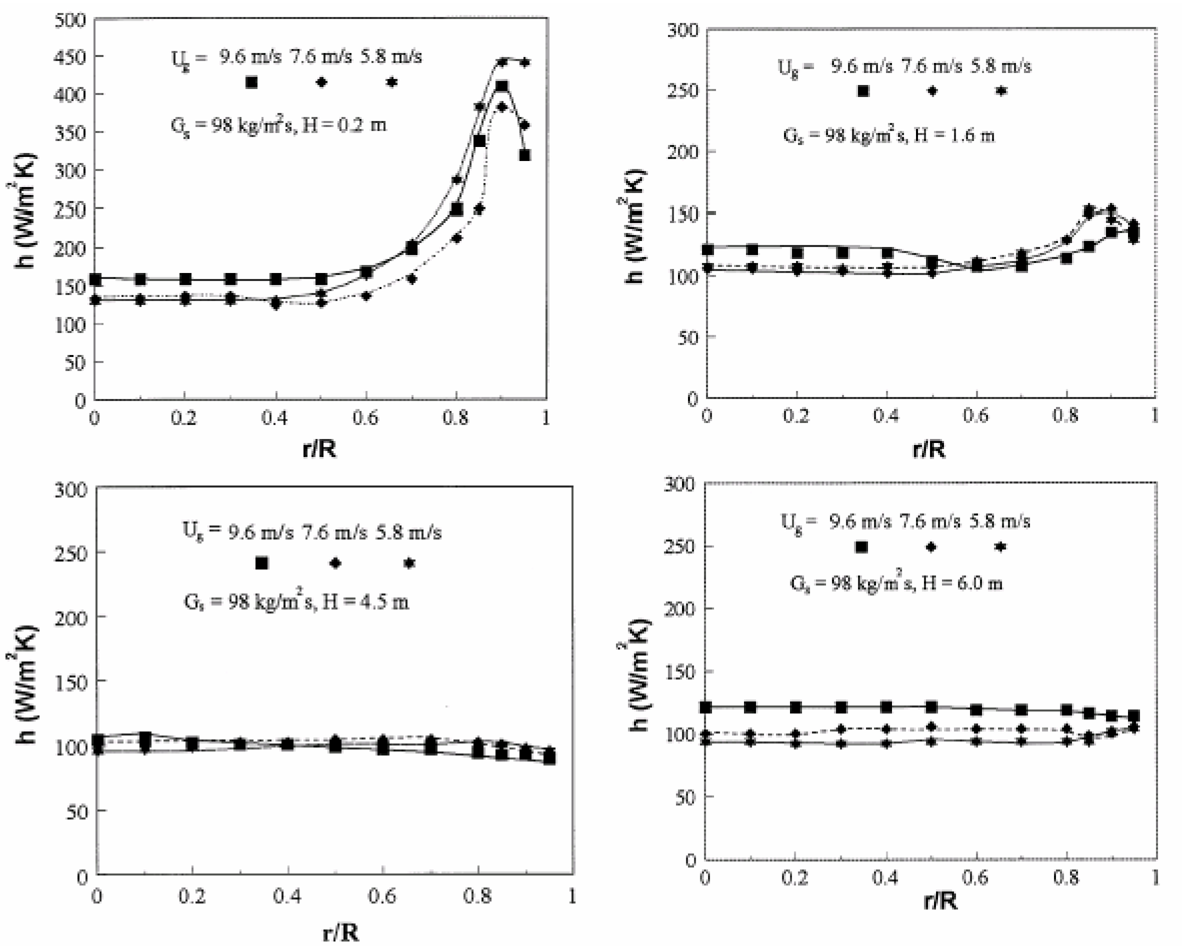

Figure 11 Effect of gas velocity on the radial distribution of the heat transfer coefficient along the downer
Source: Ma and Zhu (1999)

9. Fluid Catalytic Cracking

Fluid Catalytic Cracking (FCC) is the first application of fine-powder fluidization. The first FCC unit in industry, ESSO Model I in 1942, had both the reactor and the regenerator in the form of circulating fluidized beds. Fluidization is important to the design and operation of the FCC units. Oil fed to the FCC unit was vaporized by heat from the regenerator. The size of the unit was big because of the low activity of the acid-treated natural clay catalyst used at that time. The following models of ESSO used the down flow reactor and were reduced by size.

The performance of FCC units was gradually improved from the first model because of new catalysts and hardware improvements. Hardware improvements may include better understanding of standpipe flow and pressure balances. The improvements of FCC units lead to a reduction in unit height, hence reduce the construction and operating cost.

FCC units were developed over decades. There are modern FCC units involved with new designs. The new design riser reactor is completely vertical. This will promote a uniform radial profiles through the riser section. At the solids entrance, the riser diameter is kept small to encourage a uniform mixing of gas and solids. The riser diameter is increased after solids introduction zone because oil vapor expand after being cracked (more moles of gas lead to more volume) and help increasing resident time. The feed stream is injected through several radial nozzles. These nozzles are designed to atomize feed stream into small droplets to enhance the contact between oil vapor and solids throughout the riser.

The exit catalysts are separated by a cyclone and fall down in a standpipe. Steam is injected in the lower part of standpipe and rise counter-currently with solids to remove hydrocarbon vapor and hydrocarbon absorbed on catalyst surface. The shape and design of standpipe are very sensitive. Properly designed standpipe can circulate 1800 kg/m^2s of solids while the improper designed standpipe may achieve only one third of the proper one. Hence the improper design will lead to unnecessary larger size of standpipe.

FCC is used to crack heavy petroleum fractions into lighter products. Normally, FCC units process about 38% of the crude run in the refinery. FCC feed temperature is in between 320 and 600 ^oC boiling range. Other property ranges of FCC feed are shown below.

API gravity	10-30
Sulfur, wt%	0.1-3
Nitrogen, wt%	0.01-0.5
Carbon residue, wt%	0.1-7
Nickel and vanadium, ppm	0.1-50

Some useful products of FCC process are gasoline and olefin. Product yields are lower than theoretical yields owing to two main reasons. Heavy aromatics are not likely to crack with today's catalyst and designed products may react further.

Over past 50 years, FCC catalysts are improved. Yields are increased by 50 %. Feed resident time is decreased to a much shorter time of only a few seconds. Therefore dense-bed crackers were not needed and were replaced by CFB.

FCC catalysts are micro spheres produced by spray drying and are put in Geldart Group A powder with the following properties.

Average particle size, μm	70
Size range, μm	20-150
Sphericity	nearly 1.0
Angle of internal friction	79^o
Angle of repose	32^o
True density, kg/m^3	2500
Particle density, kg/m^3	1200-1700
Bulk density, kg/m^3	750-1000
Typical U_{mf}, m/s	0.001
Typical V_T, m/s	0.1

FCC process needs efficient feed injection, narrow RTD for both gas and solids, and shorter gas-solid contact time. The main interest is to increase selectivity of desired product, which can be gasoline or olefins. A downer is then brought into FCC industry due to its advantages over a riser. Although most of the big oil companies hold patents for downers, there is little information on this subject.

Without problems such as back mixing of particles near the wall region, particle clustering, and radial segregation of solids that occur in a riser, a downer can encourage the FCC process to reach its optimum selectivity. In a downer, solids flow in the same direction with gravity results in narrow RTD and flat radial profiles of solid holdup, solids velocity, gas velocity (Wang *et al*., 1992; Zhu *et al*., 1995). The short contact time between gas and solids is also required to prevent coke formation and over cracking. In the future with better catalyst and higher rate, the short contact time will be more needed.

10. Numerical Simulation

Computational simulations have been developed to the level that they are not only the fundamental components of multiphase flow research but also are the supports for engineering design. Numerical models for single phase flows using simple quasi-one-dimensional flow models is the simplest one to be introduced. The inclusion of the second phase is then illustrated. Eulerian-Lagrangian and Eulerian-Eulerian models are applied for either dilute or dense phase flows.

The single phase flows models were based on finite difference formulations of the continuity and Navier-Stokes equations (Harlow and Fromm, 1965). Upwind differencing scheme was used to stabilize the solutions at high Reynolds number. This study also introduced the idea of using a formulation of the continuity equation based on pressure.

The use of upwind differencing results in higher viscosity than actual in the flow field (Pantakar, 1980). This problem is considered to be severe when the stream lines do not follow the directions of the grid lines.

Tanks and tubes was studied at the imperial college. The flow field is consisted of tanks that are connected to the adjacent tanks by tubes. This concept introduced the idea of finite volume method for formulating conversion laws.

The turbulence of hydrodynamics also gained researcher's interesting. The developments in turbulence modeling led to the two equations models (Launder and Spalding, 1972). The common variables are the turbulence energy and its dissipation rate (k-ε).

10.1 Numerical Approaches

The advances in numerical technique make it possible to analyze the two-phase flow system by computer simulation. There are two popular types of models used to characterize multiphase flows in numerical simulations, the two-fluid model and models involve discrete particles simulations. Gidaspow and co-workers (Gidaspow, 1986, 1989; Tsuo and Gidaspow, 1990) use the two-fluid model and Tsuji and co-workers (Tsuji *et al*., 1992) and Sommerfeld and co-workers (Sommerfeld *et al*., 1992), Limtrakul and co-workers (Limtrakul *et al*., 2003) use the latter type of models.

The discrete phase simulations have the advantage of modeling particles' size and density distribution by specifying each particle's property since these particles are simulated one by one to calculate its velocity and its other properties but the discrete phase simulations also have the limitation of long simulation time and require a lot of computer's memory in case that there are many particles in the simulation boundaries like the case of fluidized bed reactor. In addition, models for particle-particle collisions and particle-wall collisions, and the interaction of the particles and the gas turbulences are required in the discrete phase simulations, too.

10.1.1 Lagrangian Approach

Discrete phase simulations use Lagragian approach. Lagrangian approach could be applied to both dilute and dense phase flow. In the dilute flow, the motion of particles is controlled by the particle-fluid interaction and if the flow is steady and dilute, a form of Lagragian approach is called the trajectory method (Crowe *et al*., 1977). In a dense flow, particle-particle interaction controls the dynamics of particles and the discrete element method (DEM) is necessary

10.1.2 Eulerian Approach

The use of Eulerian approach on the particle phase is referred to as two-fluid model or the Eulerian-Eulerian approach. Stokes number is an important parameter to describe particle motion. If Stokes number is small, the particles will move along with the fluid. The model might be assumed to be one phase mixture. If Stokes number is large, particles slowly response to the fluid force.

11. Models

CFBs have a complex flow behavior such as the non-uniform spatial distribution of particles, large slip velocities between the phases and the sensitivity of the hydrodynamics to the operating parameters. These effects are important to the performance of the reactors. Empirical correlations have been used but they are limited by databases used and neglect the radial gradient of the basic parameters. However, some fundamental based models can be used to predict how various parameters vary with the system conditions.

In the numerical modeling parts, the flow behavior of gas and solid can be classified as either Lagrangian or Eulerian according to the framework in which they are developed. In the Lagrangian approach, each particle has been tracked and has its own equation of motion. In dense flows, the computational requirements for Lagrangian approach are extremely high. In the Eulerian approach, each phase has only one equation of motion and can be applied to the interesting case with relatively small computational efforts but these equations contain some terms that must be chosen carefully to get the accurate results.

11.1 Two-fluid Model

Anderson and Jackson (1967) derived a two-fluid model for solid suspensions through local averaging of the point equation of motion of the gas phase and equation of motion of one single solid particle. Tsuo and Gidaspow (1990) had started the first numerical simulation of CFB in 1990.

The particle phase is treated as continuum and the momentum balance of the particle phase is locally averaged over space large enough to contain many particles

The later two-fluid model employed by Sinclair and Jackson (1989), Ocone *et al*. (1993), Bolio *et al*. (1995), Pita and Sundaresan (1991, 1993) are also consistent with Anderson and Jackson (1967).

In the works of Syamlal and Gidaspow (1985) and Gidaspow (1986), the gas phase pressure gradient term in the momentum equation invalidate the initial value problem. The normal component of solid stress based on a solid stress modulus, $G(\varepsilon)$, was then added to the equation to stabilize the numerical solutions.

Bouillard *et al*. (1989) presented two different hydrodynamics equations set, Model A and Model B. The gas phase pressure gradient term was cut off the solid phase momentum equation in model B.

The models of Gidaspow *et al*. (1989) and Tsuo and Gidaspow (1990) are similar to Model B of Bouillard *et al*. (1989) but the shear stresses were added in both solid and gas momentum equations. The solid viscous term was added to account for the particles'collisions. The constant solids viscosity for glass beads was used in the simulations of Gidaspow (1989) and the results were satisfied compared to experiments. The cluster formations at the wall regions was also correctly predicted by the simulation results.

Governing Equations

The continuity equations:

$$\frac{\partial}{\partial t}(\rho_i \varepsilon_i) + \nabla \cdot (\rho_i \varepsilon_i \vec{u}_i) = 0 \tag{1}$$

with the constraint

$$\sum \varepsilon_i = 1 \tag{2}$$

The conservation of momentum of phase i (i= gas, solid, k$\neq$ i):

$$\frac{\partial}{\partial t}(\rho_i \varepsilon_i \vec{u}_i) + \nabla \cdot (\rho_i \varepsilon_i \vec{u}_i \vec{u}_i) = -\varepsilon_i \nabla \cdot \tau_i - \beta(\vec{u}_i - \vec{u}_k) + \rho_i \varepsilon_i \vec{g} \tag{3}$$

where ρ_i is density of phase i; ε_i is volume fraction of phase i; $\vec{u}_i$ is velocity vector of phase i; τ_i is stress tensor of phase i; μ_i is viscosity of phase i; β is interphase drag coefficient.

The conservation of specie j:

$$\frac{\partial}{\partial t}(\rho_j \varepsilon_j) + \nabla \cdot (\rho_j \varepsilon_j \vec{u}_j) = R_j \tag{4}$$

where R $_j$ is rate of occurrence of species j.

The conservation of energy of phase i:

$$\frac{\partial}{\partial t}(\rho_i \varepsilon_i H_i) + \nabla \cdot (\rho_i \varepsilon_i \vec{u}_i H_i) = \\ -\varepsilon_i \frac{\partial P_i}{\partial t} + \tau_i : \nabla u_i - \nabla . q_i + h(T_i - T_k) + \sum_{m=1}^{no.\,of\ rxn} (r_m . \Delta H_{rxn,m}) \tag{5}$$

where *h* is interphase heat transfer coefficient

$$h = \frac{6k_f \varepsilon_s \varepsilon_f Nu_s}{d_p^{\ 2}} \tag{6}$$

The knudselt number (Gunn, 1978) can be defined as:

$$Nu_s = (7 - 10\varepsilon_f + 5\varepsilon_f^{\ 2})1 + 0.7\,\mathrm{Re}_s^{\ 0.2}\ \mathrm{Pr}_f^{\ 1/3} \tag{7}$$

where
$$\mathrm{Re}_s = \frac{\rho_f \left|\vec{u}_s - \vec{u}_f\right| d_s}{\mu_f} \tag{8}$$

$$\mathrm{Pr}_f = \frac{C_{p,f}\,\mu_f}{k_f} \tag{9}$$

where Re_s is particle Reynolds number; Nu_s is particle Knudselt number; Pr_f is fluid Prandtl number (indexes: 'f' refers to fluid phase; 's' refers to solid phase).

The equation for the fluctuating energy of solid called granular temperature, $\Theta_s \left(\Theta_s = 1/3 < u'^{\,2} >\right)$; where u' is particle random velocity, may be written as:

$$\frac{3}{2}\frac{\partial}{\partial t}\left(\rho_s \varepsilon_s \Theta_s\right) + \nabla \cdot \left(\rho_s \varepsilon_s \vec{u}_s \Theta_s\right) = \tau_s : \nabla \vec{u}_s + \nabla \cdot \left(k_s \nabla \Theta_s\right) - \gamma_s - 3\beta\Theta_s \tag{10}$$

where Θ_s is granular temperature; τ_s is solid phase stress; k_s is diffusion coefficient of granular temperature; γ_s is collisional dissipation of granular temperature.

Constitutive equations

The solid phase stress and pressure, and the diffusion coefficient of the granular temperature are defined as follows.

(a) Solid phase stress:

$$\tau_s = \left(-P_s + \varepsilon_s \mu_b \nabla \vec{u}_s\right)I + 2\varepsilon_s \mu_s S_s \tag{11}$$

where S_s is deformation rate; P_s is solid phase pressure; μ_b is solid bulk viscosity; μ_s is solid phase shear viscosity.

The deformation rate (S_s) can be written as:

$$S_s = \frac{1}{2}\left[\nabla \vec{u}_s + \left(\nabla \vec{u}_s\right)^T\right] - \frac{1}{3}\left(\nabla \vec{u}_S I\right) \tag{12}$$

The solid phase shear viscosity (μ_s) can be defined by:

$$\mu_s = \frac{2\mu_{s,dil}}{(1+e)g_0}\left[1+\frac{4}{5}g_0\varepsilon_s(1+e)\right]^2 + \frac{4}{5}\varepsilon_s\rho_s d_p(1+e)g_0\left(\frac{\Theta_s}{\pi}\right)^{1/2} \tag{13}$$

where d_p is particle diameter; e is particle–particle restitution coefficient.

The solid phase dilute viscosity ($\mu_{s,dil}$) is defined as:

$$\mu_{s,dil} = \frac{5\rho_s d_p\sqrt{\Theta_s\pi}}{96} \tag{14}$$

The solid bulk viscosity is defined as:

$$\mu_b = \frac{4}{3}\varepsilon_s\rho_s d_p g_0(1+e)\left(\frac{\Theta_s}{\pi}\right)^{1/2} \tag{15}$$

(b) Solid pressure:

$$P_s = \varepsilon_s\rho_s\Theta_s + 2\rho_s(1+\varepsilon)\varepsilon_s^2 g_0\Theta_s \tag{16}$$

The radial distribution function (g_0) is defined as:

$$g_0 = \frac{3}{5}\left[1-\left(\frac{\varepsilon_s}{\varepsilon_{s,\max,}}\right)^{1/3}\right]^{-1} \tag{17}$$

(c) The diffusion coefficient of the granular temperature:

$$k_s = \frac{150\rho_s d_p\sqrt{\Theta_s\pi}}{384(1+e)g_0}\left[1+\frac{6}{5}g_0\varepsilon_s(1+\varepsilon)\right]^2 + 2\varepsilon_s^2\rho_s g_0(1+e)\left(\frac{\Theta_s}{\pi}\right)^{1/2} \tag{18}$$

<u>The k-ε Turbulence Model for Each Phase</u>

The k-ε turbulence model is used for both particles and gas phase. The k-ε turbulence model was first developed for the homogeneous flow system. However, the k-ε turbulence model for the particle phase is also used here in analogous to that of the gas phase to model the big scale fluctuation of the particle phase. The use of k-ε turbulence model on the particle phase is coupled with the two-fluid model that considers the particle phase as one fluid phase. Thus this is different from the model of fluctuating energy called granular temperature (Θ). The use of k-ε turbulence model on the particle phase might helps obtaining accurate results from the simulation of the particulate flow system.

Turbulence kinetic energy of phase i (i = gas, solid; k ≠ i):

$$\frac{\partial}{\partial t}(\varepsilon_i \rho_i k_i) + \nabla.(\varepsilon_i \rho_i \vec{u}_i K_i) = \nabla.(\alpha_i \frac{\mu_{t,i}}{\sigma_k} \nabla K_i) + (\varepsilon_i G_i - \varepsilon_i \rho_i E_i) + \beta(C_{ki} K_k - C_{ik} K_i)$$
$$- \beta(\vec{u}_k - \vec{u}_i).\frac{\mu_{t,k}}{\varepsilon_k \sigma_k} \nabla \varepsilon_k + \beta(\vec{u}_k - \vec{u}_i).\frac{\mu_{t,i}}{\varepsilon_i \sigma_i} \nabla \varepsilon_i$$

Turbulence dissipation rate of phase i (i = gas, solid; k ≠ i):

$$\frac{\partial}{\partial t}(\varepsilon_i \rho_i E_i) + \nabla.(\varepsilon_i \rho_i \vec{u}_i E_i) = \nabla.(\varepsilon_i \frac{\mu_{t,i}}{\sigma_\varepsilon} \nabla E_i) + \frac{E_i}{k_i}\{C_{1\varepsilon} \varepsilon_i G_i - C_{2\varepsilon} \varepsilon_i \rho_i E_i +$$
$$C_{3\varepsilon}[\beta(C_{ki} K_k - C_{ik} K_i) - \beta(\vec{u}_k - \vec{u}_i).\frac{\mu_{t,k}}{\varepsilon_k \sigma_k} \nabla \varepsilon_k + \beta(\vec{u}_k - \vec{u}_i).\frac{\mu_{t,i}}{\varepsilon_i \sigma_i} \nabla \varepsilon_i]\}$$

where K_i is turbulence kinetic energy of phase i; E_i is turbulence dissipation rate of phase i; $\mu_{t,i}$ is turbulence viscosity of phase i; G_i is the production of turbulence kinetic energy.

The turbulent viscosity ($\mu_{t,i}$) is computed from

$$\mu_{t,i} = \rho_i C_\mu \frac{K_i^2}{E_i}$$

and the production of turbulence kinetic energy (G_i) is computed from

$$G_i = \mu_{t.i}\left(\nabla \vec{u}_i + (\nabla \vec{u}_i)^T\right) : \nabla \vec{u}_i$$

$$C_{ki} = 2 \text{ and } C_{ik} = 2 * \left(\frac{\eta_{ki}}{1 + \eta_{ki}}\right)$$

where η_{ki} is the ratio between the two characteristic times and is written as

$$\eta_{ki} = \frac{t_{t,ki}}{t_{F,ki}}$$

where $t_{F,ki}$ is the characteristic particle relaxation time connected with inertial effects acting on a dispersed phase; $t_{t,ki}$ is the Lagrangian integral time scale calculated along particle trajectories.

The characteristic particle relaxation time connected with inertial effects acting on a dispersed phase is defined as

$$t_{F,ki} = \frac{\varepsilon_k \rho_i}{\beta}\left(\frac{\rho_k}{\rho_i} + C_V\right)$$

where the added-mass coefficient, $C_V = 0.5$.

The Lagrangian integral time scale calculated along particle trajectories, mainly affected by the crossing-trajectory effect (Csanady, 1963) is defined as

$$t_{t,ki} = \frac{t_{t,i}}{\sqrt{1 + C_\beta \xi^2}}$$

where $t_{t,i}$ is a characteristic time of the energetic turbulent eddies defined as

$$t_{t,i} = \frac{3}{2} C_\mu \frac{K_i}{E_i}$$

$$\xi = \frac{\left|\vec{u}_k - \vec{u}_i\right| t_{t,i}}{L_{t,i}}$$

and

$$C_\beta = 1.8 - 1.35 \cos^2 \theta$$

The length scale of the turbulent eddies ($L_{t,i}$) is defined as

$$L_{t,i} = \sqrt{\frac{3}{2}} C_\mu \frac{K_i^{3/2}}{E_i}$$

and θ is the angle between the mean particle velocity and the mean relative velocity.

$C_{1\varepsilon}$, $C_{2\varepsilon}$, $C_{3\varepsilon}$, C_μ are constants where $C_{1\varepsilon} = 0.09$, $C_{2\varepsilon} = 1.44$, $C_{3\varepsilon} = 1.92$, $C_\mu = 1.3$.

11.2 Discrete Phase Model

For the multiphase flow, the discrete second phase is also allowed to be model by Fluent in a Lagrangian frame of reference in addition to the two-fluid model, which uses the Eulerian approach. Unlike Eulerian model in Fluent, the discrete phase model has the benefit of using the option to include catalytic reaction that takes place on the solid catalyst particles surfaces. This second phase consists of sphere particles which may include droplets of bubbles but for the application of circulating fluidized bed, means solid particles. The discrete phase trajectory is calculated by using a Lagrangian formulation that includes the discrete phase inertia, drag force, and the gravity force for both steady and unsteady flows. The effects of turbulence in the gas phase on the dispersion of particles can be included by choosing the stochastic model options available in the discrete phase model as will be mentioned in the Fluent setting part.

For the gas phase:

The position of each particle can be calculated from the following equations.

$$\vec{R} = \vec{r}_o + \vec{v}_p dt \tag{19}$$

$$\vec{v}_p = \vec{v}_{po} + \vec{a}_p dt \tag{20}$$

where $\vec{R}$ is particle position; $\vec{r}_o$ is particle position of the former time step; $\vec{v}_p$ is particle velocity; $\vec{v}_{po}$ is particle velocity of the former time step; $\vec{a}_p$ is particle acceleration rate; *dt* is time interval.

The force balance on solid particles in the x-direction is described in this equation.

$$\vec{a}_p = \frac{dv_p}{dt} = F_D(\vec{u}_g - \vec{v}_p) + \frac{\vec{g}_x(\rho_p - \rho_g)}{\rho_p} + \vec{F}_x \tag{21}$$

; $\vec{u}_g$ is gas velocity

where $F_D(\vec{u}_g - \vec{v}_p)$ is the drag force per unit particle mass.

$$F_D = \frac{18\mu}{\rho_p d_p^2}\frac{C_D \mathrm{Re}}{24} \tag{22}$$

Re is the relative Reynolds number, which is defined as

$$\mathrm{Re} = \frac{\rho\left|\vec{v}_p - \vec{u}_g\right| d_p}{\mu_g}$$

For smooth sphere particles

$C_D = a_1 + a_2 / Re + a_3 / Re^2$

where a_1, a_2, a_3 and are constants that apply for smooth spherical particles over several ranges of Re given by Morsi and Alexander.

The term 'F_x' in equation (21) includes 'the virtual mass force' required to accelerate the fluid surrounding the particle and the force from the pressure gradient in fluid phase.

For the gas phase:

The continuity equations:

$$\frac{\partial}{\partial t}\left(\rho_g \varepsilon_g\right) + \nabla \cdot \left(\rho_g \varepsilon_g \vec{u}_g\right) = 0 \qquad (23)$$

The conservation of momentum of gas phase:

$$\frac{\partial}{\partial t}\left(\rho_g \varepsilon_g \vec{u}_g\right) + \nabla \cdot \left(\rho_g \varepsilon_g \vec{u}_g \vec{u}_g\right) = -\nabla \varepsilon_g P - \beta\left(\vec{u}_g - \vec{v}_p\right) + \rho_g \varepsilon_g \vec{g} \qquad (24)$$

where ρ_g is gas density; $\vec{u}_g$ is gas velocity; $\vec{v}_p$ is the local average of particle velocities; ε_g is gas volume fraction; β is interphase drag coefficient; $\vec{g}$ is gravity force.

11.3 Discrete Element Method (DEM)

The ideas of DEM are similar to those of discrete phase model but include the effect of particles interaction, hence available for dense particles phase flow. The interactions between particles can be separated to the normal force and the tangential force that can be described by three mechanisms that are spring, dashpot, and friction force.

This model interests in the movement of each particle (Cundall and Strack, 1979) by calculating the position and velocity of each particle. The velocities of particles are affected by the impact of force on the particle. The acceleration of particles can be calculated directly from impacted forces. The movements of particles are described in two kinds, the distance movement and the angular movement.

Acceleration of distance movement: $$\vec{a}_p = \frac{\vec{f}}{m_p} + \vec{g} \qquad (25)$$

where $\vec{a}_p$ is particle acceleration rate; $\vec{f}$ is force acting on the particle; m_p is mass of the particle; $\vec{g}$ is gravity force.

The forces acting on the particle are the force from collisions and drag forces between solid and gas phases.

Acceleration of angular movement: $$\vec{\alpha} = \frac{\vec{T}}{I} \quad (26)$$

With the distance velocity and angular velocity as followed.

Distance velocity: $$\vec{v}_p = \vec{v}_{po} + \vec{a}_{po} dt \quad (27)$$

Angular velocity: $$\vec{\omega}_p = \vec{\omega}_{po} + \vec{\alpha}_{po} dt \quad (28)$$

where $\vec{v}_p$ is the particle velocity; $\vec{v}_{po}$ is the particle velocity of the former time step; $\vec{a}_p$ is the particle acceleration rate; $\vec{a}_{po}$ is the particle acceleration rate of the former time step; $\vec{\omega}_p$ is the particle angular velocity; $\vec{\omega}_{po}$ is the particle angular velocity of the former time step; $\vec{\alpha}_p$ is the particle angular acceleration rate; $\vec{\alpha}_{po}$ is the particle angular acceleration rate of the former time step; *dt* is the time interval.

The position after the time value *dt* consumed is then calculated by the following equation.

Position of a particle: $$\vec{r} = \vec{r}_o + \vec{v}_o dt \quad (29)$$
where $\vec{r}$ is the particle position; $\vec{r}_o$ is the particle position of the former time step.

11.4 Semi-empirical models

There are some models that simplify the gas and solid flow patterns and calculate a conversion of reactants. These models can be calculated directly without the helps of computers. The sample of these are shown by the following models.

11.4.1 Core-Annulus Model

The core-annulus model divides fluidized bed into two zones, core and annulus. Each zone has uniform solid distribution. Gas is assumed to have a plug flow in the core region and is stagnant in the annulus zone. Mass transfer occurs at the interface between two zones. The model is illustrated in Figure 13.

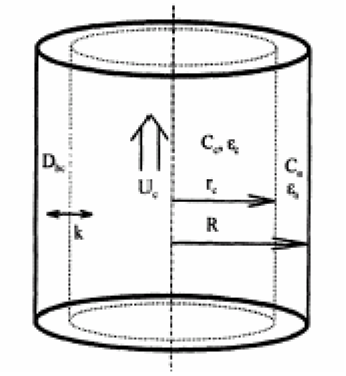

Figure 12 Core-annulus model
Source: Namkang *et al*. (1997)

11.4.2 Two-regions Model

Kunii and Levenspeil have developed the two-regions model to describe hydrodynamics behavior in circulating fluidized bed. This model has dense region at bottom and lean region at the top of CFB. Each region also has two zones called core zone and wall zone. The core zone in the lean region is bigger than in the dense region as shown in Figure 13 (Levenspeil 2001). The solid fractions in the wall and core zone are uniform in their regions. The conversion of reactant A can be calculated from C_{AO}/C_A from equation 30.

$$\ln\frac{C_{A0}}{C_A} = \left[f^{*}\delta_d k''' + \frac{1}{\dfrac{1}{\delta_d K_{CW}} + \dfrac{1}{f_w(1-\delta_d)k'''}} \right]\frac{H_d}{u_0} + \left[f^{*}\delta_l k''' + \frac{1}{\dfrac{1}{\delta_l K_{CW}} + \dfrac{1}{f_w(1-\delta_l)k'''}} \right]\frac{H_l}{u_0} \qquad (30)$$

where f is solid fraction; δ is core/bed area factor; K is mass transfer coefficient; H is bed height; u_o is superficial gas velocity.

The sub-index *d* refers to dense zone; *l* refers to lean zone; *C* refers to core zone; *W* refers to wall zone. At the present time, the data for f_w, f^*, δ are available but not for K_{cw}. Once the reasonable values for K_{cw} are obtained, the performance of these reactors will be predicted.

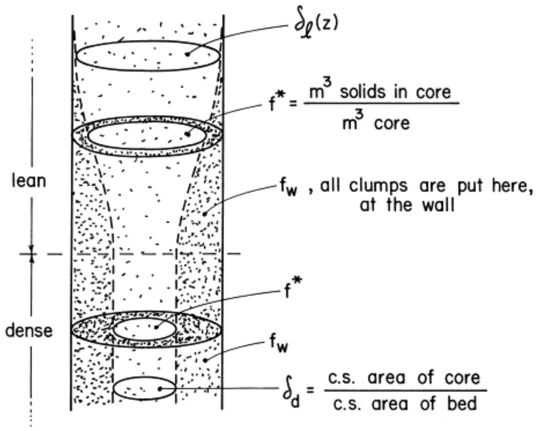

Figure 13 Core-annulus model from Kunii and Levenspiel model
Source: Levenspeil (2001)

MATERIALS AND METHODS

Materials

1. Computers and Networking Devices

1.1) Personal computers: Pentium IV

1.2) Gigabit Ethernet Switch and CAT 5 network cables

2. Software

2.1) Operating system: Linux distribution

2.2) Grid generation: Gambit 2.2

2.3) Simulation of fluid dynamics and reaction: Fluent 6.2

Methods

Simulation of 2-D Models

A 2-D simulation can be carried out with the assumptions of axisymmetry or symmetry. Both assumptions can be used to describe a circulating fluidized bed downer in a limit of no side pipe-attachments to the system. In these assumptions gas and solid velocities in a downer cylinder are not a function of θ direction and the θ components of these velocities are zero. Thus only the R and Z components are interested. However, in a real 3-D downer column, there are inlet and outlet parts connected to the side walls. When a 2-D simulation is carried out, the system is just considered as a 2-D rectangular with inlet and outlet pipes attached to a wall boundary.

In 2-D axisymmetric and symmetrical assumptions, the domain of calculation becomes 2-D with radius direction in the range of 0-R and the system height in the range of 0-H as shown in Figure 14(a) and Figure 15(a). With these assumptions, the simulation loses its capability to describe both unaxisymmetric and unsymmetrical downers because the way that feed and exit streams attach to only one side of the downer. Therefore both axisymmetric and symmetrical assumptions have their limits to represent the real downer reactor if there are non-symmetrical inlets or outlets attached to the downer.

With symmetrical assumption, the domain in Figure 14(a) represents quadrilateral tube with no end effects from front and back walls (infinitely thick) shown in Figure 14(b). The attached inlet and outlet on the wall boundary of domain in Figure 14(a) will extend throughout the depth of both side walls in a 3-D implication as seen in Figure 14(b).

For the other meaning of the 2-D model in Figure 15(a), the system can be assumed axisymmetry. Axisymmetric assumption of the 2-D model in Figure 1(a) can be explain as the cylinder with axisymmetry (Figure 15(b)). The axisymmetric assumption will assume that the inlet pipe or outlet pipe attached on the wall in one side of the rectangular domain has its end attached to all over the downer perimeter at the same height.

Without axisymmetric and symmetrical assumptions, a 2D simulation looks like the front, or back, projection of the downer reactor (Figure 16(a)). This type of 2D domain can only explain the real downer as a quadrilateral tube but it has an advantage in the way that entrance or exit streams can be attached to only one side of the downer. The attached entrance or exit also extend throughout the side-end of a downer as shown in Figure 16(b) as well. However, this full projection model cannot described the cylindrical shape downer.

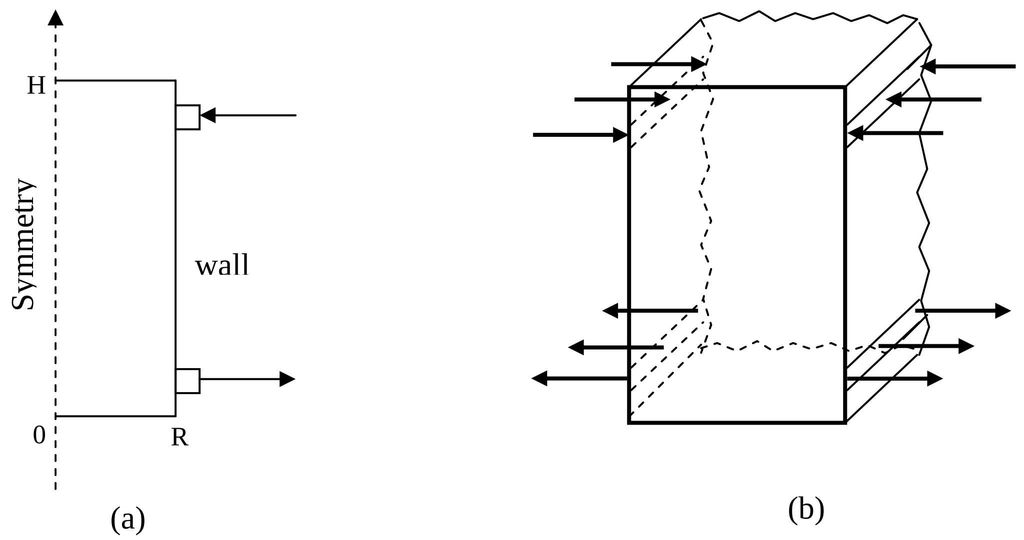

Figure 14 (a) a 2-D symmetrical model, (b) implication of a 2-D symmetrical model representing a rectangular tube

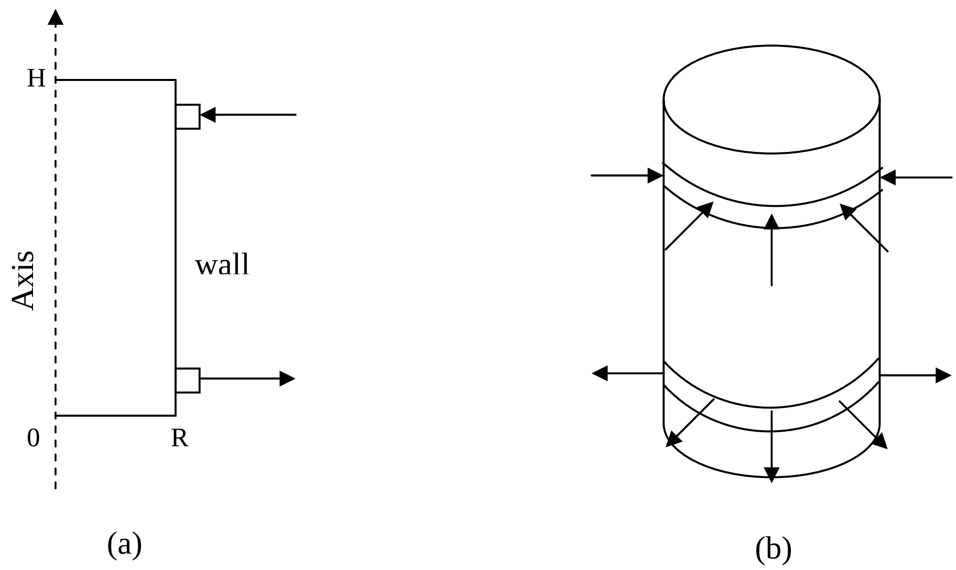

Figure 15 (a) a 2-D axisymmetric model, (b) implication of a 2-D axisymmetric model representing a cylinder downer column

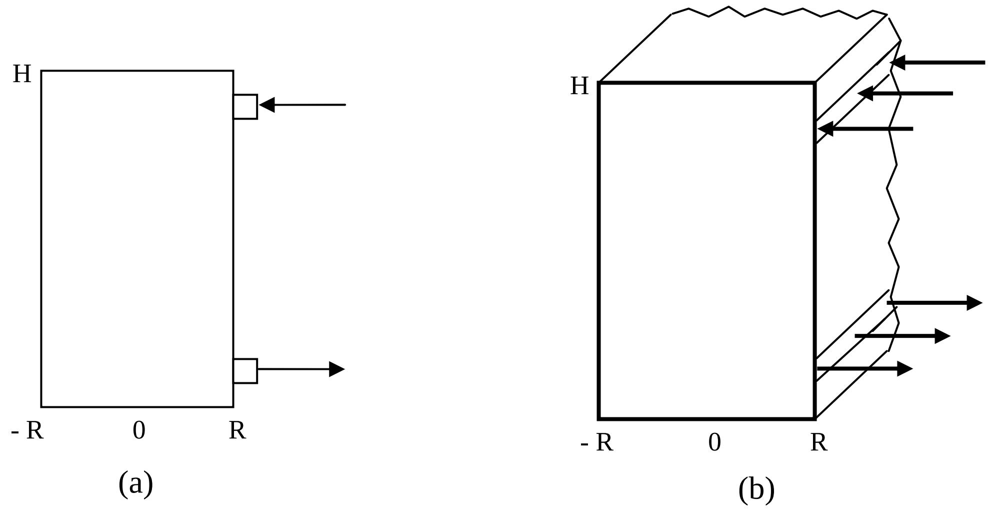

Figure 16 (a) a full projection 2-D model with side attachments, (b) implication of a full projection 2-D model with side attachments

Considering a 2-D domain with entrance on the top and exit at the bottom of the rectangular domain with wall boundary conditions on both sides of the rectangular domain as shown in Figure 17(a). This type of domain is symmetrical and can be used to describe both the quadrilateral downer that have entrance and exit on the top and bottom respectively (shown in Figure 17(b)).

The hydrodynamics result obtained from the computer simulation of the domain in Figure 17(a) is not symmetry even if the domain is symmetrical. The imbalance occurs during the generation of the computational cells in the domain or by the round-off error generated by the computer can create the imbalance between the left and the right side of the domain. There are chances that particles entering the domain will swing left and right while moving down the column due to the non-symmetry of variables in this domain. This problem is shown by the contour plot in Figure 18. The yellow contour represents a locust of particles while the blue one represents the area with low content of particles. For time dependent analysis, at any fixed height, the locust of particles also changes their positions from side to side with time, too. If enough time is used for time averaging, this simulation might represent more realistic results. However, the full projection model in Figure 17(a) will not include the effect of the depth dimension in the simulation. While the full projection model represent the 2-D rectangular reactor, all conventional downers used by both industrials and educations are of the cylinder shape nowadays. Hence the simulation results of the full projection model will not describe the real hydrodynamics in the downer.

In this research, the cylindrical downer with no side attachments on the downer column is studied although there are side attachments at the top separator and bottom storage tank. Hence the axisymmetric assumption is used to correctly represent the reactor and avoid problems occurred with the full projection domain.

The details of a downer reactor model used in this study will be described in the next chapter.

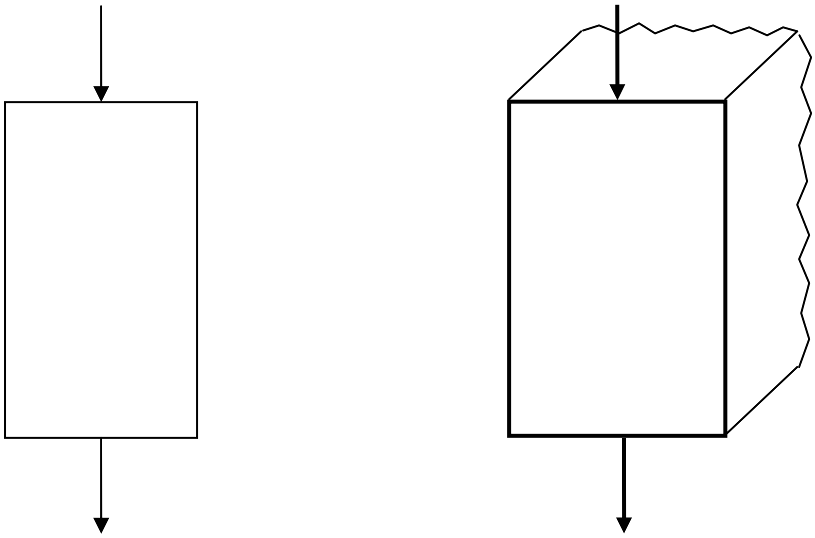

(a) (b)

Figure 17 (a) a full projection 2-D model with no side attachment, (b) implication of a full projection 2-D model with no side attachment

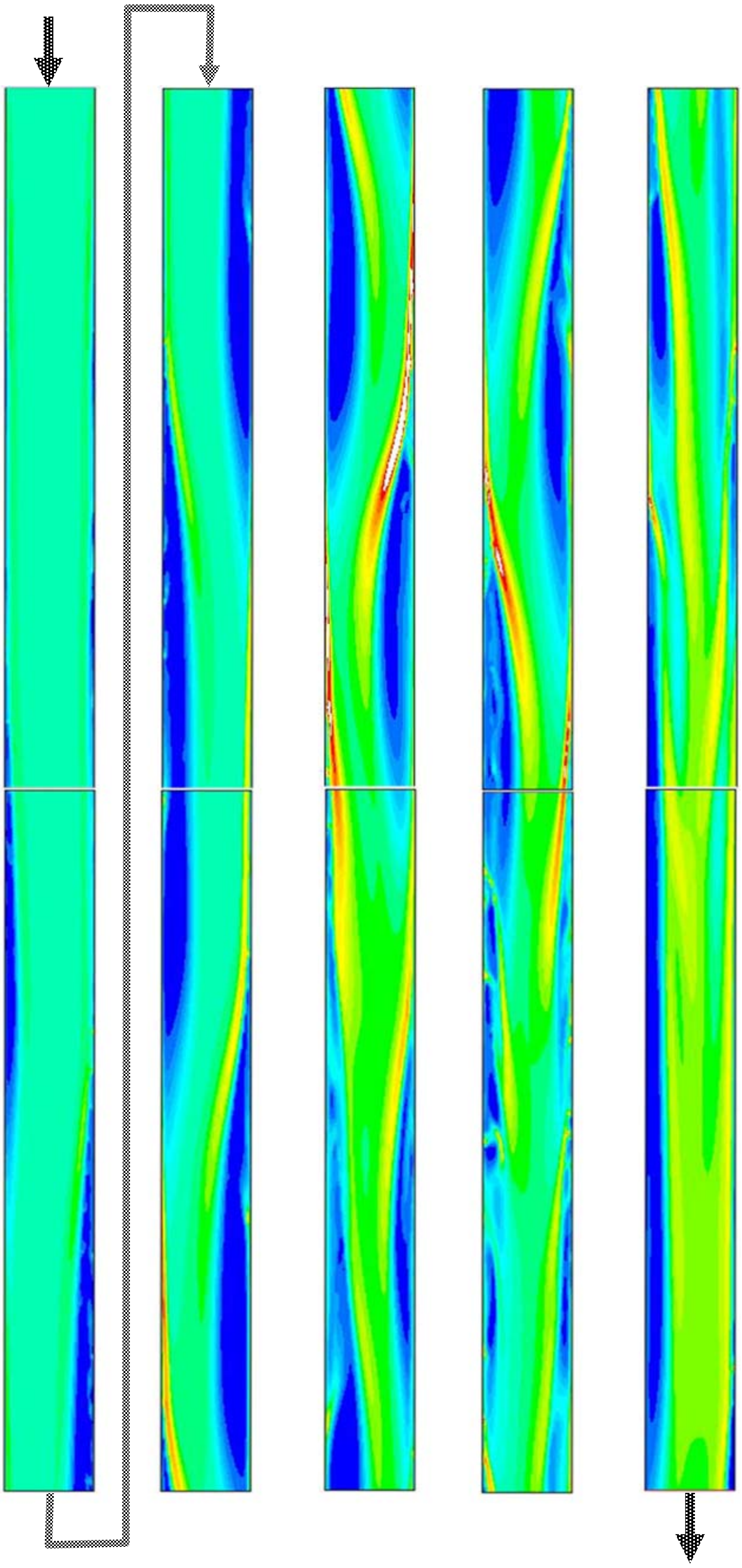

Figure 18 Contours of solid volume fraction show problems occur with full projection domain

Geometry Domain

As mentioned in the earlier section, the simulation of the reactor 2-D full projection domain has capability to illustrate the unsymmetrical pipe-attachments to central domain but as a slab of 2-D domain not the cylinder shape. Since symmetrical model cannot represents a cylindrical downer because it uses rectangular coordinate, axisymmetric model, which uses cylindrical coordinate, is used in this work instead.

Axisymmetric assumption of 2-D model in Figure 19 will represent the 3-D reactor as volume created by rotating the 2-D model around the axis. As a result, the downer column and the upper storage tank that are on the centerline will be of cylindrical shape as needed. The 3-D upper storage tank will become a drum with the same radius as its 2-D width and the same height as its 2-D model and the downer column will become a cylindrical tube with the same radius as its 2-D width. The riser shape will look like a circular shell with thickness equal to its 2-D model width. Inlets and outlets on the horizontal plane of the model will become horizontal circular shape. Inlets and outlets on the vertical plane of the model will become the vertical circular surfaces. These surfaces are created by rotating the inlets or outlets around the domain axis as shown in Figure 20. The implementing 3-D shapes of the 2-D downer model in this calculation may be different to a real geometry downer. In order to correctly describe the shape of a real downer reactor, the 3-D model should be used instead. However, simulating the 3-D model of a complicated downer reactor, which comprises of many components, lasts for months. As a result, the axisymmetric model is used to simplify a downer reactor to a 2-D model and still represents the downer column cylindrical shape. Simplification of a downer reactor to a 2-D model can save enormous times. A 2-D simulation with the help of parallel computing on 3 computers only takes a few days.

Each parts of this downer reactor model is described in the ‘downer components’ section. Boundary conditions, initial conditions, model parameters, and numerical methods used in this simulation are also described following this topic.

1. Downer components

This research studies solids movement in a downer reactor. A downer reactor model consists of a particle storage tank, particle distributing tubes, a particle distributor, a downer column, a riser column, and two gas-solid separators located at the end of the downer and the riser. The overall model is represented in Figure 19. The model geometries of the top part, particle distributing tubes, and the bottom part are shown in Figure 21, Figure 22, and Figure 23 respectively. Particles first stay in the top storage tank initially, then falls into distributor through particle distributing tubes. The reactant gas enters the domain at the top of distributor and mixes with particles in distributor, then, both gas and solids flow into a downer where reactions take place. After leaving downer, gas and solids are separated by the bottom separator. Gas, which now becomes product gas, leaves the domain at the bottom separator. On the contrary, solids are recycled through a riser, which uses the air to lift solids up to the top. Solids are then separated from air by the top separator and return to the storage tank. The details of downer components are described as follows.

1.1 Particle storage tank

There are two storage tanks in this downer reactor model; top storage tank and bottom storage tank. The top storage tank is above a downer column and its purpose is to feed particles into the downer column. The bottom storage tank is used to store used particles flowing out of a downer after being separated from product gas.

1.1.1 Top storage tank

A top storage tank is used to store the particles at the beginning of simulation and the particles that are recycled from a riser. Particles in the storage tank are maintained at the minimum fluidized bed condition (ε_{mf}) by the storage tank fluidized gas, which is set at the minimum fluidized velocity of the particles (u_{mf}). This is done in order to maintain constant particle flux to the downer column.

Particle level in the storage tank is important to the performance of the circulating fluidized bed downer. High particle level will give more solid circulation rate than the lower one. There are solid distributing tubes at the bottom of the storage tank. The uniformity of solids distributed from each tubes is also important. Uneven solid flux through each ejecting tubes into solid distributor can create a non-uniform solid concentration in the downer column, hence decreases the uniformity of solid resident time as well as the downer performance.

1.1.2 Bottom storage tank

A bottom storage tank is a bottom part of the bottom separator tank. Particles from a downer move toward a bottom wall of the bend and flow into a bottom storage tank. It is used to collect particles that flow out of a downer column and supply the particles accumulating there through the riser back to the storage tank. The amount of particles enters the riser is controlled by the width of connection area connected to the riser as shown in Figure 23.

As mentioned before that the particle level in the top storage tank is important to control the particle flux into the downer column, the width of the connection edge to the riser is then adjusted to equate the amount of particles supplied back to the top storage tank with the particles flow out of the top storage tank to the downer column. The amount of time needed for the particle level in the top storage tank to reach its steady state is then the time particles travel from the bottom storage tank to the top storage tank. Since there is no reaction occurred in the riser, the temporary deviation of particle flux around its designed value has no important. Hence, unlike particles in the top storage tank, particles in bottom storage tank are not fluidized.

Some of product gas that enters the bottom storage tank along with particles is separated out through the vent of the bottom storage tank. Particles in bottom storage tank help preventing circulating air in the riser flowing into the storage tank. Its level is designed to provide enough pressure head to overcome the pressure in an early section of the riser where they were connected by a small channel.

1.2 Particle distributor

Particle distributor is where particles first contact with the main fluidizing gas. There are 12 particle distributing tubes connected between the particle storage tank and the particle distributor. Particles in the top storage tank have to pass through these particle distributing tubes to enter the particle distributor.

On the top of particle distributor, there are 13 main fluidizing gas distributor inlets between particle distributing tubes. The area of the main fluidizing gas inlets is the opening area at the top of distributor that is not connected to the particle distributing tubes. The main fluidizing gas superficial velocity (U_{sg}) will be the value mention in this work instead of the gas velocity setting at the main fluidizing gas inlet boundary. This calculation is done by multiplying the designed superficial gas velocity with the ratio of the downer cross-section area to the main fluidizing gas inlet area.

The reason that many feeding tubes are evenly distributed between the main fluidizing gas inlets is to disperse particles across the downer column before they enter the downer column. The height of distributor tank allows particles to disperse and mix with the gas. After mixing with each other in the distributor, gas and particles then enter the downer column together as mixing fluids. The uniformity of particle dispersion is important to the performance of the circulating fluidized bed downer as mentioned before.

1.3 Downer column

A downer column is the main part of the system where reactions take place. This downer is 9.3 metres long and 0.1 metres in diameter. Particles and gas should be distributed uniformly as much as possible before entering a downer column to give the best downer performance. However, the non-uniform distribution of both gas and particle phases when they first enter the downer column, which is called the distributor effect, occurs at the top of the downer. This effect might wear out at the very beginning of the downer or last until the end of the column.

1.4 Riser column

A 0.05 m. diameter riser is used to circulate the used particles back to the storage tank. Riser length is comparable to downer length. The amount of time that particles stay in a riser allows particles to cool down or heat up depends on the types of reaction, which are exothermic or endothermic respectively.

1.5 Gas-solid separators

Gas-solid separators use the method of centrifugal force. Most of product gas leaves the domain at the outlet below the downer. Solids, which are heavier, are swing to the wall at the turning point and pass through the small extra chamber, which is right under the product gas outlet, to the separator tank. The separator tank also allows the leftover gas to leave the domain at its vent.

The separators are used two places in the system. The bottom separator connected at the bottom of the downer is used to separate product gas from particles. Particles then flow into the riser and lifted up by circulating air. The recycled particles are then separated again after leaving the riser at the top separator, which then sends these particles back to the top storage tank.

The top separator tank is connected with the riser by two bends. However, there is only one bend between the downer and the bottom separator tank. The bottom part of the bottom separator tank is used as the bottom particle storage tank as described early in the storage tank section. Like the top separator tank, the bottom separator tank uses its vent for the remaining product gas to be separated from stream of particles.

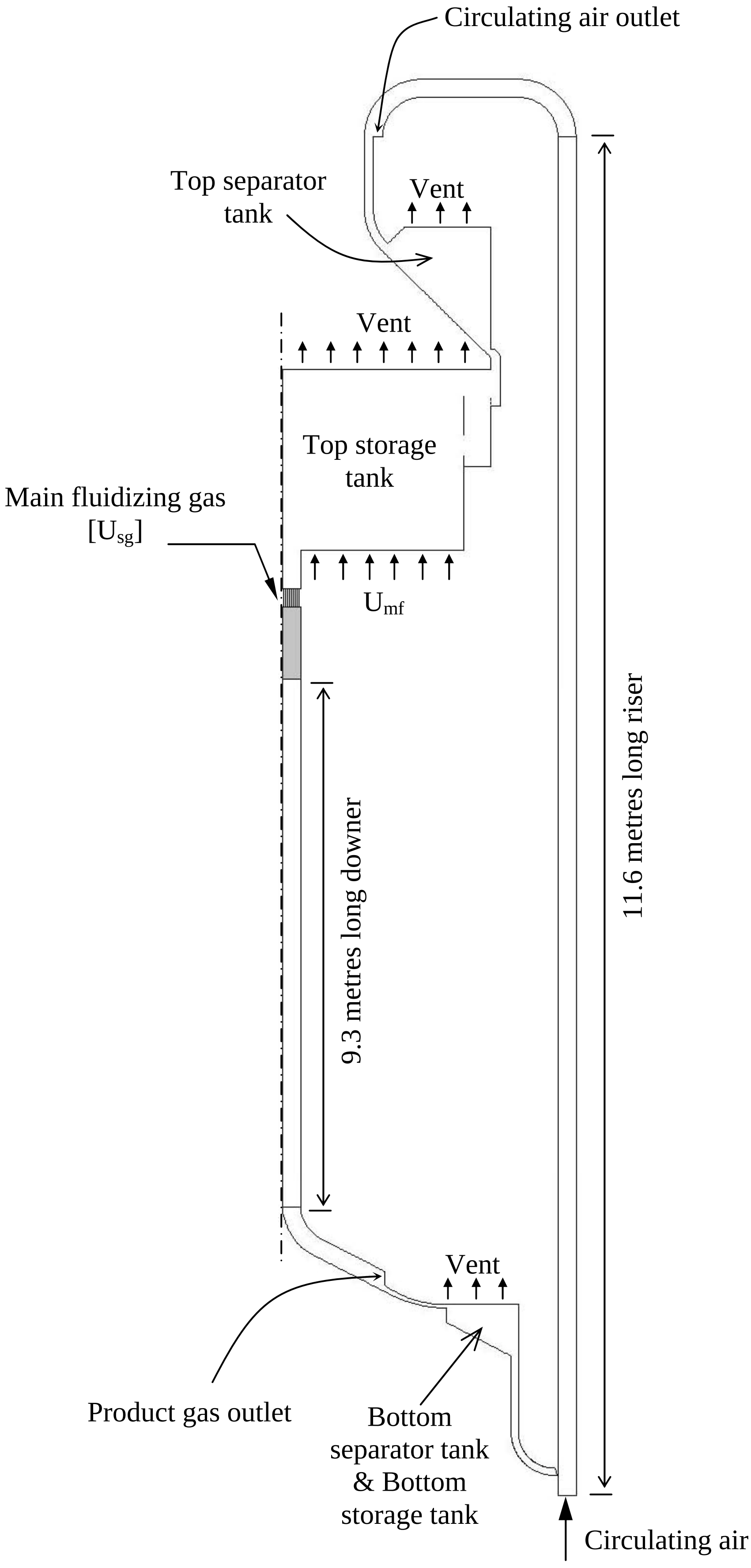

Figure 19 Model geometry

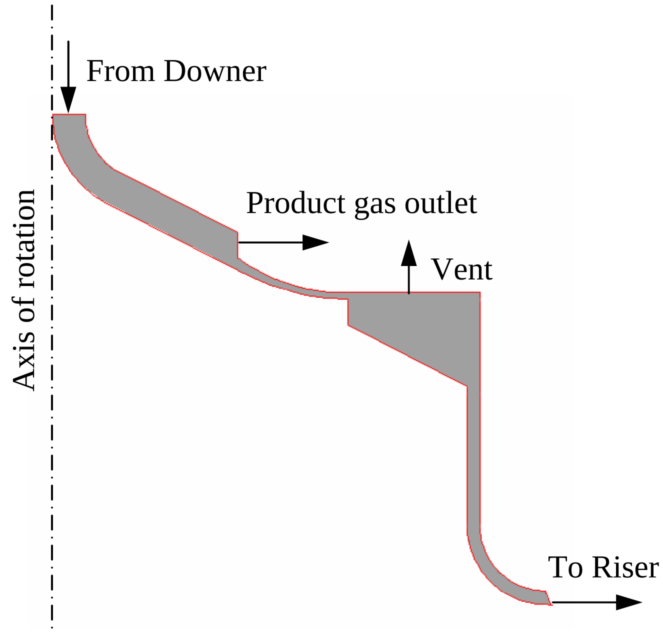

(a)

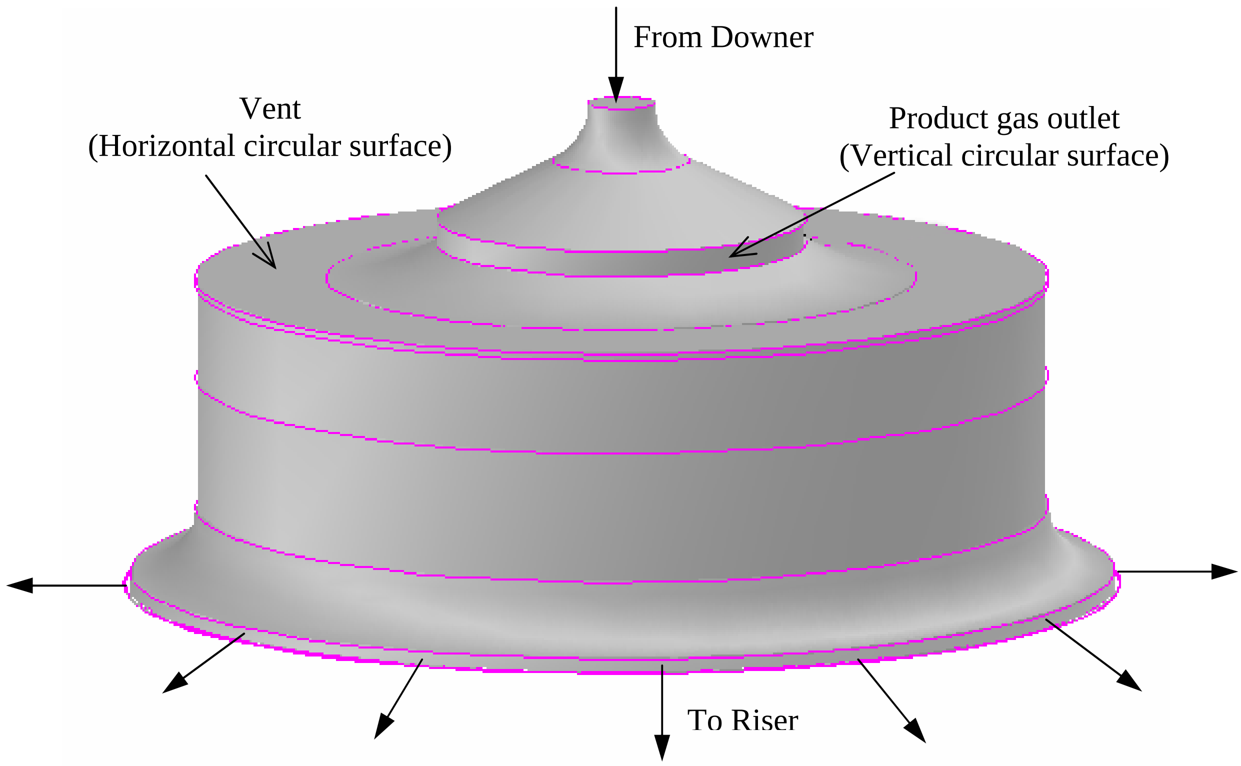

(b)

Figure 20 3-D implementation of 2-D inlets and outlets; (a) 2-D model, (b) the geometry that the 2-D model with axisymmetric assumption represent

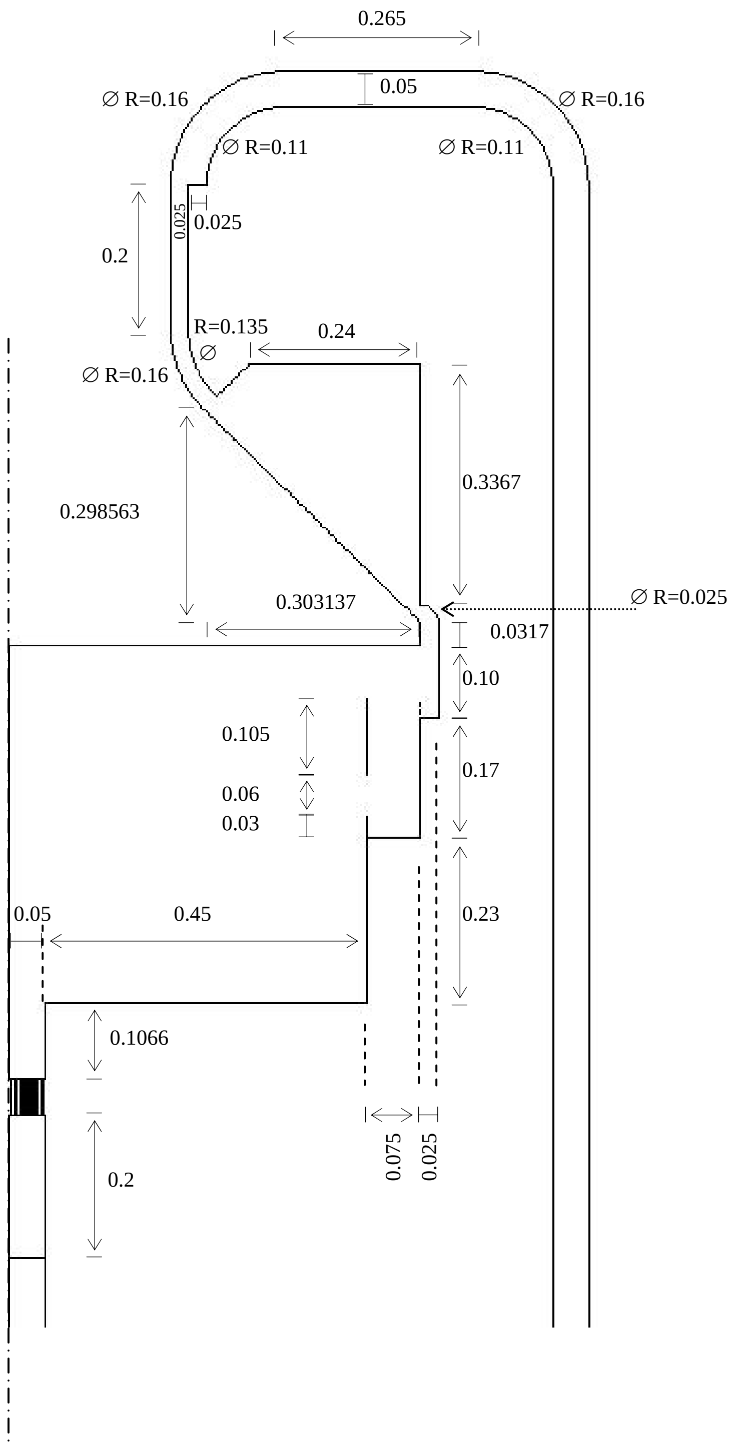

Figure 21 Top section geometry (length unit is meter)

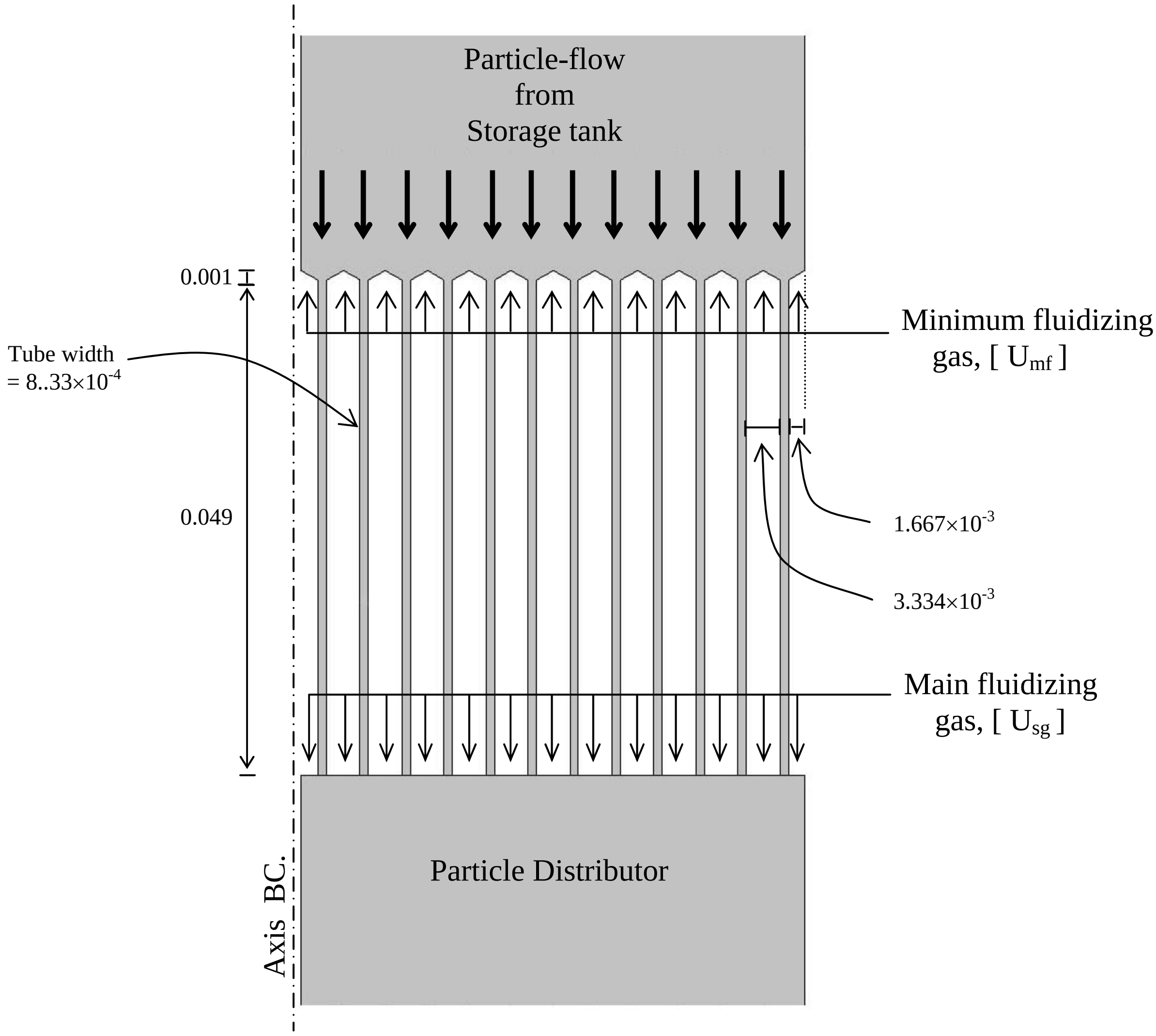

No. of tubes	12
Tube width (m)	8.33×10^{-4}
Distance between tubes (m)	3.334×10^{-3}
Distance between axis and leftmost tube (m)	1.667×10^{-3}
Distance between rightmost tube and right edge (m)	1.667×10^{-3}
No. of main fluidizing gas inlets	13
No. of minimum fluidizing gas inlets (incline lines)	24

Figure 22 Particle distributing tubes geometry (length unit is meter)

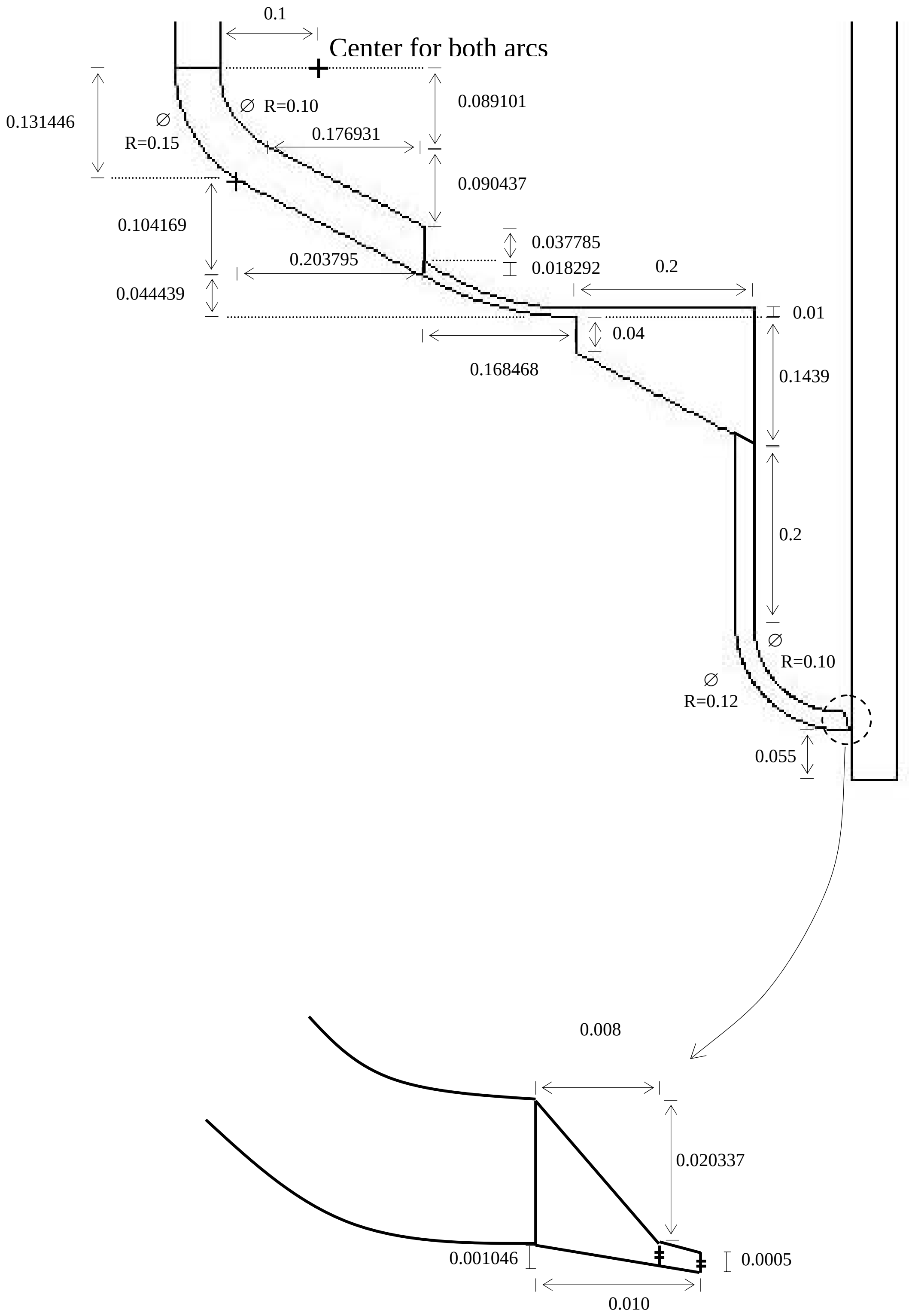

Figure 23 Bottom section geometry (length unit is meter)

2. Boundary Conditions

All walls in the domain are non-slip for both gas and solid phases except for particle distributing tubes and the particle distributor walls that are free slip walls (no friction). The free slip walls at distributing tubes are set to maintain a steady particle flux. In addition, the free slip setting at the distributor wall is to let particles distribute uniformly in the distributor without the effect of wall friction. If the non-slip condition is used at the distributor wall, there will be an accumulation of particles near the wall because of the parabolic gas velocity profile. On the contrary, if the boundary condition is free slip wall (no friction loss), particles will distribute uniformly. This free slip boundary condition setting may not be true in the real downer reactor and is set to provide uniform radial solid holdup profile to the downer. To model the free slip wall in a real downer reactor, the downer reactor must be redesigned. The downer distributor diameter may be set bigger than the downer diameter and the particle distributing tubes must be positioned in the core zone. Hence, the contacting area between the flows in the core and the stagnant region in the annulus of the distributor will act like a free surface that is used in this work.

All outlets are atmospheric pressure outlets. There are three velocity inlets; the storage tank fluidizing gas (U_{mf}), the main fluidized gas (U_{sg}) at the top of downer, and the circulating air (U_{air}) at the bottom of a riser.

Storage tank fluidized gas, U_{mf} = 0.05 m/s

Main fluidizing gas superficial velocity, U_{sg} =10 m/s

Circulating air, U_{air} = 10 m/s

At the centerline of the downer, the axis boundary condition is applied. The model is assumed to be axisymmetric around the axis. This axis boundary condition will assume our downer to be a cylinder with 0.1 m. in diameter, which is better than the symmetry boundary condition that cannot clearly represents a cylinder-shape downer. For multiphase system, the axis boundary condition that uses cylinder coordinate will correct solid dispersion in a radial direction since the radial diffusion area gets bigger with further radial position. All boundary conditions and their values are listed in table 1.

Table 1 Boundary conditions of the downer reactor model

Boundary	Boundary type	Value
Centerline		
Centerline	Axis	$\frac{\partial \vec{v}_p}{\partial r} = 0$, $\frac{\partial \vec{v}_g}{\partial r} = 0$, $\frac{\partial P}{\partial r} = 0$
Inlets		
Storage tank fluidized gas, (U_{mf})	Velocity inlet	
r-component velocity		0 m/s
y-component velocity		0.05 m/s
Turbulence		No turbulence
Main fluidized gas, (U_{gas})	Velocity inlet	
Velocity magnitude		10 m/s
Turbulence intensity		5.92 %
Turbulence length scale		0.000233 m
Circulating air, (U_{air})	Velocity inlet	
Velocity magnitude		10 m/s
Turbulence intensity		3.98 %
Turbulence length scale		0.007 m
Outlets and Vents		
Product gas outlet	Outlet vent	1 atm
Circulating air outlet	Outlet vent	1 atm
Top separator tank vent	Outlet vent	1 atm
Bottom separator tank vent	Outlet vent	1 atm
Top storage tank vent	Outlet vent	1 atm
Walls		
Distributor wall	Free slip wall	$\frac{\partial \vec{\mathrm{v}}_\mathrm{p}}{\partial \vec{\mathrm{n}}} = 0$, $\frac{\partial \vec{\mathrm{v}}_\mathrm{g}}{\partial \vec{\mathrm{n}}} = 0$
Other walls	Non-slip wall	$\vec{\mathrm{v}}_\mathrm{p} = 0, \vec{\mathrm{v}}_\mathrm{g} = 0$

3. Initial Conditions

Initially, the velocities of both gas and solids everywhere else in the domain except a downer column are zero. In a downer column, gas velocity is set at 10 m/s in a negative y-axis direction to initiate the downflow of particles from storage tank. Without undergoing this method, the main fluidized gas sometimes turns upward and flow into an upper storage tank. The reason of this phenomenon is that the high pressure-drop in a downer column creates a high pressure at the top of a downer column. Fluidizing gas is then turned upward by the pressure difference. But once particles start to flow down the tube, their momentum creates a larger force than the pressure difference. There is no solid present in the column initially. The granular temperature (particle fluctuating energy, $\Theta_s \left(\Theta_s = 1/3 < u'^2 >\right)$; where u' is the mean square of particle random velocity) in the downer is initially 10^{-4} m^2/s^2 which is the same as the inlet granular temperature.

Solid volume fraction of top storage tank is initially set at 0.3 to maintain minimum fluidized bed solid volume fraction (ε_{mf}). Solid volume fraction of bottom storage tank is initially set at 0.6 as maximum packing limit of the catalyst. Initial conditions of all variables divided for each part of the domain are shown in Table 2.

Table 2 Initial conditions of the downer reactor model

Domain	**Variable**	**Value**
Everywhere	Pressure	1 atm
	Gas phase	
Everywhere except	y-component of $\vec{u}_g$	0 m/s
Downer column		-10 m/s
Everywhere	r-component of $\vec{u}_g$	0 m/s
Everywhere	Turbulence kinetic energy (K_g)	1 m^2/s^2
Everywhere	Turbulence dissipation rate (E_g)	1 m^2/s^3
	Particle phase	
Everywhere except	Particle volume fraction	0
Upper storage tank		0.3
Downer storage tank		0.6
Everywhere	y-component of $\vec{u}_s$	0 m/s
Everywhere	r-component of $\vec{u}_s$	0 m/s
Everywhere	Turbulence kinetic energy (K_s)	1 m^2/s^2
Everywhere	Turbulence dissipation rate (E_s)	1 m^2/s^3
Everywhere	Granular temperature (Θ_s)	0.0001 m^2/s^2

4. Model parameters

An axisymmetric assumption is applied to the model as described in previous section. The downer reactor model uses eulerian-eulerian multiphase model, which is described in the literature review section, with k-ε turbulence models on both gas and particle phases.

The application of k-ε turbulence model on particle phase is analogous to the k-ε turbulence model of gas phase. Many researchers have applied the use of turbulence models on the solid phase and get satisfied results. Cheng *et al*. (1999) combined the kinetic theory with the k_p equation, developed by Zhou (1994), and successfully simulated the hydrodynamics in downer reactors. Zheng *et al*. (2001) also applied the k-ε turbulence model on particle phase for the simulation of a riser reactor. The simulation results show satisfactory agreement with experimental data. These works show that the particulate turbulence bears essential influence on hydrodynamics in fluidized bed reactors. In Table 3. below, the turbulence parameters used in the equation of granular temperature are shown. These values are typical values used for turbulent model and also shown in Mathematical model section.

Table 3 Turbulence parameters

Turbulence parameters	Value
C_μ	0.09
$C_{1\varepsilon}$	1.44
$C_{2\varepsilon}$	1.92
$C_{3\varepsilon}$	1.3

5. Particles and gas properties

Particles used in this simulation are modeled from FCC particles. FCC particles are catalyst for the Fluid Catalytic Cracking reaction. The size of the particles is very small to maximize the surface area of catalyst. The particle properties are described in Table 4.

The coefficient of restitution is the value that quantifies the elasticity of collisions. Its value is ranged from 0, for fully inelastic collisions, to 1, for fully elastic collisions. It was utilized by Jenkins and Savage (1983) to account for the loss of energy in particle collisions. In this model, the particle-particle collision (inter-particle collision) restitution coefficient is 0.9 .

Since this work only simulates hydrodynamics in a downer reactor, there is no need to use several fluids for each gas inlets. The only fluid used is air. The properties of air are shown in Table 4.

Table 4 Particle and air properties

Particle properties	Value
Diameter (μm)	67
Density (kg/m^3)	1500
Particle-particle restitution coefficient (e_{ss})	0.9
Air properties	**Value**
Density (kg/m^3)	1.225
Viscosity (kg/m.s)	1.789×10^{-5}

6. Operating conditions

There is a 9.81 m/s^2 gravity force applied to this simulation in a negative-y direction. This gravity force has a large influence on the hydrodynamics in the downer reactor because the FCC particles used in this simulation are dense. The gravity force cannot be neglected in the simulation of fluidized bed reactor.

Table 5 Operating conditions

Operating conditions	Value
Time interval	10^{-3} s
Circulation rate	100 kg/m^{2}s
Gas Inlet velocity	
Minimum fluidizing gas (U_{mf}) velocity	0.05 m/s
Main fluidizing gas (U_{sg}) velocity	10 m/s
Circulating air (U_{air}) velocity	10 m/s
Downer	
Downer radius	0.05 m
Downer length	9.3 m
Distributor	
Distributor radius	0.05 m
Distributor length	0.2 m
Riser	
Riser width	0.05 m
Riser length	11.6 m

7. Numerical methods

The unsteady state time dependent analysis is used. The time interval used is 0.001 second. Each time interval allows 60 iterations as maximum number of iterations to converge. The convergence occurs when every variable-residuals reach 10^{-6}. The calculation of each time step will be stopped if the solution converges or the maximum number of iterations is reached, depending on either of which occurs first. Once the calculation of that time step is stopped, the calculation of next time step begins.

The finite volume method is used to solve the transport equation together with the first order upwind differencing scheme. The pressure variable is solved by SIMPLE method (Semi-Implicit Method for Pressure-Linked Equations) developed by Patankar (1980).

Because of the non-linearity of the equation being solved, it is necessary to control the change in value of each variable. This is achieved by reducing the change in variable value produced during an iteration. This method is called under-relaxation. Under-relaxation method uses the under-relaxation factors to reduce the change in value for each flow variables by the following formula. The values of under-relaxation factors are also shown in Table 6.

$$\phi = \phi_{old} + \alpha\Delta\phi$$

where ϕ is the value of variable
ϕ_{old} is the value before the calculation of this time step
$\Delta\phi$ is the change in value after the calculation of this time step
α is the under-relaxation factor

Table 6 Under-Relaxation factors for simulation variables

Under-Relaxation factors	Value
Pressure	0.3
Density	1
Body Forces	1
Momentum	0.3
Volume fraction	0.3
Granular temperature	0.2
Turbulence kinetic energy	0.8
Turbulence dissipation rate	0.8
Turbulence viscosity	1

Mathematical Model

1. Governing Equations

The continuity equations:

$$\frac{\partial}{\partial t}(\rho_i \varepsilon_i) + \nabla \cdot (\rho_i \varepsilon_i \vec{u}_i) = 0$$

with the constraint $\sum \varepsilon_i = 1$

where ρ_i is density of phase i; ε_i is volume fraction of phase i; u_i is velocity vector of phase i.

The conservation of momentum of phase i (i= gas, solid; k $\neq$ i)

$$\frac{\partial}{\partial t}(\rho_i \varepsilon_i \vec{u}_i) + \nabla \cdot (\rho_i \varepsilon_i \vec{u}_i \vec{u}_i) = -\varepsilon_i \nabla \cdot \tau_i - \beta(\vec{u}_i - \vec{u}_k) + \rho_i \varepsilon_i g$$

where τ_i is stress tensor of phase i; β is interphase drag coefficient and can be generally expressed by this equation

$$\beta = \frac{\varepsilon_s \rho_s f}{t_s}$$

where t_s is particulate relaxation time: $t_s = \dfrac{\rho_s d_s^2}{18\mu_f}$

where d_s is the diameter of particles; f is a function that is defined differently by different researchers.

All definitions of f include a drag function (C_D) that is based on the relative Reynolds number (Re_s). It is this drag function that differs among the exchange-coefficient models.

For dilute solid phase flow with solid fraction lower than 0.2, the correlation of developed by Wen and Yu (1966) is used. If the solid fraction is higher than 0.2, the correlation developed by Ergun (1952) is used instead. The equations below are written for convenience and are in the form that excludes the function '*f*' and the particulate relaxation time (t_s).

For $\varepsilon_s \leq 0.2$; $\beta = \dfrac{3}{4} C_D \dfrac{\varepsilon_s \varepsilon_f \rho_f}{d_s} \left|\vec{u}_s - \vec{u}_f\right| \varepsilon_f^{-2.65}$

where the drag function defined as: $C_D = \dfrac{24}{\varepsilon_f \operatorname{Re}_s}\left[1 + 0.15(\varepsilon_f \operatorname{Re}_s)^{0.687}\right]$

and the relative Reynolds number: $\mathrm{Re}_s = \dfrac{\rho_f d_s \left|\vec{u}_s - \vec{u}_f\right|}{\mu_f}$

For $\varepsilon_s > 0.2$; $\beta = 150\dfrac{\varepsilon_s(1-\varepsilon_f)\mu_f}{\varepsilon_f d_s^2} + 1.75\dfrac{\rho_f \varepsilon_s \left|\vec{u}_s - \vec{u}_f\right|}{d_s}$

The equation for the fluctuating energy of solid called granular temperature, $\Theta_s\left(\Theta_s = 1/3 < u'^2 >\right)$; where u' is particle random velocity, may be written as:

$$\frac{3}{2}\frac{\partial}{\partial t}\left(\rho_s \varepsilon_s \Theta_s\right) = \tau_s : \nabla\vec{u}_s - \gamma_s - 3\beta\Theta_s$$

where γ_s is collisional dissipation of granular temperature described by Lun *et al* (1984). The last term was derived by Gidaspow (1992) and represents the transfer of the kinetic energy of random fluctuations in particle velocity from solid phase to gas phase.

2. Constitutive equations

The solid phase stress and pressure of the granular temperature are defined as follows.

(a) Solid phase stress:

$$\tau_s = \left(-P_s + \varepsilon_s \mu_b \nabla u_s\right)I + 2\varepsilon_s \mu_s S_s$$

where S_s is deformation rate; P_s is solid phase pressure; μ_b is solid bulk viscosity; μ_s is solid phase shear viscosity.

The deformation rate (S_s) can be written as:

$$S_s = \frac{1}{2}\left[\nabla\vec{u}_s + \left(\nabla\vec{u}_s\right)^T\right] - \frac{1}{3}\left(\nabla\vec{u}_S I\right)$$

The solid phase shear viscosity (μ_s) derived by Gidaspow (1992) can be defined by:

$$\mu_s = \frac{2\mu_{s,dil}}{(1+e)g_0}\left[1 + \frac{4}{5}g_0\varepsilon_s(1+e)\right]^2 + \frac{4}{5}\varepsilon_s \rho_s d_s (1+e) g_0 \left(\frac{\Theta_s}{\pi}\right)^{1/2}$$

where d_p is particle diameter; e is particle–particle restitution coefficient.

The solid phase dilute viscosity ($\mu_{s,dil}$) is defined as:

$$\mu_{s,dil} = \frac{5\rho_s d_p \sqrt{\Theta_s \pi}}{96}$$

The solid bulk viscosity derived by Lun *et al*. (1984) is defined as:

$$\mu_b = \frac{4}{3}\varepsilon_s \rho_s d_p g_0 (1+e)\left(\frac{\Theta_s}{\pi}\right)^{1/2}$$

(b) Solid pressure:

Solid pressure is derived by Lun *et al*. (1984) and composed of a kinetic term and a second term due to particle collisions:

$$P_s = \varepsilon_s \rho_s \Theta_s + 2\rho_s (1+\varepsilon)\varepsilon_s^2 g_0 \Theta_s$$

The radial distribution function (g_0) is a correction factor that modifies the collisional probability for dense particles flow derived by Ogawa *et al*. (1980) and is defined as:

$$g_0 = \frac{3}{5}\left[1-\left(\frac{\varepsilon_s}{\varepsilon_{s,\max,}}\right)^{1/3}\right]^{-1}$$

3. The k-ε Turbulence Model for Each Phase

In this work, the k-ε turbulence model is used for both particles and gas phase. The k-ε turbulence model was first developed for the homogeneous flow system. However, the k-ε turbulence model for the particle phase is also used here in analogous to that of the gas phase to model the big scale fluctuation of the particle phase. The use of k-ε turbulence model on the particle phase is coupled with the two-fluid model that considers the particle phase as one fluid phase. Thus this is different from the model of fluctuating energy called granular temperature (Θ). The use of k-ε turbulence model on the particle phase might helps obtaining accurate results from the simulation of the particulate flow system.

Turbulence kinetic energy of phase i (i = gas, solid; k$\neq$ i):

$$\frac{\partial}{\partial t}(\varepsilon_i \rho_i k_i) + \nabla.(\varepsilon_i \rho_i \vec{u}_i K_i) = \nabla.(\alpha_i \frac{\mu_{t,i}}{\sigma_k}\nabla K_i) + (\varepsilon_i G_i - \varepsilon_i \rho_i E_i) + \beta(C_{ki}K_k - C_{ik}K_i)$$

$$-\beta(\vec{u}_k - \vec{u}_i).\frac{\mu_{t,k}}{\varepsilon_k \sigma_k}\nabla \varepsilon_k + \beta(\vec{u}_k - \vec{u}_i).\frac{\mu_{t,i}}{\varepsilon_i \sigma_i}\nabla \varepsilon_i$$

Turbulence dissipation rate of phase i (i = gas, solid; k$\neq$ i):

$$\frac{\partial}{\partial t}(\varepsilon_i \rho_i E_i) + \nabla.(\varepsilon_i \rho_i \vec{u}_i E_i) = \nabla.(\varepsilon_i \frac{\mu_{t,i}}{\sigma_\varepsilon} \nabla E_i) + \frac{E_i}{k_i}\{C_{1\varepsilon}\varepsilon_i G_i - C_{2\varepsilon}\varepsilon_i \rho_i E_i +$$

$$C_{3\varepsilon}[\beta(C_{ki}K_k - C_{ik}K_i) - \beta(\vec{u}_k - \vec{u}_i).\frac{\mu_{t,k}}{\varepsilon_k \sigma_k}\nabla\varepsilon_k + \beta(\vec{u}_k - \vec{u}_i).\frac{\mu_{t,i}}{\varepsilon_i \sigma_i}\nabla\varepsilon_i]\}$$

where K_i is turbulence kinetic energy of phase i; E_i is turbulence dissipation rate of phase i; $\mu_{t,i}$ is turbulence viscosity of phase i; G_i is the production of turbulence kinetic energy.

The turbulent viscosity ($\mu_{t,i}$) is computed from

$$\mu_{t,i} = \rho_i C_\mu \frac{K_i^2}{E_i}$$

and the production of turbulence kinetic energy (G_i) is computed from

$$G_i = \mu_{t.i}\left(\nabla\vec{u}_i + (\nabla\vec{u}_i)^T\right) : \nabla\vec{u}_i$$

$$C_{ki} = 2 \text{ and } C_{ik} = 2 * \left(\frac{\eta_{ki}}{1+\eta_{ki}}\right)$$

where η_{ki} is the ratio between the two characteristic times and is written as

$$\eta_{ki} = \frac{t_{t,ki}}{t_{F,ki}}$$

where $t_{F,ki}$ is the characteristic particle relaxation time connected with inertial effects acting on a dispersed phase; $t_{t,ki}$ is the Lagrangian integral time scale calculated along particle trajectories.

The characteristic particle relaxation time connected with inertial effects acting on a dispersed phase is defined as

$$t_{F,ki} = \frac{\varepsilon_k \rho_i}{\beta}\left(\frac{\rho_k}{\rho_i} + C_V\right)$$

where the added-mass coefficient, C_V = 0.5 .

The Lagrangian integral time scale calculated along particle trajectories, mainly affected by the crossing-trajectory effect (Csanady, 1963) is defined as

$$t_{t,ki} = \frac{t_{t,i}}{\sqrt{1 + C_\beta \xi^2}}$$

where $t_{t,i}$ is a characteristic time of the energetic turbulent eddies defined as

$$t_{t,i} = \frac{3}{2} C_\mu \frac{K_i}{E_i}$$

$$\xi = \frac{|\vec{u}_k - \vec{u}_i| t_{t,i}}{L_{t,i}}$$

and

$$C_\beta = 1.8 - 1.35 \cos^2 \theta$$

The length scale of the turbulent eddies ($L_{t,i}$) is defined as

$$L_{t,i} = \sqrt{\frac{3}{2}} C_\mu \frac{K_i^{3/2}}{E_i}$$

and θ is the angle between the mean particle velocity and the mean relative velocity.

$C_{1\varepsilon}$, $C_{2\varepsilon}$, $C_{3\varepsilon}$, C_μ are constants where $C_{1\varepsilon}$ = 0.09, $C_{2\varepsilon}$ = 1.44, $C_{3\varepsilon}$ = 1.92, C_μ = 1.3 .

RESULTS AND DISCUSSIONS

The model of a full-loop downer reactor is developed in this research. This downer reactor consists of a downer column, particle storage tanks, gas-solid separators, and a riser column. All these components are designed together to be able to operate simultaneously. Hydrodynamics results from the simulation of the downer reactor after reaching steady state will be discussed.

The hydrodynamics behavior in a downer column is the main interest in this research because it is where reactions take place. The axial and radial profiles of solid holdup and velocity are studied. Solid fraction and velocities of both phases are illustrated throughout the column by graphs, solid volume fraction contours, and velocity vector plots. In addition, the effect of solid circulating rate (G_s) on hydrodynamics behavior in a downer column is observed. The hydrodynamics in a downer column obtained by numerical simulations will be compared to the experimental results.

The separation of gas and solids is also important in a circulating fluidized bed reactor because the catalyst particles need to be recovered from the gas streams. The fluid catalytic cracking (FCC) catalysts are small and expensive. The cost of FCC catalysts increases the need to recover them as much as possible. However, their small sizes make them difficult to be separated from gas. Hence, the gas-solid separators need to be designed in the way that can achieve high recovery yield of small particles. The solid volume fraction contours and velocity vector plots are used to demonstrate the separating efficiency of solid particles from the gas stream in the gas-solid separators.

Designs of Model Components

Geometry design is important to the performance of the downer reactor. Improper designs of the downer components can lead to undesired hydrodynamic behaviors such as non-uniform radial solid distribution in the downer column and loss of expensive particles. Many components of the downer reactor model do not work properly as expected during this work and need to be re-designed. Some of these components such as the solid distributing tubes and the gas-solid separators are important to the performances and operating cost of the downer reactor. In this section, the designing of the particle distributing tubes and gas-solid separator are discussed. The old designs of these components and their troubles are also shown here as the case studies.

1. Solid Distributing Tubes

The solid distributing tubes connect the top storage tank to the distributor, which is above the downer column. The design of the distributing tubes affects how well solids are distributed, which is very important to the downer reactor performance. A large number of small tubes can give the same solid flux but better solid distribution than a few number of big tubes. The ability of solids to distribute in the radial direction uniformly is needed and is used to determine the number of the solid distributing tubes. If solids distribute uniformly, only a few distributing tubes are needed.

In this section, two models with different solid distributing tubes are compared. These two cases have 4 and 12 distributing tubes but have the same total tube area (0.01 m). The case with 4 tubes has bigger tubes with 0.0025 m in diameter while the case with 12 tubes has 0.000833 m in diameter tubes. The shapes of these two cases are shown in Figure 24.

These two cases have the same solid flow rate through the solid distributing tubes at 1 kg/s. Figure 25 shows the axial solid holdup profiles of both cases. The solid holdups at the top of both cases are closed to each other. The difference in solid holdup is only 2×10^{-4}, which is about 2.5 % of the average solid holdup. The axial solid velocity profiles of both cases are similar to each other as shown in Figure 26.

Figure 27 and Figure 28 show the radial solid holdup profiles at 0.02 and 6.227 m. At 0.02 m from the downer entrance, the radial solid holdup profile of the 4-tubes case is not as smooth as that of the 12-tubes cases. The solid holdup peaks are at the same radial position of the distributing tubes. This non-uniform radial profiles can still be seen at 6.227 m but with smaller amplitudes.

Figure 29 and Figure 30 show the radial solid velocity profiles at 0.02 and 6.227 m. At 0.02 m from the downer entrance, the radial solid velocity profile of the 4-tubes case is lower than that of the 12-tubes case. This might occur from the lower effective drag force because solids are not exposed themselves to the gas phase uniformly. However, in this simulation, the gas-drag is large because of very small size of particles. The solid velocity of the 4-tubes case catches up with that of the 12-tubes case and the solid velocity profiles at 6.227 m are similar. At the entrance the solid velocity profile of 12-tubes case is also more uniform than the 4-tubes case. However, the solid velocity profiles are similarly uniform after fully develop no matter of the number of solid distributing tubes.

By comparing these two models with different solid distributing tubes, the model with 4 solid distributing tubes does not have the uniform radial solid distribution. Since uniform solid distribution is important to the performance of the downer, the downer with 4 distributing tubes will give lower selectivity than that with 12 distributing tubes. For the FCC reactions, the downer with non-uniform radial distribution such as this 4 distributing tubes model will produce the under-cracking or over-cracking products. Therefore, a model with 12 particle distributing tubes is used in this work

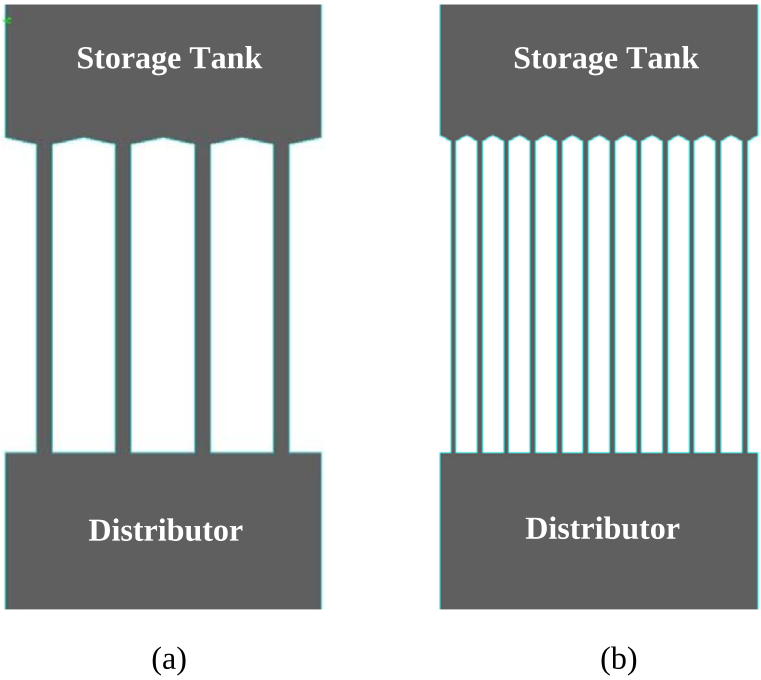

Figure 24 The solid distributing tubes; (a) 4-tubes system, (b) 12-tubes system

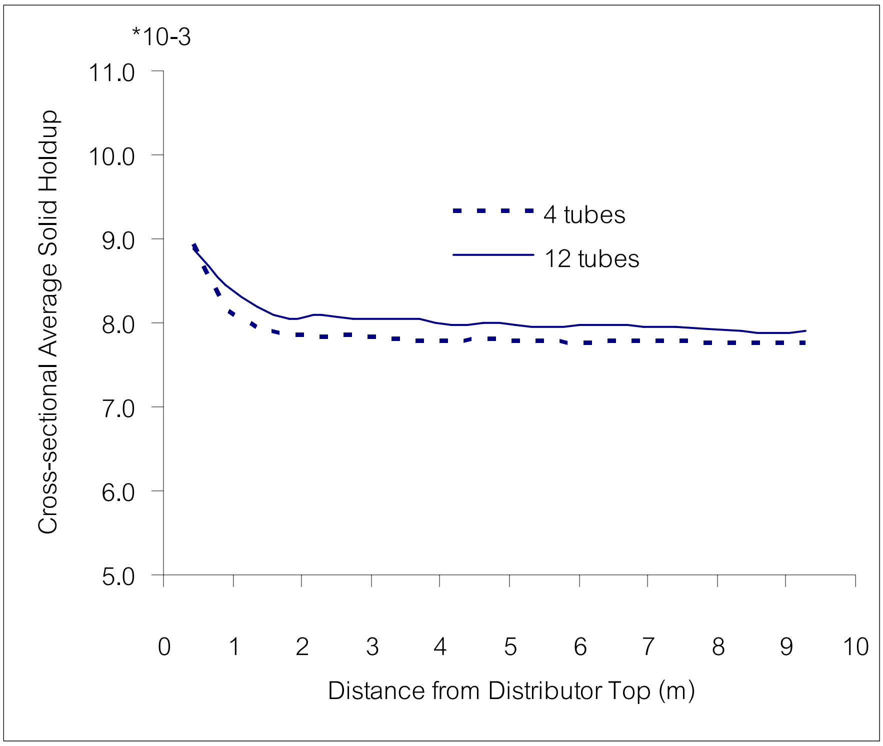

Figure 25 Axial solid holdup profiles at superficial gas velocity (U_{sg}) of 10 m/s and solid circulation rate of 130 kg/m^{2}s

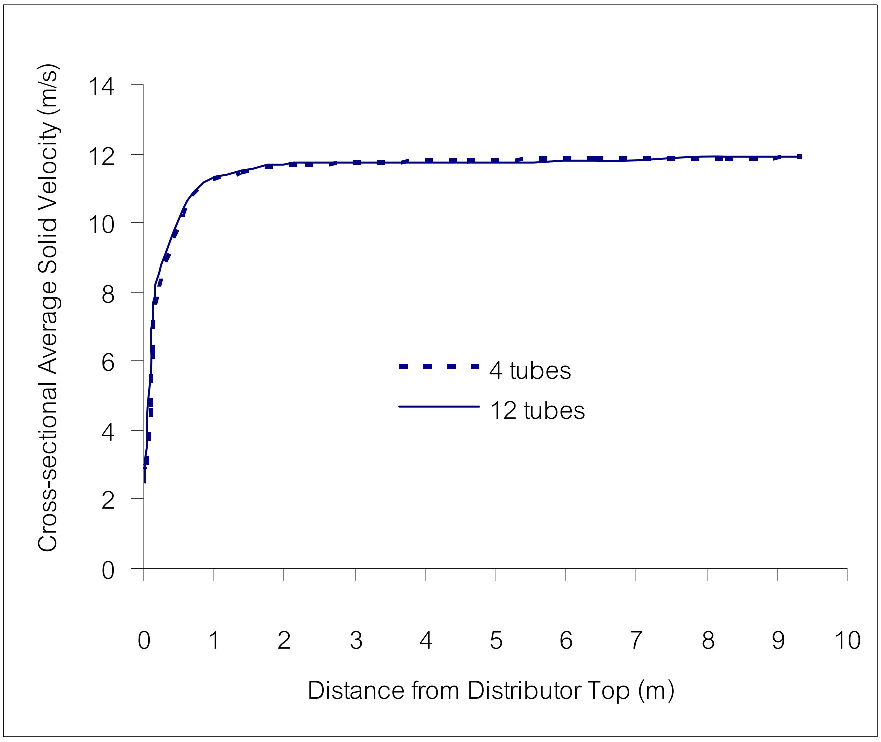

Figure 26 Axial solid velocity profiles at superficial gas velocity (U_{sg}) of 10 m/s and solid circulation rate of 130 kg/m^{2}s

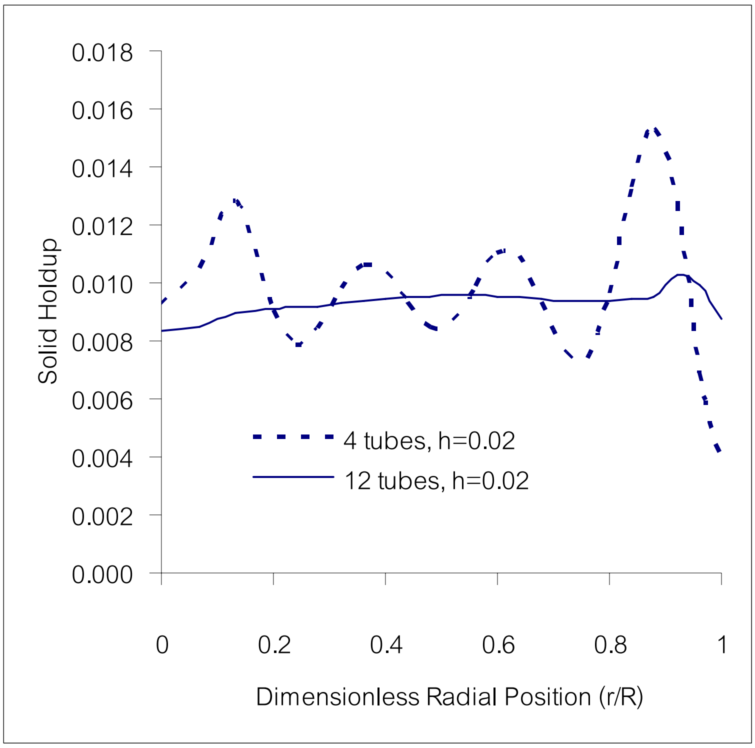

Figure 27 Radial solid holdup profiles at 0.02 m from downer entrance at superficial gas velocity (U_{sg}) of 10 m/s and solid circulation rate of 130 kg/m^{2}s

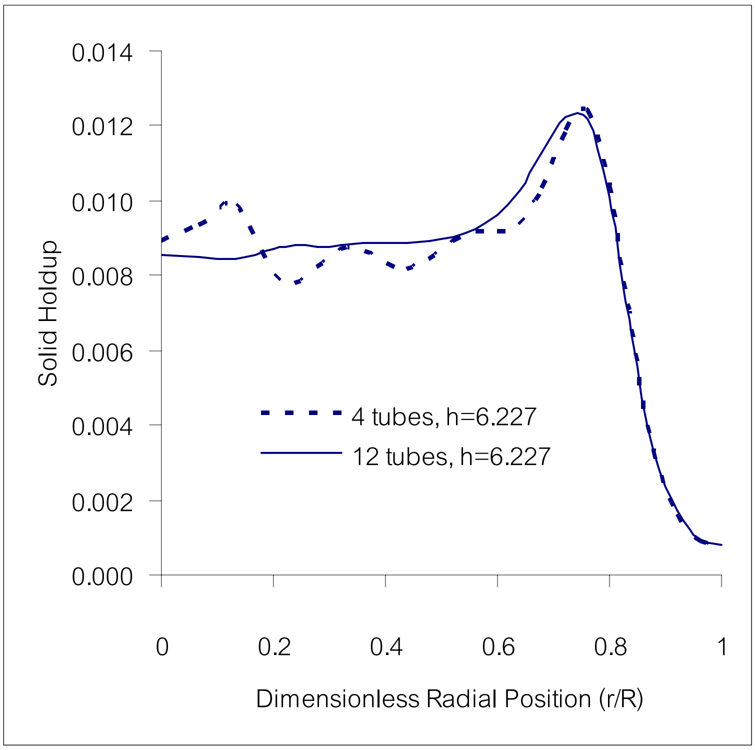

Figure 28 Radial solid holdup profiles at 6.227 m from downer entrance at superficial gas velocity (U_{sg}) of 10 m/s and solid circulation rate of 130 kg/m^{2}s

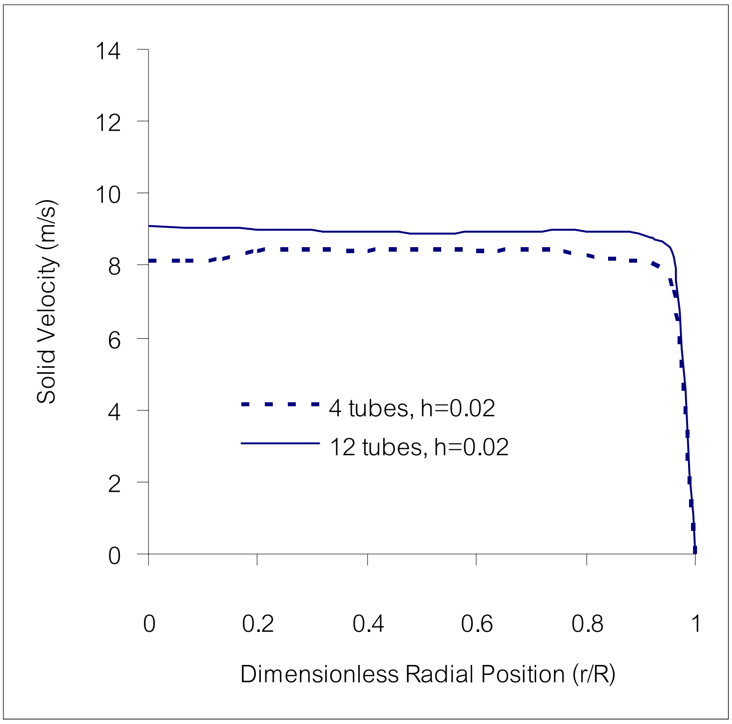

Figure 29 Radial solid velocity profiles at 0.02 m from downer entrance at superficial gas velocity (U_{sg}) of 10 m/s and solid circulation rate of 130 kg/m^2s

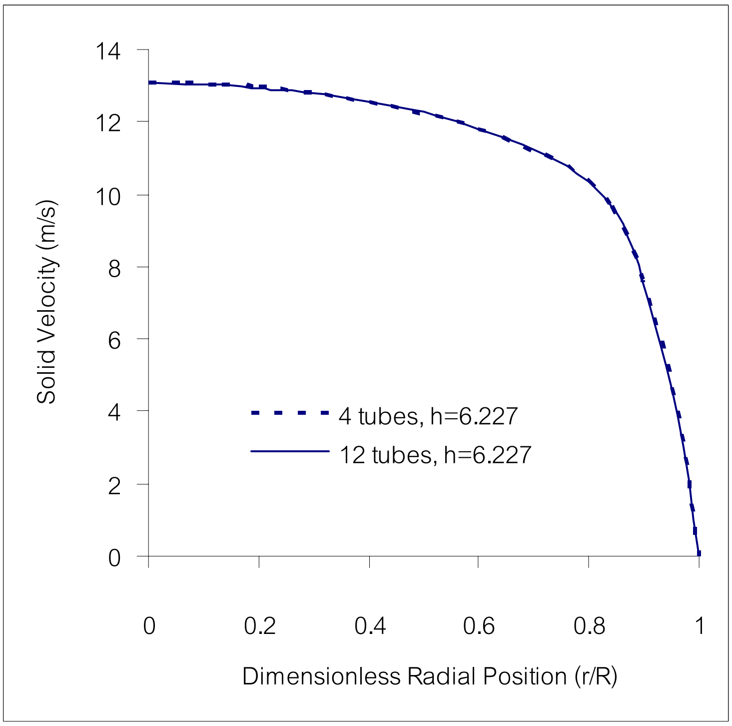

Figure 30 Radial solid velocity profiles at 6.227 m from downer entrance at superficial gas velocity (U_{sg}) of 10 m/s and solid circulation rate of 130 kg/m^2s

2. Gas-Solid Separators

The gas-solid separators are designed to separate fluid catalytic cracking (FCC) particles from the mixture of gas and particles. In a real 3-D downer reactor, the cyclone is used to separate gas and FCC particles. Since the FCC particles are very expensive, they need to be recovered as much as possible. Hence, at least two cyclones are used per a separation unit; there are 2 separation units in a downer reactor, one at the top and one at the bottom of a downer reactor.

Since the real cyclone cannot be modeled in 2 dimensions, the settling tank is the simplest equipment to replace the cyclone and was used at the beginning of this work. Two designs of the settling tanks are shown here to represent how they work. The geometry of both settling tanks are shown in Figure 31. The inlet is on the right side of the geometry. There are two outlets in each settling tank. The ambient pressure (1 atm) is specified at both outlets. The top outlet is designed for gas to leave while the bottom one is designed for solids because they are heavier than gas. The bottom outlet is designed to be small to prevent the gas flows through it. The volume fraction of particles of the inlet flow is 6.7×10^{-3} for both cases.

In the first design of the settling tank, the inlet flow is too fast (10 m/s) and hit the wall on the opposite side as shown in Figure 32. Particles collect themselves at the wall and leave at both outlets. There are 50% of particles leaving the separator at the top outlet. The second design of the settling tank is the correction of the first design. The geometry of the second design is bigger than the first one. The inlet size is enlarged 5 times to reduce the speed of the inlet flow from 10 m/s to 2 m/s, keeping the same flow rates of gas and particles. The slow flow allows particles to settling down before hitting the wall. However, 48 % of FCC particles still leave the top outlet. This is because the FCC particles are small (67 µm i.d.), hence they have high surface to weight ratio resulting in the enormous gas-drag that overcomes the gravity force. The particles cannot be separated out by the gravity force that apply in the settling tank and still follow the gas stream. The solid holdup contour and velocity vector plot of the second designed settling tank are shown in Figure 33.

To solve these troubles, the gas-solid separator described in the next section is used. The solid holdup contour and velocity vector plot are also shown in that section to demonstrate how the separator works. The gas-solid separator uses the concept of centrifugal force to separate gas and solids like what happens in the real cyclone. This gas-solid separator also has a benefit in dealing with high flow rate comparing to the settling tank, which has to be much larger to deal with the high flow rate.

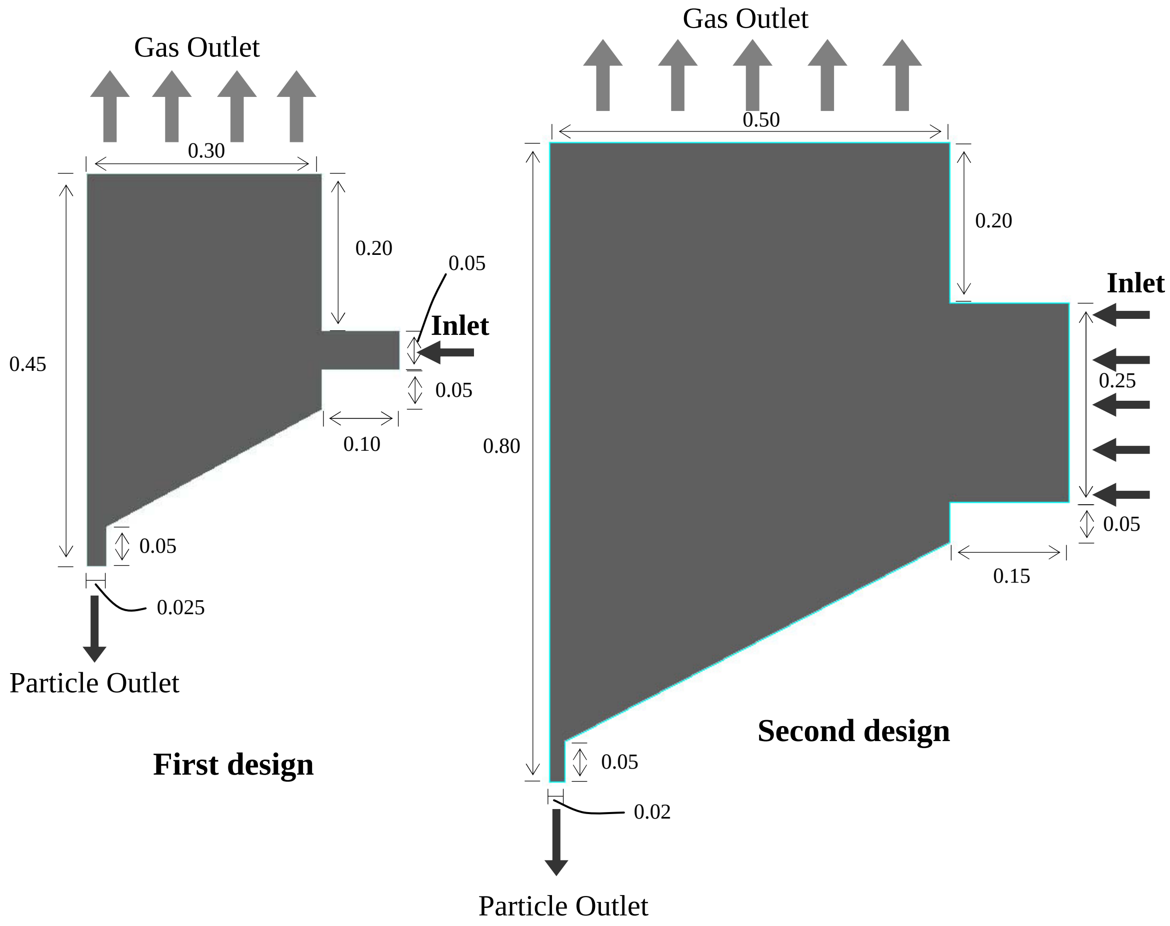

Figure 31 The first and second designs of the settling tanks

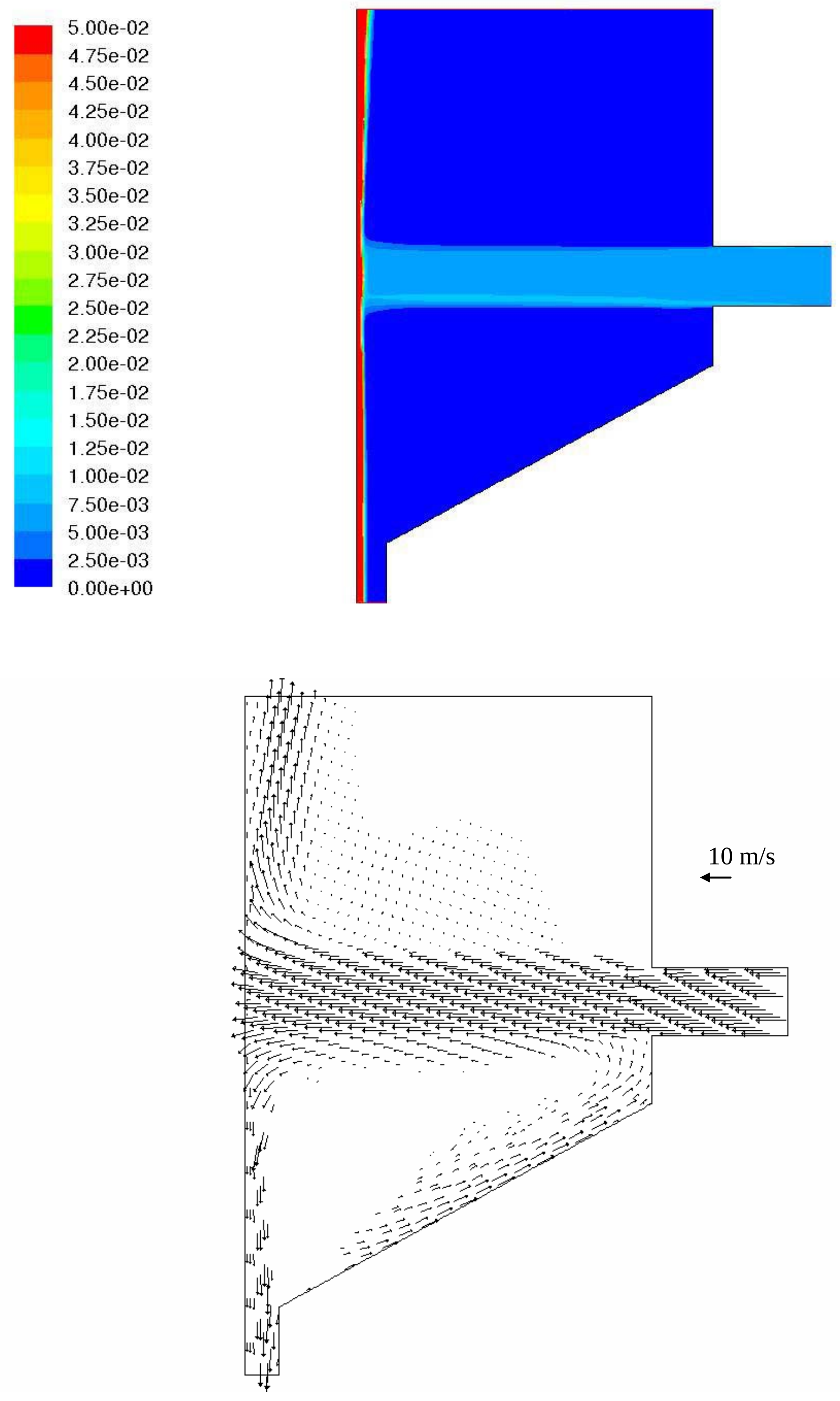

Figure 32 The solid holdup contour and velocity vector plots of the first design showing too much speed of the inlet flow

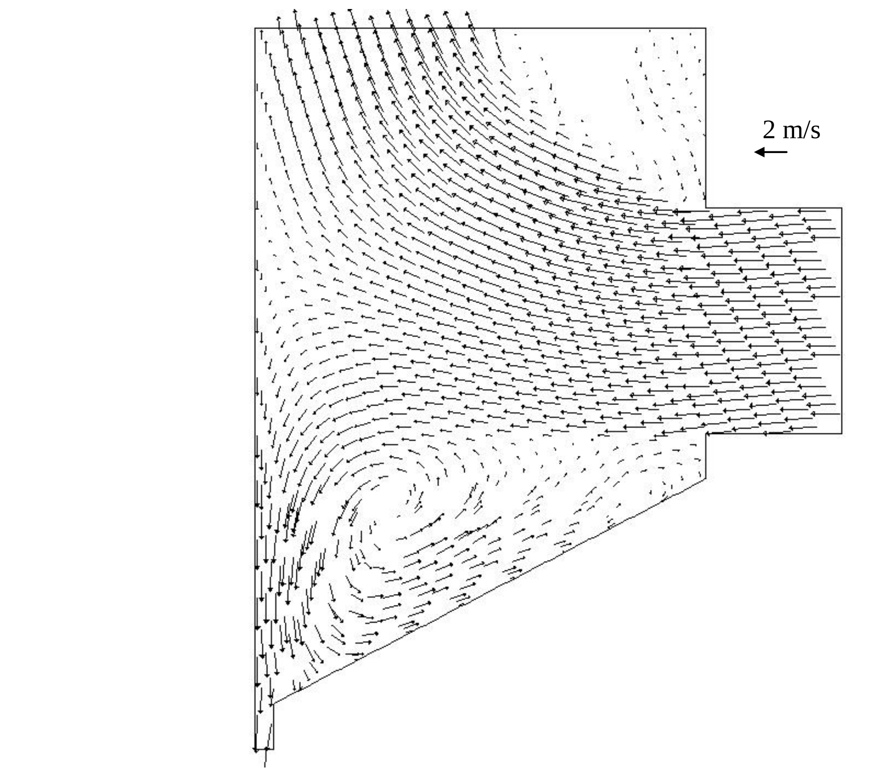

Figure 33 Solid holdup contour and velocity vector plot of the second designed settling tank

Separation of Gas and Particles

In this downer reactor model, gas and particles need to be separated at two locations as shown in Figure 34. The first location is at the bottom of the model, after the particles pass through a downer. The second location is at the top of the model after the particles leave the riser column. At the top of the downer, the reactant gas mixes with solids and reacts. At the end of the downer, gas, which becomes the product gas, must be separated from solids here. After being separated from the product gas, solids are transferred to the bottom storage tank. The bottom storage tank supplies solid stream to the riser column. Solids that are fed to the riser column are lifted by circulating air to the top of the riser. These solids will be separated after they leave the riser to be recycled to the top storage tank, which supplies solids directly to the downer reactor.

Vector and contour plots at the places where the separation of gas and solids occurs are used to represent how the separation process works.

1. Separation of Product Gas and Used Catalyst at the Bottom of the Downer Column

After solids leave a dower column and enter the 60^o bend, they are moving towards the lower wall of the bend because of their inertia as shown in the vector plot in Figure 36. In this downer study, solids density is 1500 kg/m^3 and is much higher than gas density. The difference of density between solid and gas phases helps separating them. The small solid particle, which is only 67 μm, has high surface to weight ratio, hence increasing drag coefficient between solids and gas. By this reason, it is almost impossible to separate solids from gas by other methods such as using the settling tank. The settling tank uses only gravity force to settle solids which cannot overcome the drag force of the gas phase that brings solids along with the gas phase to the top outlet of the tank. The contour of solid volume fraction is shown in Figure 35. The solid velocity vector plotted in Figure 36 shows how solids move toward the lower wall of the bend and separated into a small channel leading to the bottom storage tank. The areas absented from the vector arrows have no solids.

2. Separation of Circulating Air and Recycling Catalyst at the Top of the Riser Column

As mentioned in the above section, solids flowing through the downer column are brought to the bottom storage tank, which supply a stream of solids to the riser. Circulating air brings solids up to the top of the riser, where they must be separated and transferred to the top storage tank.

Considering the 3-D geometry of this 2-D axisymmetric domain shown in Figure 34, the cross section area of all horizontal paths in the domain will increase with the distance from the axis of the domain as shown in Figure 20, which is the axisymmetric axis. At the bottom of the downer, both solids and gas move away from the axis to the higher cross section area hence lower their own velocities. These solids can be easily separated by only one bend. However, the separation method at the top of the riser becomes much more difficult because the high amount of air used to lift the solids through the riser. The velocities of air and solids increase when they move toward the axis of the domain due to the decreasing cross section area. After passing two 90^o bends, solids are swing to the outer wall of the bends and more than half of the circulating air at the inner wall is separated out of the domain at the circulating air outlet. The amount of air that does not leave the circulating air outlet still follows solids into the separating channel and needs to be removed from solids stream before solids enter the top storage tank. At this point, the separation unit is used (the top separator) to remove the air from solids through its vent.

All components involving the top separation processes are shown in Figure 37 (contours of solid volume fraction) and Figure 38 (solid velocity vector plot). These components include two 90^o bends and a separation unit. There are low content of solids in most of the area of the riser except the area in the downflow pipe as represented by the blue color (solid holdup range of $0 - 1.5\times10^{-4}$). However, since there are some solids in that area, the velocity vector is represented. On the other hand, the blue contour in the top separator tank represents no solid at all and there is no vector shown in that position. Figure 39 and Figure 40 are the contour and vector plots representing the separation at the first bend. The vector plot shows that the first bend is not enough to swing all solids to the wall and the second bend is needed. Solids that move towards the outer wall of these two bends are then flowing into the top separator. The design of the top separator is to keep solid velocity vector pointed to the bottom outlet channel and keeping the channel narrow enough to prevent the air flux coming with solid stream from entering this channel. Figure 41 and Figure 42 represent the solid flow in the top separator. Solids are leaded to the bottom channel by their own momentums. On the other hand, the air will be vented out through the top outlet of the top separator at atmospheric pressure. Figure 43 represents the gas velocity vector plot of the top separator showing the gas flow out of the top vent. The small dots in this Figure are the vectors representing very slow gas velocity moving up to the vent.

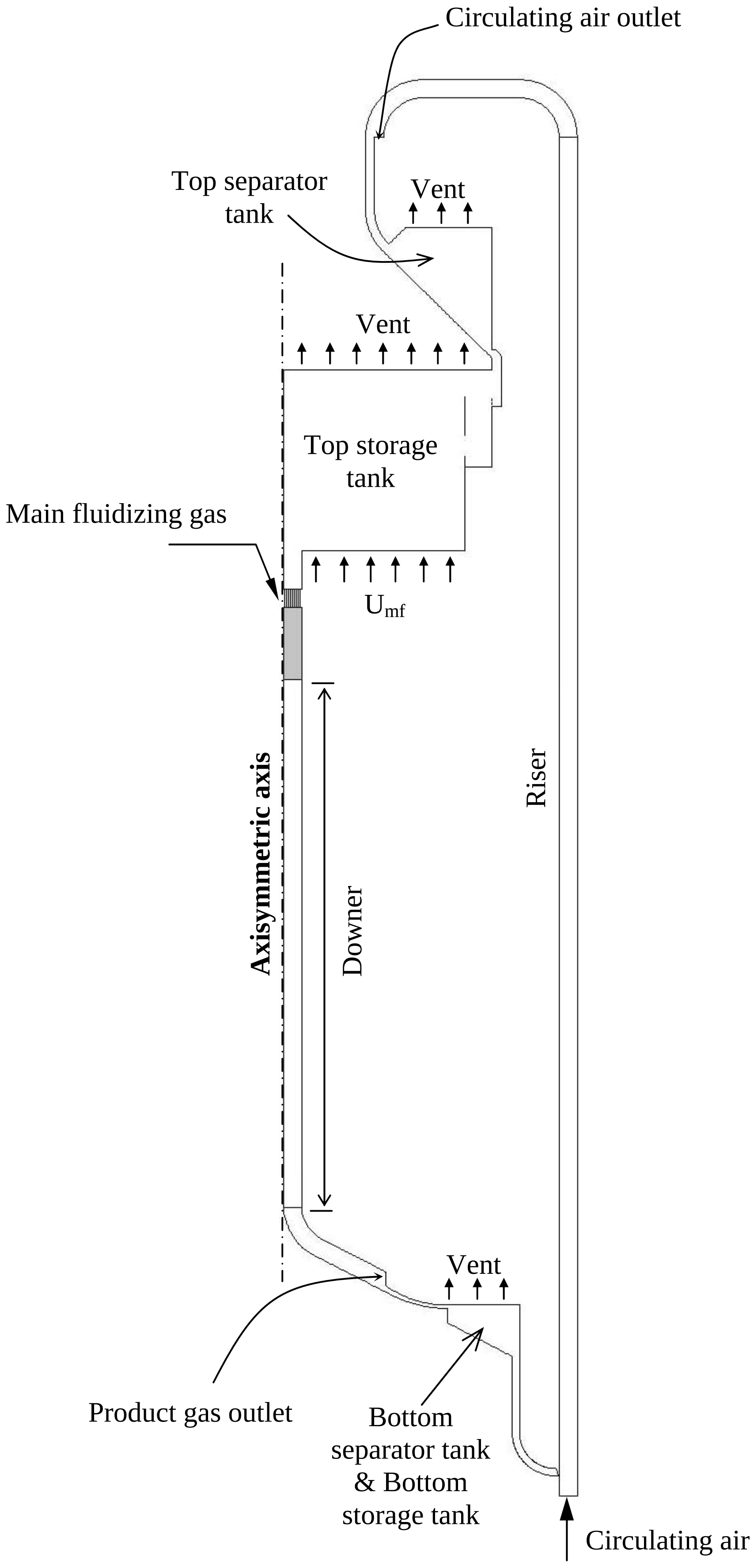

Figure 34 Downer reactor model

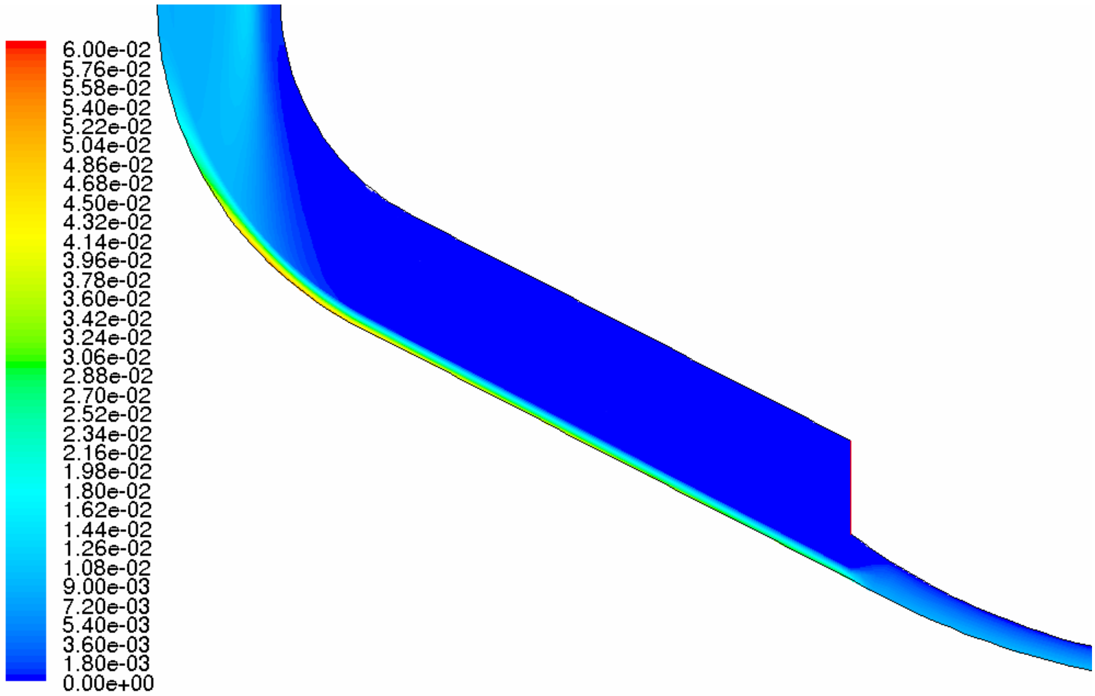

Figure 35 Solid holdup contour at the bend below downer column

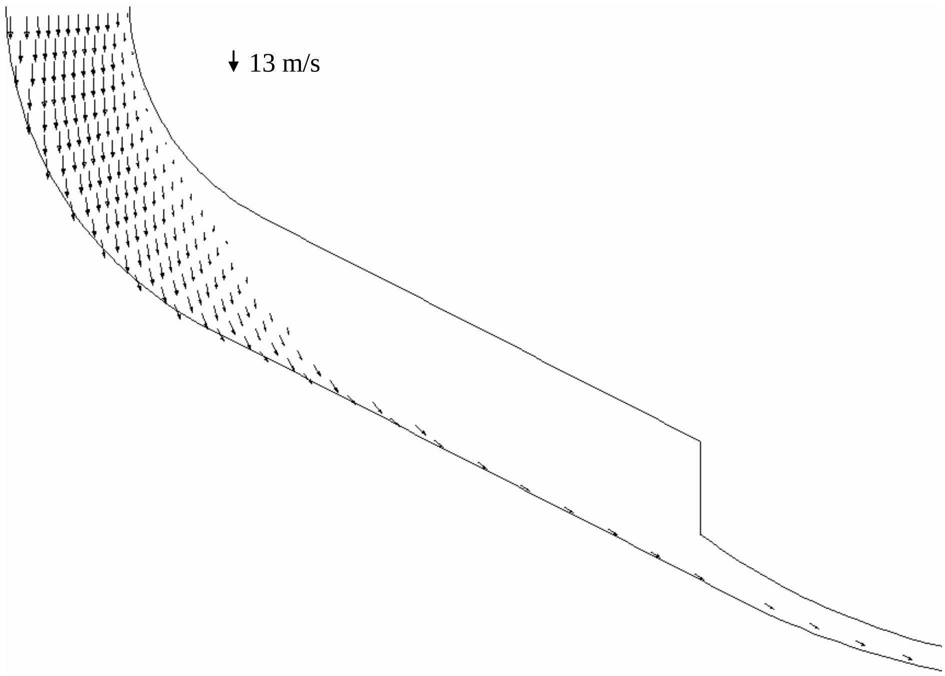

Figure 36 Solid velocity vectors at the bend below downer column

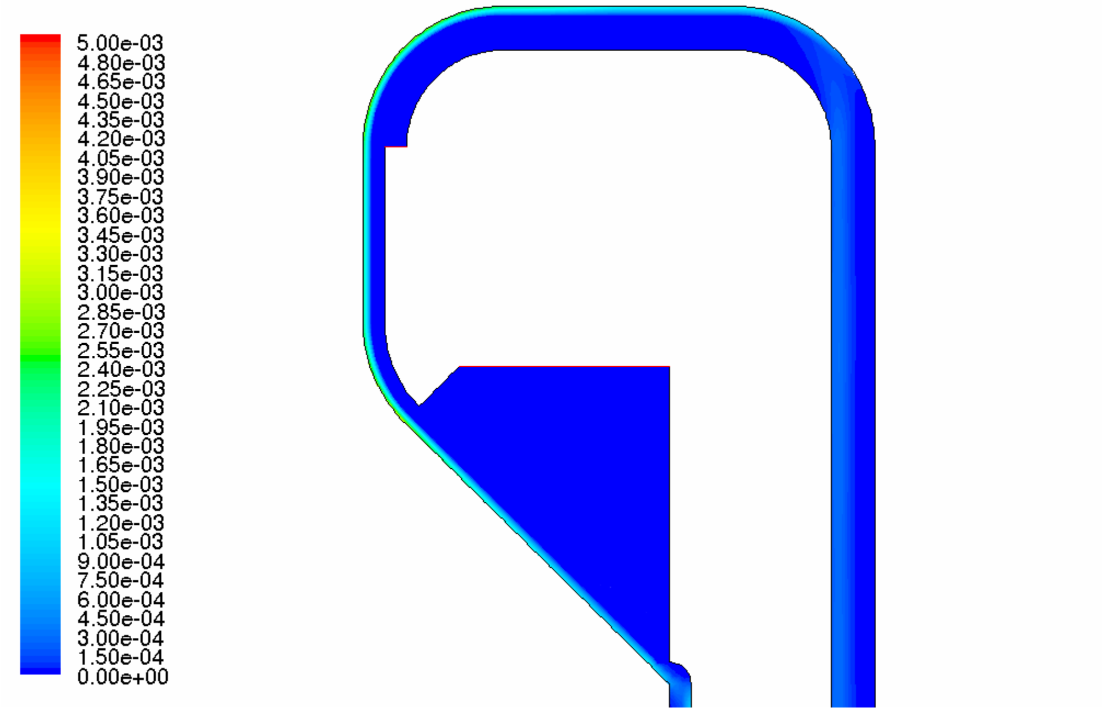

Figure 37 Overall contour plot of solid holdup at the top

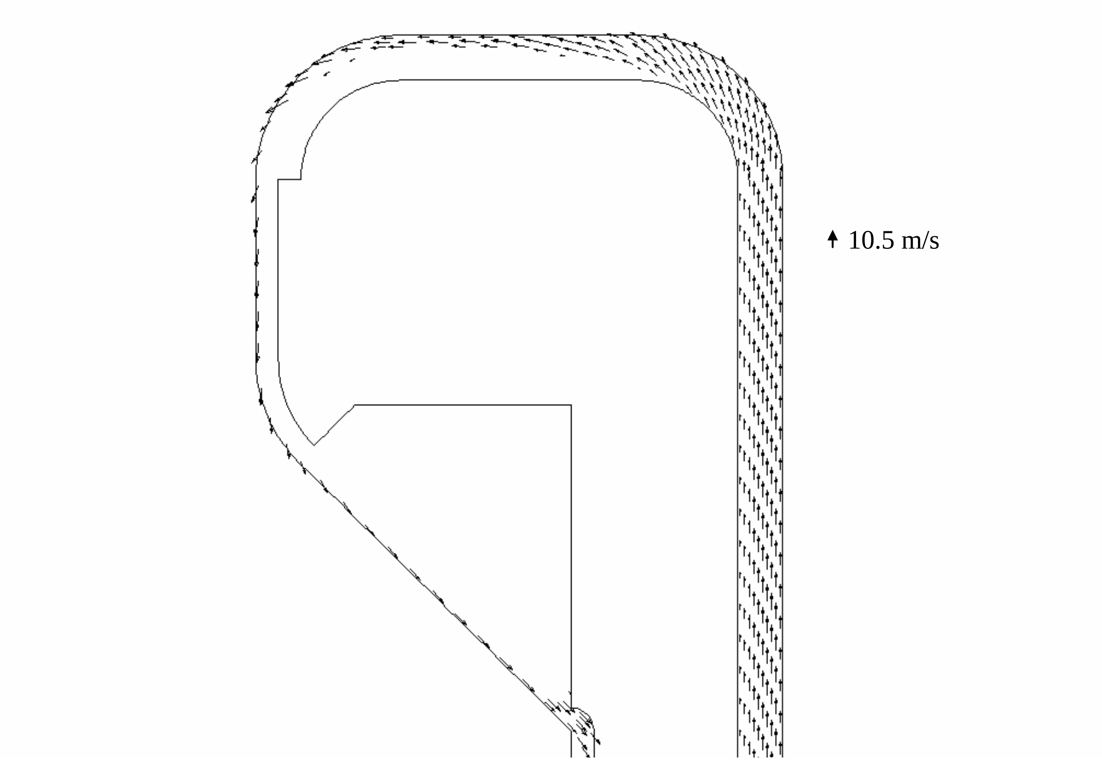

Figure 38 Overall vector plot of solid velocity at the top

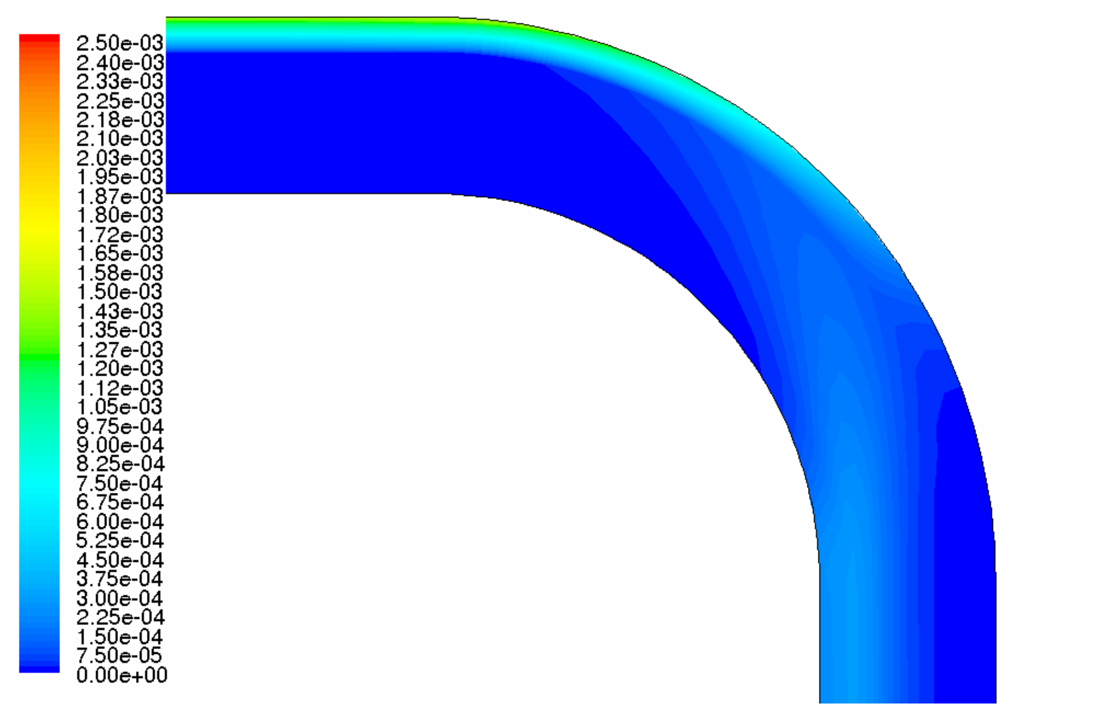

Figure 39 Solid holdup contour at the first bend on the top of riser column

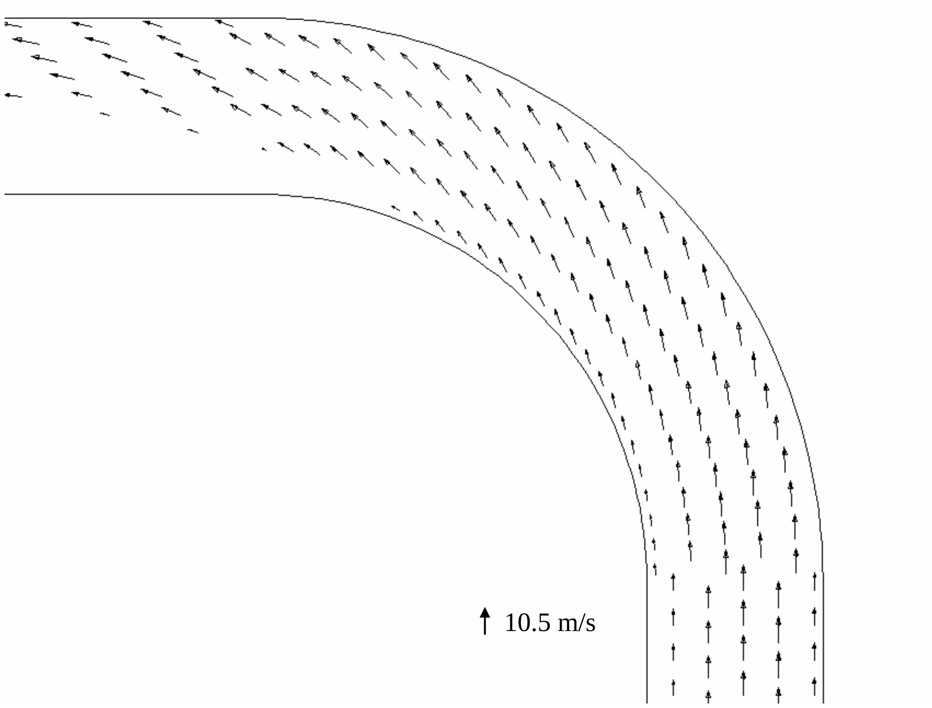

Figure 40 Solid velocity vectors at the first bend on the top of riser column

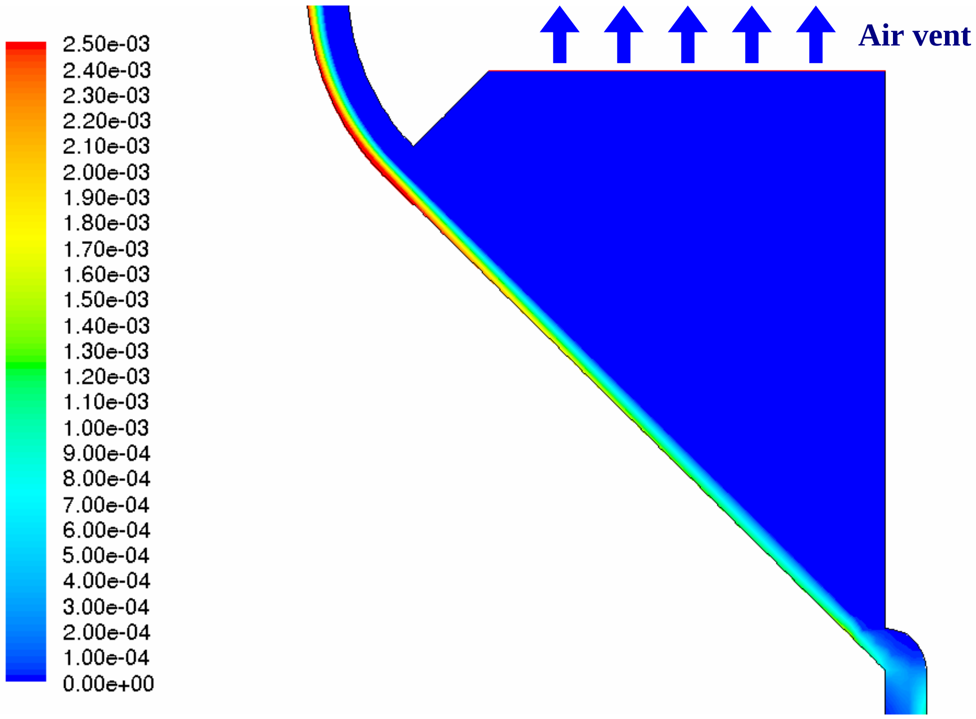

Figure 41 Solid holdup contour in the separation unit

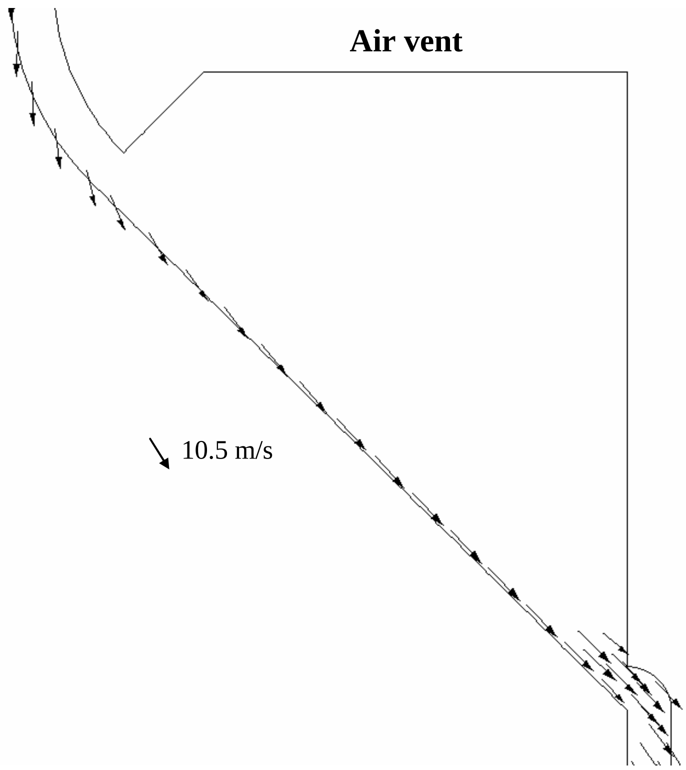

Figure 42 Solid velocity vectors in the separation unit

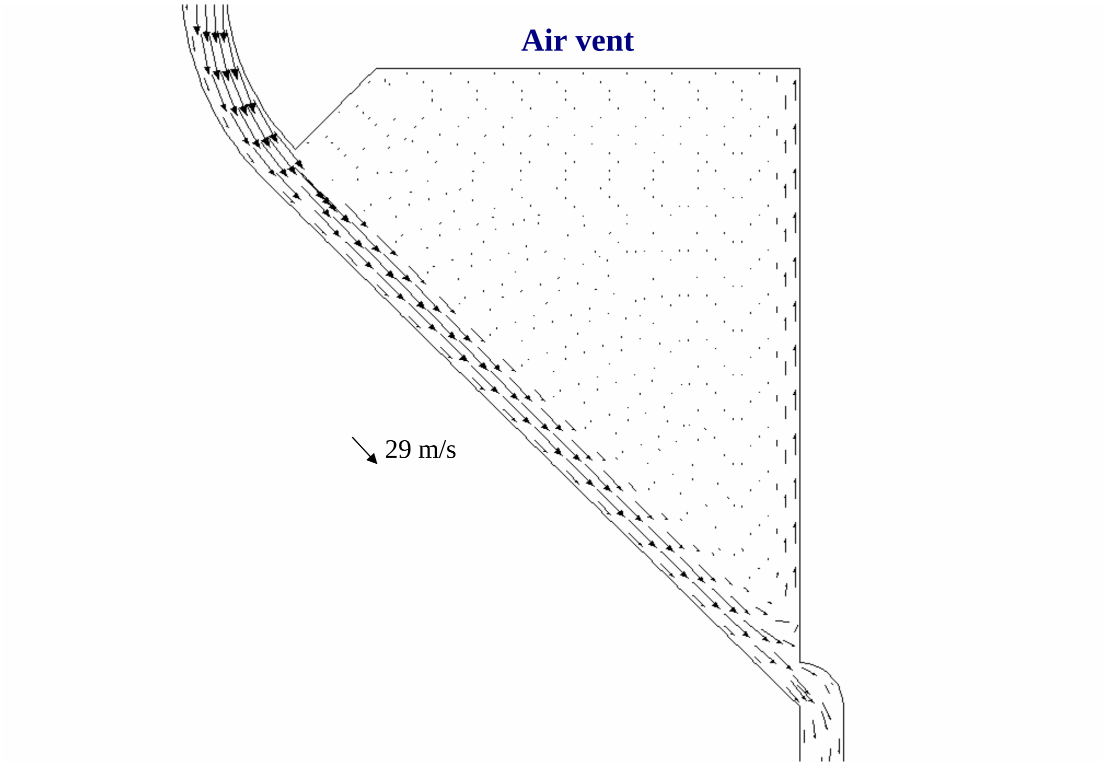

Figure 43 Gas phase velocity vectors in the separation unit

Hydrodynamics in a Riser Column

A riser column is used to circulate used particles to the top storage tank. An air inlet with 10 m/s in velocity is at the bottom of the riser. The air from the bottom blows particles, which are fed from the bottom storage tank, up to the top separator tank. The reactor model is shown in Figure 34. Since the riser column in this model is only used to circulate used particles with no reaction, the hydrodynamics here will not affect the performance of the reactor.

Figure 44 shows solid holdup contour and velocity vector plots. Solids are fed from the bottom separator tank; therefore the solid concentration near the feed point is always higher than other areas as seen in Figure 44. The radial distribution of solid holdup gradually changes at the beginning after fed to the riser and then remain unchanged along the height of the riser as seen in the solid holdup contour.

Figure 45 shows the gas and solid velocity vector near the solid feeding point at the bottom section of the riser. The gas velocity in the riser at the area near the feed is slowed down because solids are injected there. In the area above the feeding point, gas and solids in the same location are likely to have the same values of velocities.

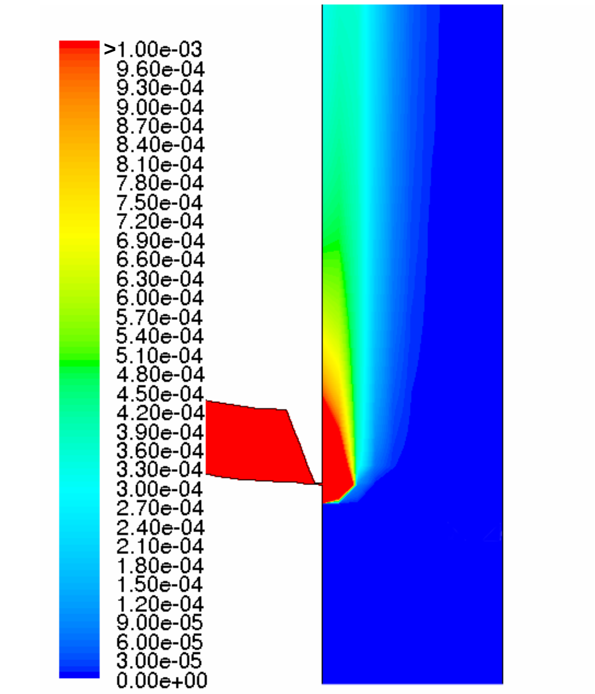

Figure 44 Solid holdup contour at the feeding point

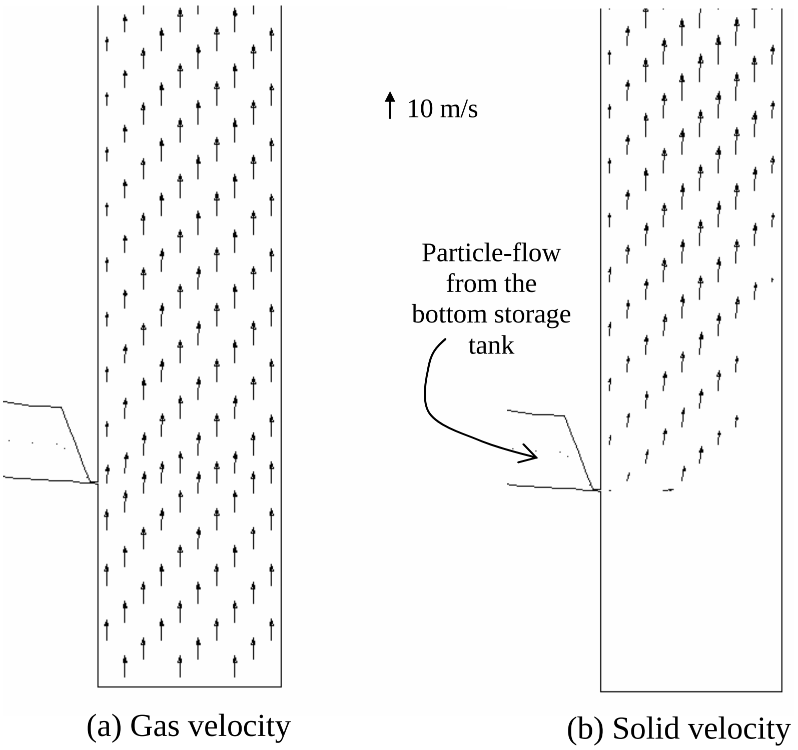

Figure 45 (a) Gas velocity vector plot at the feeding point, (b) Solid velocity vector plot at the feeding point

The axial solid holdup profile in the riser column is shown in Figure 46. The holdup is high near the riser inlet because solids are injected near the bottom of the riser. The holdup value decreases in the first meter, where solids accelerate themselves. How ever, after 2 m from the riser inlet, solid holdup gradually increases with fluctuation. The fluctuation in solid holdup is about 2.5 %. The increasing holdup is caused by the gravity. Gravity in the riser acts on the opposite direction of the flow, which is different from the downer. Hence, solids near the end of the riser are slowed down and accumulate themselves over there.

Figure 47 shows the radial profiles of solid holdup at different distances above the feeding point. Solids are injected from the left side of the riser. At 0.05 m above the feeding point, solids are accumulated near the left wall. Some part of solids on the left move to the right side of the riser while moving up the riser column but most of them still stay on the left side. After 2 m, solid holdup profile is close to fully develop and changes only little from 2 m to 6 m above the feeding point.

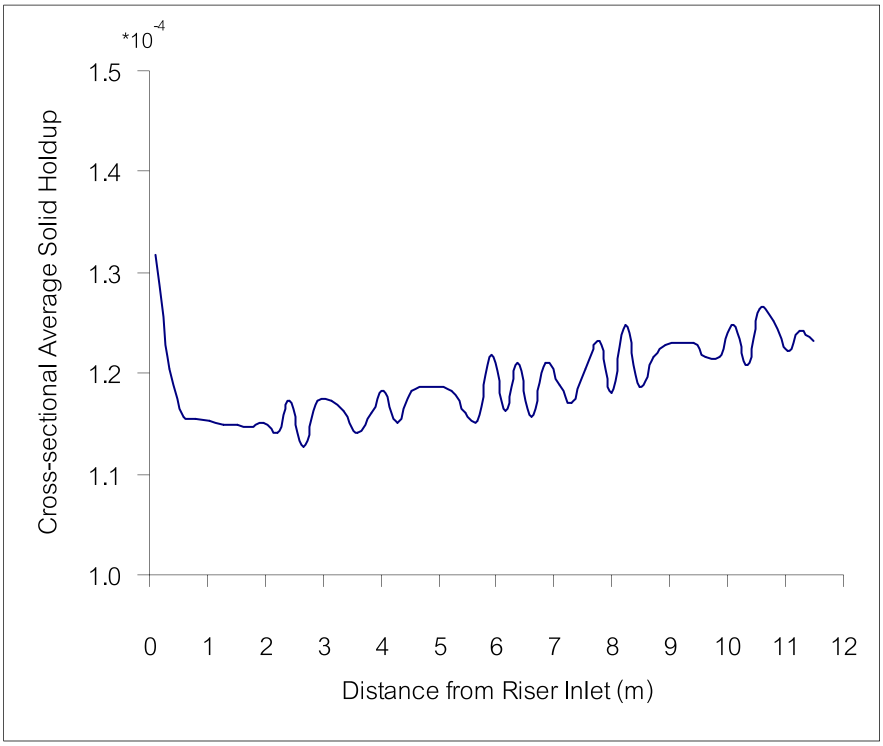

Figure 46 Axial solid holdup profile in the riser column

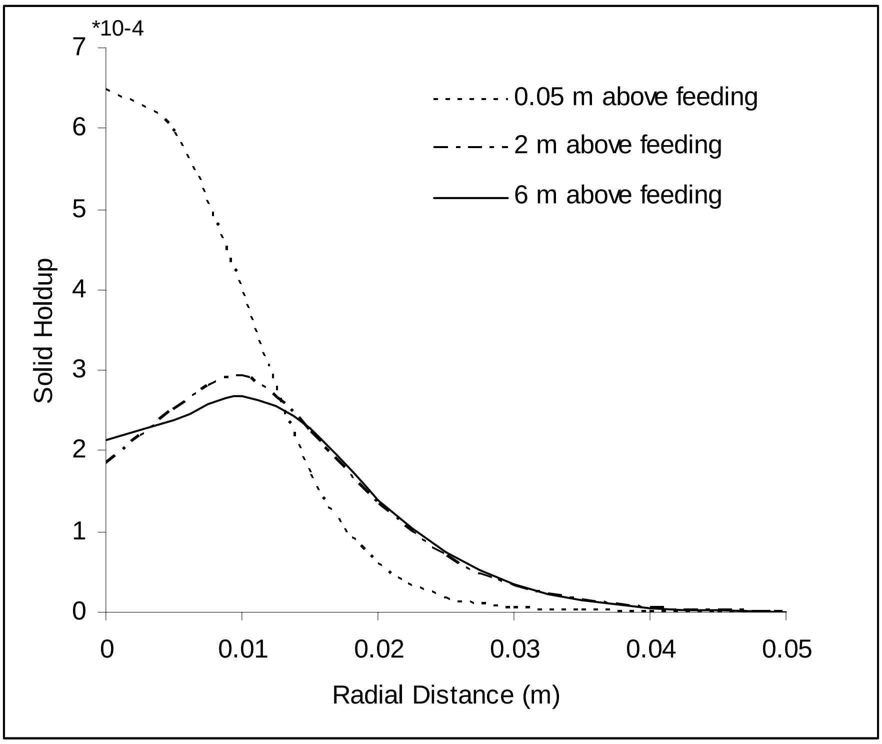

Figure 47 Radial solid holdup profiles in the riser column

Hydrodynamics in a Downer Column

1. Solid Holdup Contour and Velocity Vector plot

In the distributor above the downer, the wall of the distributor is free slip leading solids to uniformly distribute with uniform velocity along the downer radius. However, in the main downer, the boundary condition at the downer wall is set to non-slip. Therefore, with non-slip condition at the wall, the hydrodynamics in the main downer should be different from that in the distributor. These results illustrated by solid holdup contour and velocity vector plots lead to the conclusion that particulate flow in a fluidized bed downer are divided into core and annulus zones due to the effect of the non-slip boundary at the downer wall.

Figure 48 shows the solid holdup contour and velocity vector plots of the first meter section of the downer at superficial feed gas velocity (U_{sg}) of 10 m/s and solid circulation rate of 130 kg/m^{2}s. This first section shows the most changing in solid distribution in the downer. Solids entering the downer column from the particle distributor are divided to core and annulus zones at the first meter as shown in contour plots on the left side of Figure 48. Each section in this Figure 48 contains 0.5 meters section of the downer starting from the downer entrance. The downer entrance is the top edge of the most left picture in this figure. The solid volume fraction contour is first uniform at the downer entrance and then starts dividing into two zones with a locust of high solid concentration (solid holdup peak) seen as the red zone. Here, the green zone on the right side of solid holdup peak is the position used to separate the core zone and the annulus zone. The blue contour at the wall indicates that there is low content of particles in this area because solids migrate from the annulus zone near the wall to the core zone. The width of the blue contour gradually increases with more distance from the downer entrance since solids keep migrating to the center until they reach the fully develop zone, where the radial distribution profiles of solids stop changing with more distance from the downer entrance, further down the column.

Solid velocity vector plot is shown on the right side of Figure 48. At the entrance of the downer column, the velocity of solids is uniform along the radius of the downer as seen by the equal length arrows. After entering the downer, solids at the wall move slower and change direction toward the center. The incline vectors indicate that solids in these areas have a significant velocity component in the direction toward the center of the downer column (-r direction). The maximum velocity vectors at the center represent the solid velocity at 13 m/s while the minimum velocity vectors near the wall represent the solid velocity around 2.85 m/s. The vector plot of solid velocity shows that there is no back flow in the downer column and the flow is closer to the ideal plug flow compared to other kinds of fluidized bed, in which back flow always occur. Particle holdup and particle velocity in the riser column of Huilin *et al*. (2003) are shown in Figure 49. Particles in the riser are accumulated near the wall and fall down. As a result, the hydrodynamics in a riser is further from the plug flow regime than the hydrodynamics in a downer.

The solid holdup contour of the whole length of the downer column is shown in Figure 50. Each picture of downer sections represents 0.93 meters of the downer starting from the left. Solids in the downer are divided into core and annulus zones and the distribution of solids is stable along the downer length. The contour of solid holdup has reached the fully develop zone after some distance more than 2 meters as shown in the third column in Figure 50. In the fully develop zone, the core and annulus zones still exist. The blue contour near the downer wall represents the solid-free area. The green contour next to the blue one is the boundary separating core and annulus zones. Solid holdup peak can still be seen as the red zone near the wall. The widest yellow contours on the left of each picture are the core zone where solids distribute uniformly. The radial profiles of solid holdup at various distances from the downer entrance will be represented clearly by the graphs in the section 2.

After a period of 2 seconds of simulation, solid stream from the bottom storage tank that flow through the riser have reached the top storage tank. This solid stream flow rate into the top storage tank is designed to be equal to its outflow rate to the downer (by specify the width of solid feeding tube connected to the riser) to stabilize the amount of solids in the top storage tank, hence steady the solid flux into the downer. After the solid flux into the downer is stabilized, hydrodynamics in the downer will come to steady state condition and the simulation results do not need to be averaged over a period of time before analyzed. Hence, simulation results of a downer could be retrieved at any point of time after the solid flux from the top storage tank has been steady. The solid holdup contours in the downer and the riser at any particular times are shown in Figure 51. In this figure, it can be seen that only 1 second is enough to fill the downer with particles while it takes 2 seconds to fill the riser with particles even though both fluidized gases are fed at 10 m/s. This is because particles in the riser flow in the opposite direction with the gravity force.

2. Axial Profiles of Solid Holdup and Velocity

Axial solid holdup profile is plotted in Figure 52. The solid holdup drops dramatically in the first 2 meters below the entrance of the downer column. Axial solid holdup profile might be affected by the axial velocity profile of solids that is shown in Figure 53. Considering the system at steady state condition, when solid velocity increases along with the downer axial position, the solid holdup will drop to maintain the same constant flux to satisfy mass conservation of solid particles. As a result, the decreasing of solid holdup profile in the first 2 meters is related to the high increasing of solid velocity in the first 2 meters of the downer.

The superficial gas velocity is set at 10 m/s, however, solids enter the distributor at the speed of 2.4 m/s as seen in Figure 53. The large difference between gas and solid velocity at the entrance above solid distributor, where the contacting of gas and solids occurs, creates enormous drag force. At the top of the downer, solid velocity increases rapidly because the big drag force and the gravity work in the same direction. This top section (about 0.7 meter) with high increasing of solid velocity of the downer is called as the first acceleration zone. After 0.7 m. below the downer entrance, solid velocity increases slower because they have reached the gas velocity and are only accelerated by the gravity. This position is the end of the first acceleration zone but the start of the second acceleration zone where they accelerated at slower rate. After 2 meters from the downer entrance, solid velocity almost becomes constant. The downer section after 2 meters is called the constant velocity zone because solids stop increasing their velocities in this zone. The results here agree well with the work of Nattha *et al*., 2005, which reports the positions at 1 m. as the position dividing the first and second acceleration zone, and 2 m. as the position dividing second acceleration zone and the constant velocity zone.

The final value of solid velocity after fully develop (Figure 53) is about 12 m/s, which is more than superficial gas velocity (10 m/s). However, solid velocity is not locally greater than gas velocity as shown by the radial profiles of gas and solid velocities at 4 m., where gas and solid enter the constant velocity zone for some distances, as shown in Figure 54. At 0.7 meter, where the first acceleration zone ends, solids still keep accelerating even their local velocities have reached the velocity of the gas phase. The reason is that solids migrate from the annulus zone, which has lower velocity, to the core zone and then be able to move faster. Hence the increasing in mass averaged velocity of solids might occur from two reasons. The first reason is the forces that act on solids comprising of both drag force and gravity force that happen in the first acceleration zone. The second reason is that solids migrate to the higher velocity zone at the core as that occurs in the second acceleration zone at 0.7-2 meters. Both solid velocity and holdup averaged from 4-6 meters are plotted against the radial position on the same graph in Figure 55 showing that the solid majorities stay in the core zone with higher velocity, thus explains why mass averaging of solid velocity gives higher value than gas velocity even if their local velocities are the same.

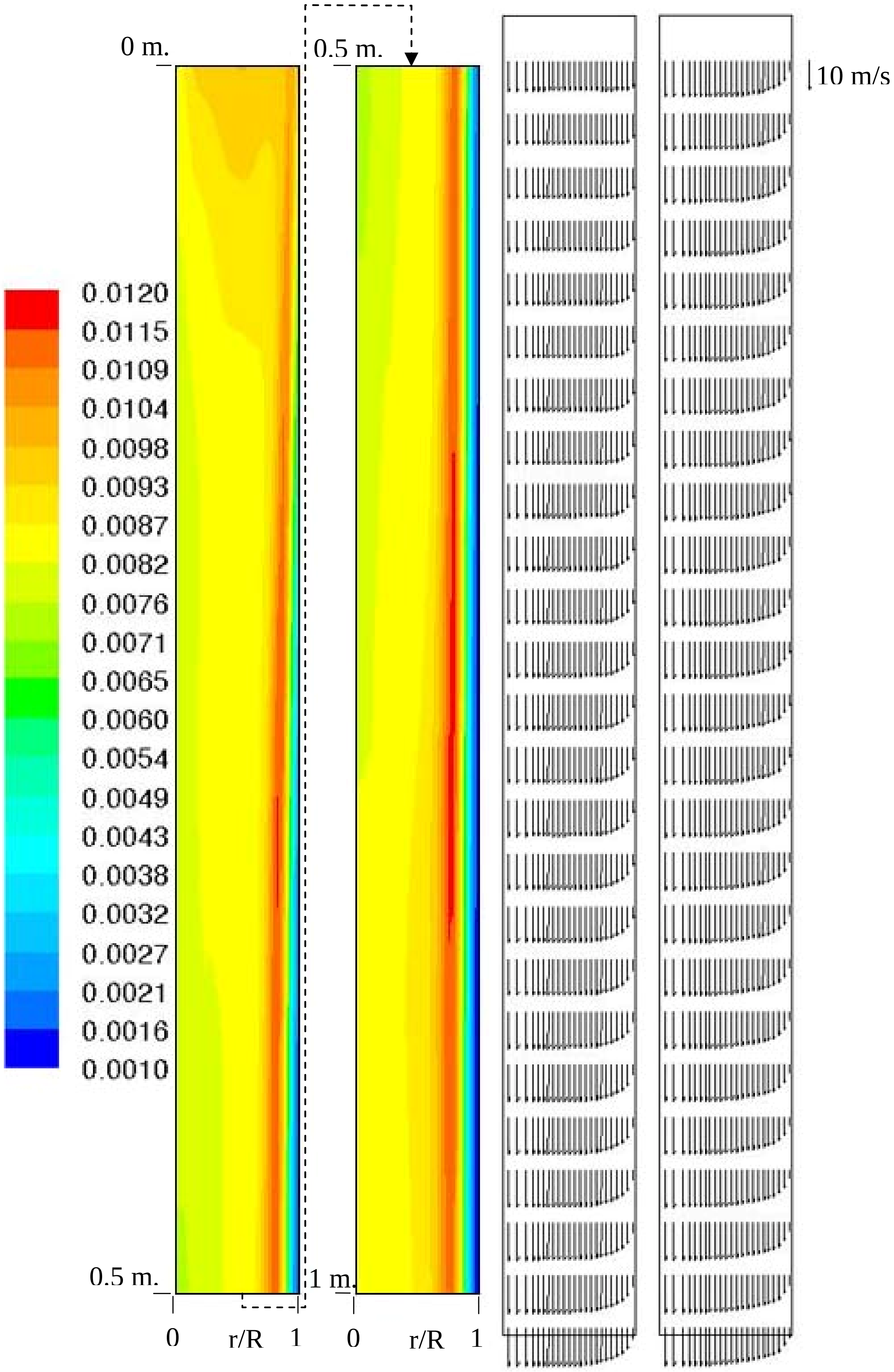

Figure 48 Solid holdup contour and velocity vector plots of the first meter section of the 0.1 m in diameter and 9.3 meters long downer with 67 μm. particles at superficial gas velocity (U_{sg}) of 10 m/s and solid circulation rate of 130 kg/m^{2}s

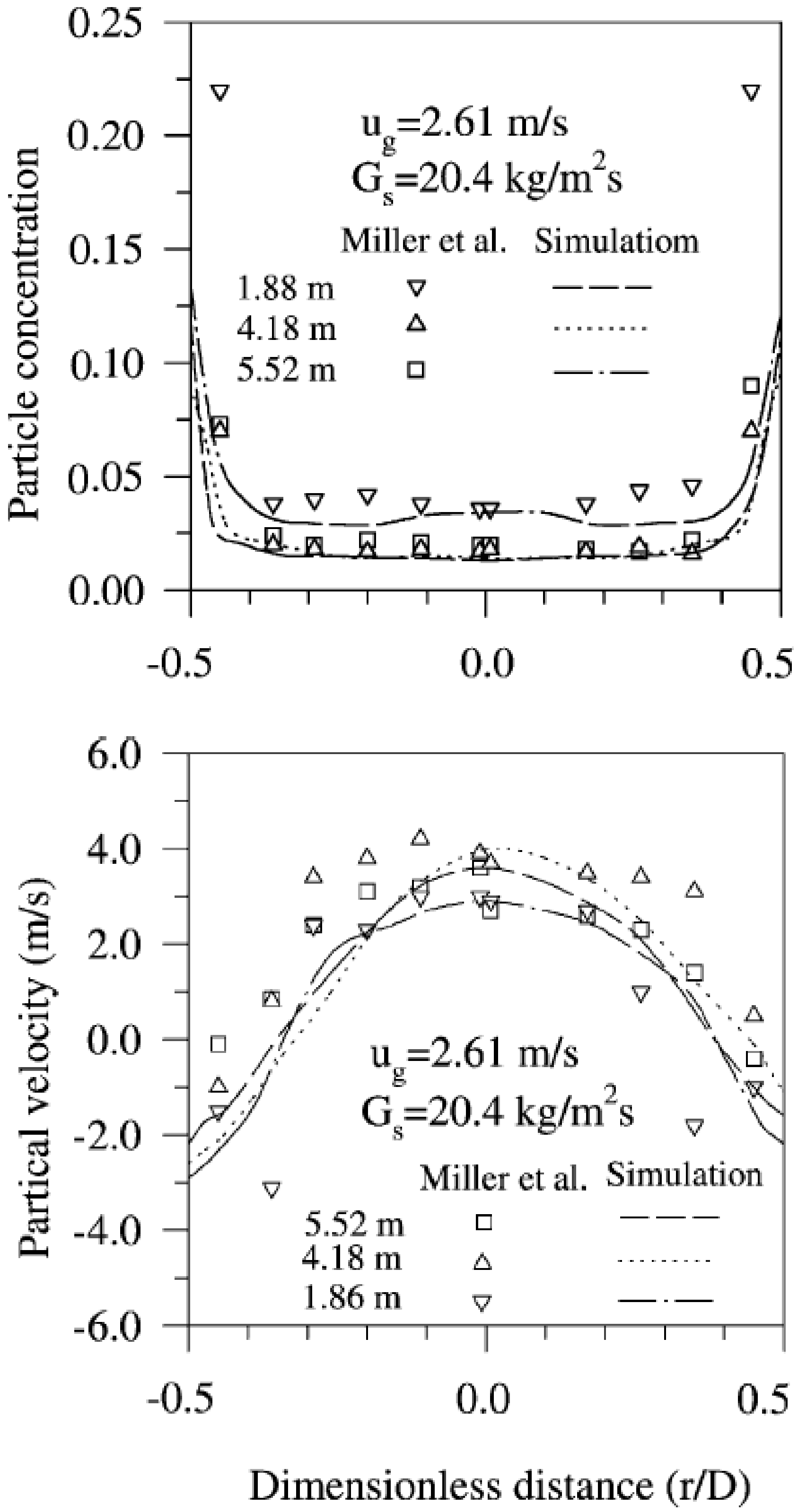

Figure 49 Hydrodynamics in a riser; (a) Radial particle concentration profile, (b) Radial particle velocity profile

Source: Huilin *et al*. (2003)

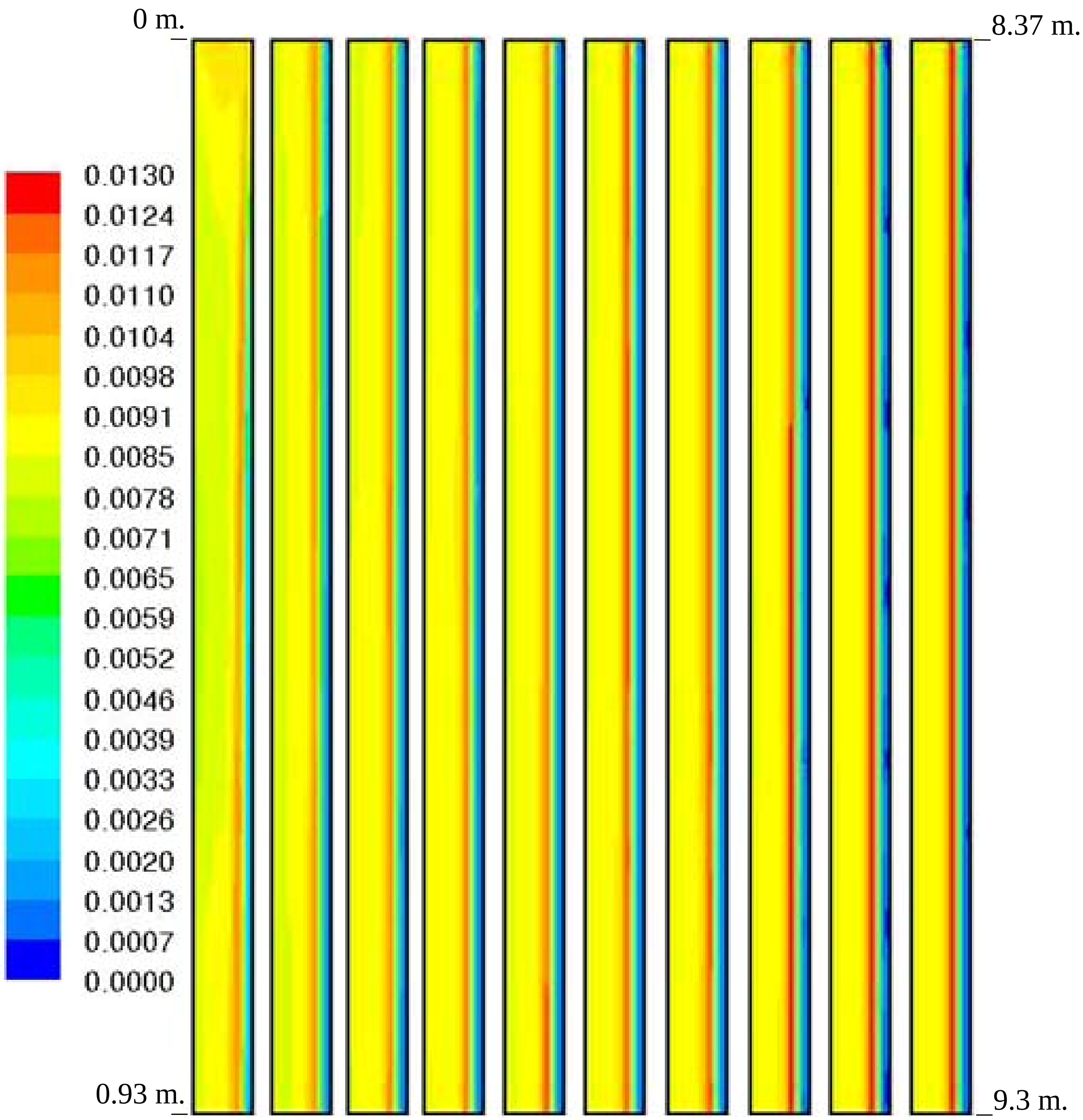

Figure 50 Solid contour of the 0.1 meter in diameter and 9.3 meters long downer with 67 μm. particles at superficial gas velocity (U_{sg}) of 10 m/s and solid circulation rate of 130 kg/m^2s

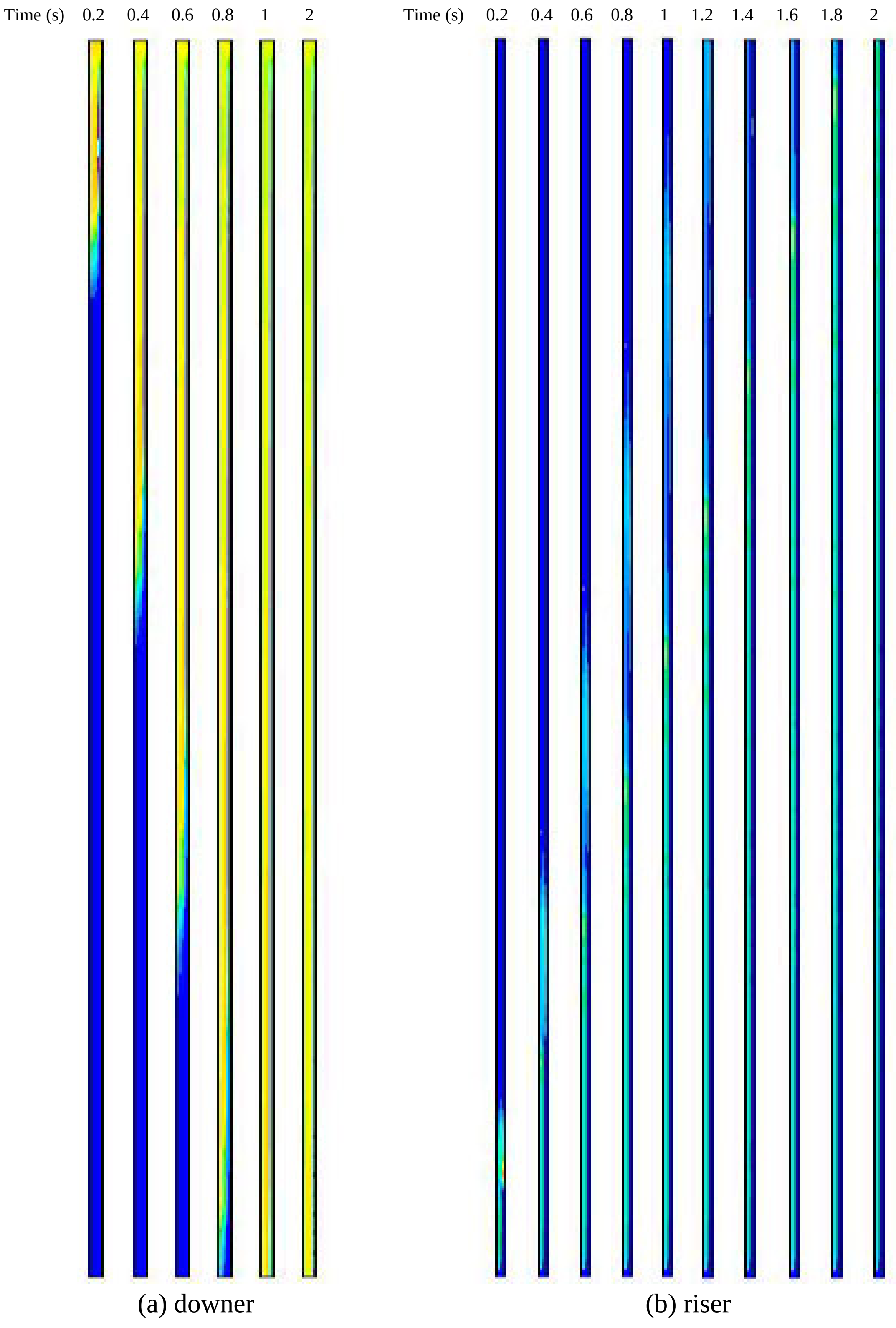

Figure 51 Solid holdup contours in downer and riser at specified times; (a) downer, (b) riser

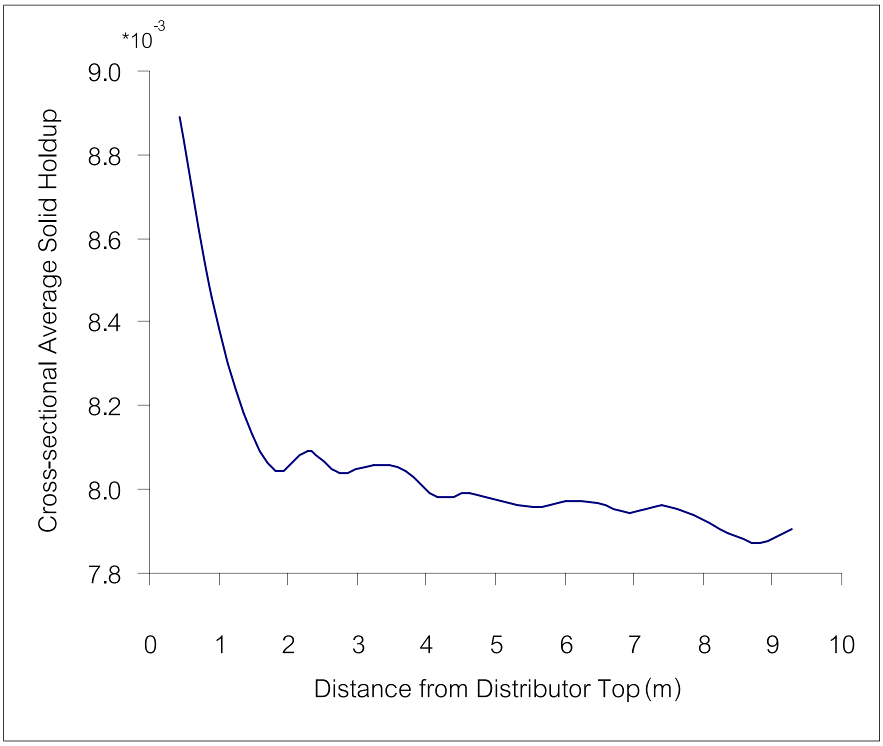

Figure 52 Axial solid holdup profile at superficial gas velocity (U_{sg}) of 10 m/s and solid circulation rate of 130 kg/m^{2}s

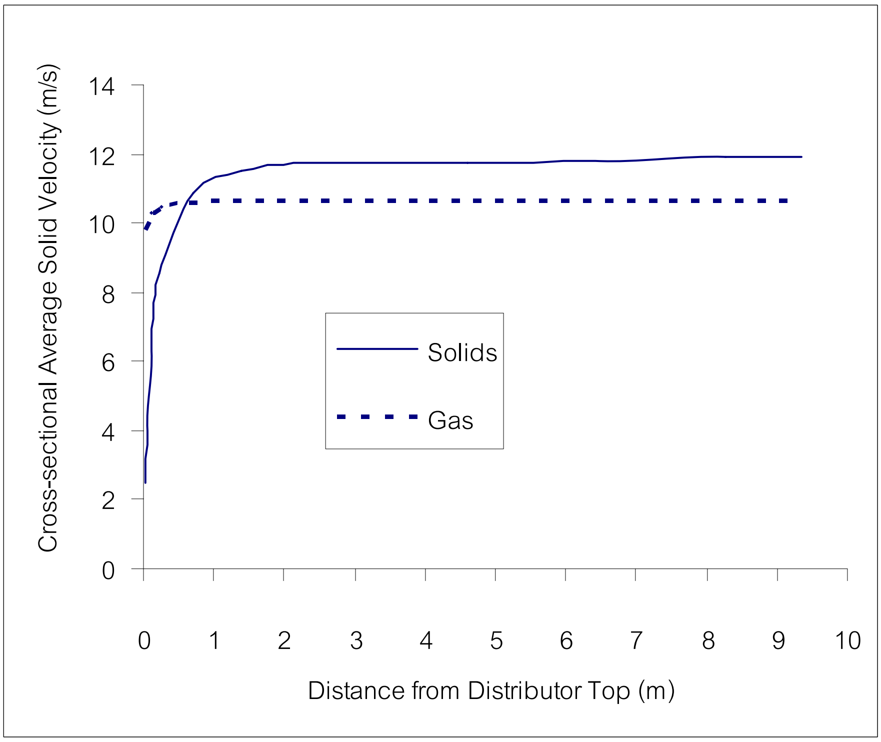

Figure 53 Axial solids velocity profile at superficial gas velocity (U_{sg}) of 10 m/s and solid circulation rate of 130 kg/m^{2}s starting from distributor top

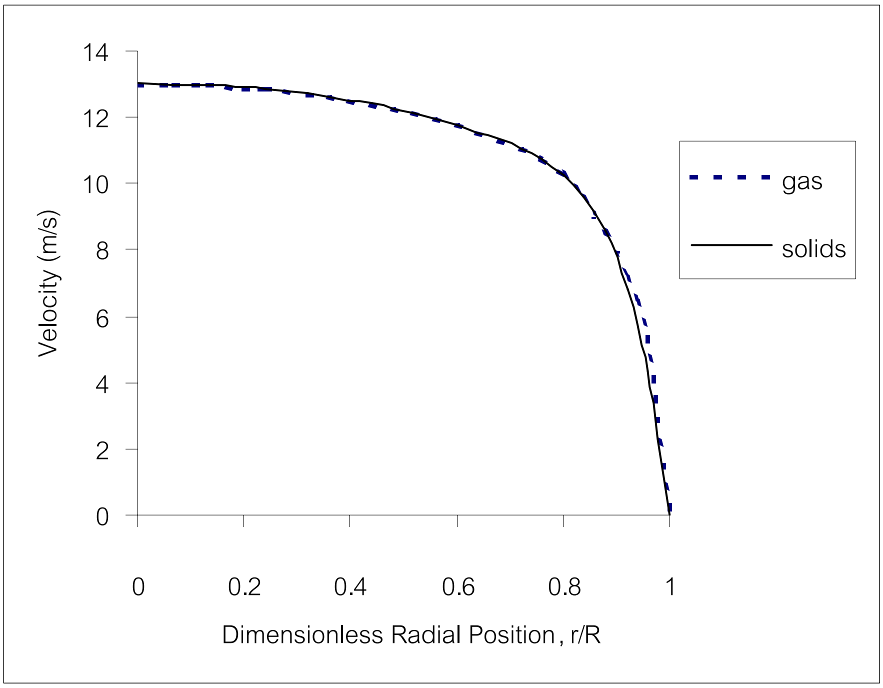

Figure 54 Radial velocity profile of gas and solids at 4.398 m. from downer top at superficial gas velocity (U_{sg}) of 10 m/s and solid circulation rate of 130 kg/m^2s

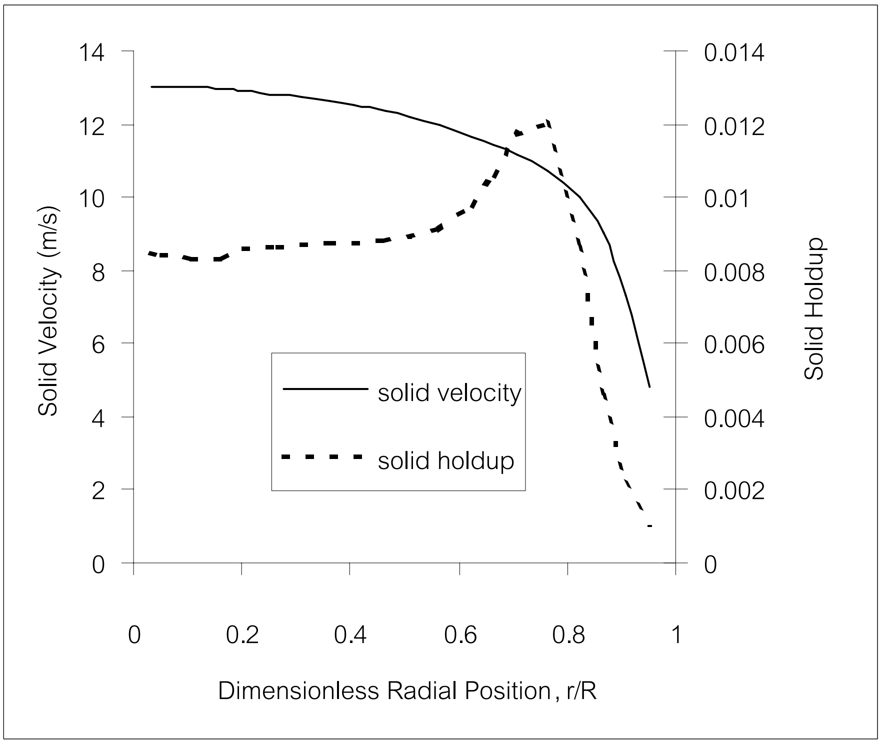

Figure 55 Compare radial solid velocity profile and radial solid holdup profile averaged from 4-6 m. from downer entrance at superficial gas velocity (U_{sg}) of 10 m/s and solid circulation rate of 130 kg/m^2s

3. Axial Profile of Static Pressure

In the homogeneous flow, pressure-loss is the result of the friction between fluid and the wall. The pressure-loss in homogeneous flow is almost linearly dependent to the distance in the flow direction. However, in a particulate flow, pressure could decrease by the momentum transfer from fluid to solid phase beside the loss from wall-friction. The cross-sectional average axial pressure plot is shown in Figure 56. The pressure drops dramatically in the first meter because the momentum of gas is transferred to accelerate solids that are much slower at the beginning section of the downer in the first acceleration zone. This result agrees well with the axial solid velocity profile. From 1 to 2 meters, pressure decreases at slower rate indicating the second acceleration zone. These results can be seen clearer with the axial profile of the pressure gradient that is shown in Figure 57. The pressure gradient sharply increases until changes its slope at 1 meter and comes to a constant slope at 2 meters from the downer entrance. The pressure-drop after 2 meters is mainly the result of the friction-loss at the downer wall.

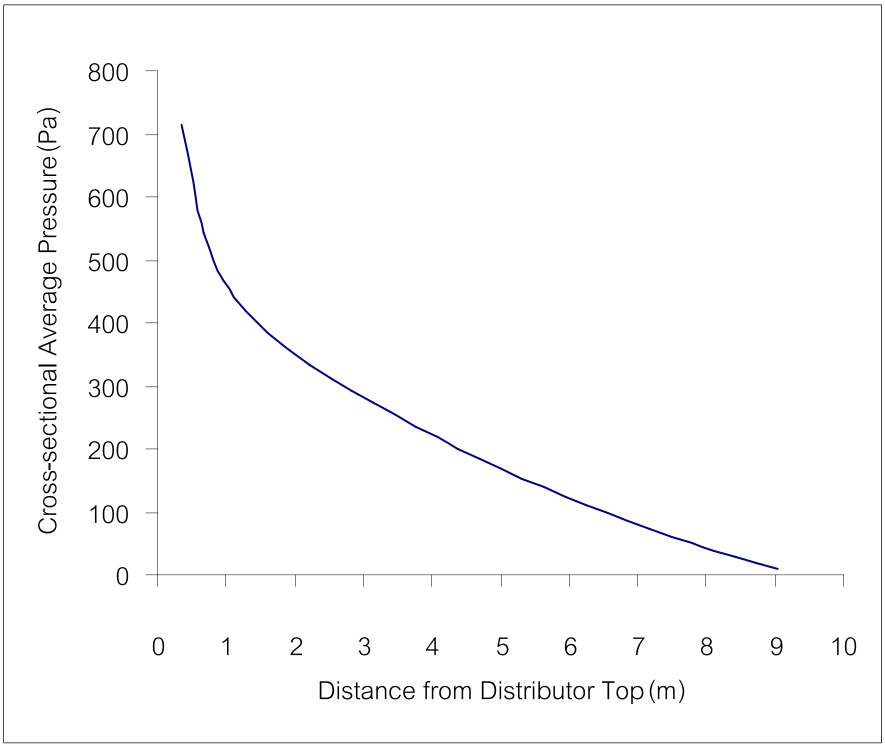

Figure 56 Axial static pressure profile at superficial gas velocity (U_{sg}) of 10 m/s and solid circulation rate of 130 kg/m^{2}s

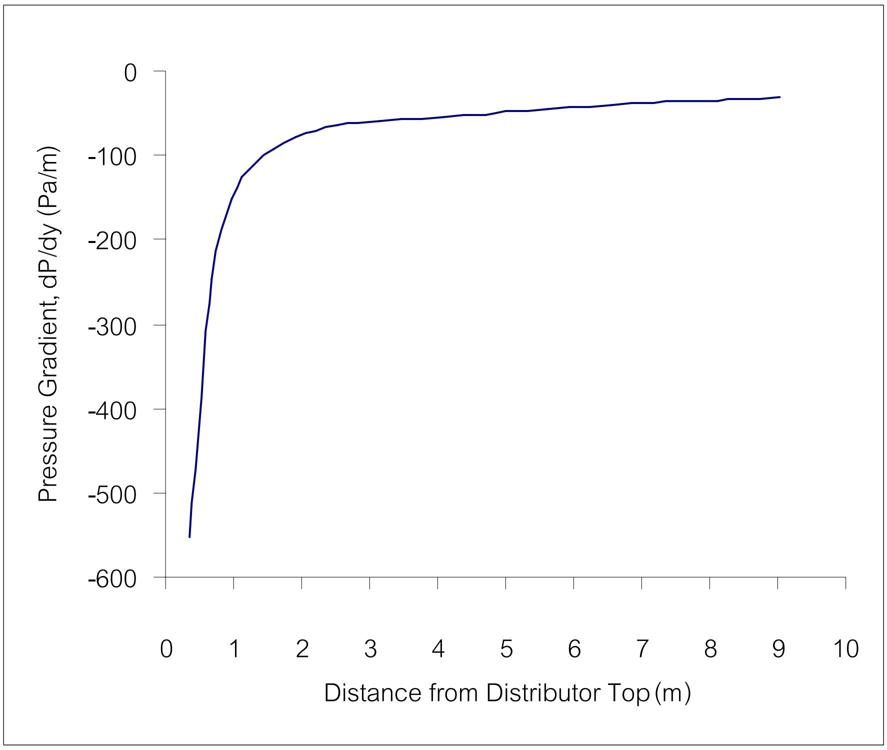

Figure 57 Axial pressure gradient (dp/dy) profile at superficial gas velocity (U_{sg}) of 10 m/s and solid circulation rate of 130 kg/m^{2}s

4. Radial Profiles of Solid Holdup and Velocity

In Figure 58, the radial solid holdup profiles at different axial position (h) are plotted. At the downer entrance (h=0.02 m.), solids distribute almost uniformly except at the center and the wall. Solids holdup profile is separated into core and annulus zone. The core zone has a uniform solid holdup while the annulus zone contains low content of solids. In this case, which has solid circulation rate of 134 kg/m^{2}s, the flat core has a uniform solid holdup of 0.009 at all axial positions. The average solid hold up in the annulus is about 2-3 times lower than the core holdup in this case. The low solid holdup in the annulus decreases the effective volume of the reactor because reactions take place only on the solids.

Down the column, solids at the wall move toward the center and create the peak of radial solid holdup profile. The solid holdup profiles present a peak at r/R = 0.6-0.8 as reported by many researchers (Yang *et al.*, 1991; Bai *et al.*, 1991; Wang *et al.*, 1992). The solid holdup peak moves toward the center at slower rate along the downer length. At 6 meters below the downer entrance, the solid concentration peak almost stops moving to the center. Solid holdup at the peak is 0.013, which is about 40-50 % higher than the value in the core..

As discussed earlier at the beginning of this part that solids are divided into core and annulus zones due to the effect of non-slip wall and create the solid holdup peak. In the core zone, solid and gas velocities do not increase much toward the center. After reaching gas velocity, solids that have more gravity force acting on themselves than gas try to move faster by shifting their positions toward the center where gas velocity is higher (lower drag). But the change in gas velocity decreases near the center, hence this might be the reason that the solid holdup peak moves toward center slower along the length of downer column.

Figure 59 shows solid velocity profiles at different axial positions. Solid velocity at the wall is always zero because of the non-slip condition. At the top of the downer (h=0.02 m.), solid velocity profile is quite uniform around 8 m/s. At 2.112 m. from the downer entrance, the solid velocity profile almost reaches its fully developed state. Solid velocity profile in the core is flat and decreases toward the wall in the annulus zone. The non-slip boundary at the wall should not affect the solid velocity profile in the core zone since there is low solid content in the annulus zone. Since most of solids stay in the core region where solid velocity does not vary much with the radial position, the residence time distribution (RTD) of the solid phase in a downer should be uniform and closer to that of plug flow than other types of fluidized bed reactors.

The solid velocity profile in a downer separates to core and annulus zones because of the effect of gas velocity that is low in the wall region and higher in the core zone. Even if the profiles look like the parabolic shape of homogeneous fluid flow in a pipe, the value in the core region is more flat and have a sharp drop at r/R= 0.85, which is the same point that solid volume fraction getting lower than its average value. Hence, the dimensionless radius position of 0.85 is the separation point between the core zone where most of the particles reside and the annulus zone, which becomes the stagnant region due to its slow flow and low solid content (low reaction).

Because solid particles are as small as 67 μm., the drag coefficient is high. This high value of drag coefficient makes the gas and solid radial velocity profile close to each other. The flat-like profile in the core of radial solid velocity profile in Figure 59 can be explained as a disturbance of a homogeneous gas system profile (parabolic) by the existence of solid particles. This profile shift from the parabolic shape proves that the existence of solid in a downer makes the flow more like plug flow and enhances the reactor performance.

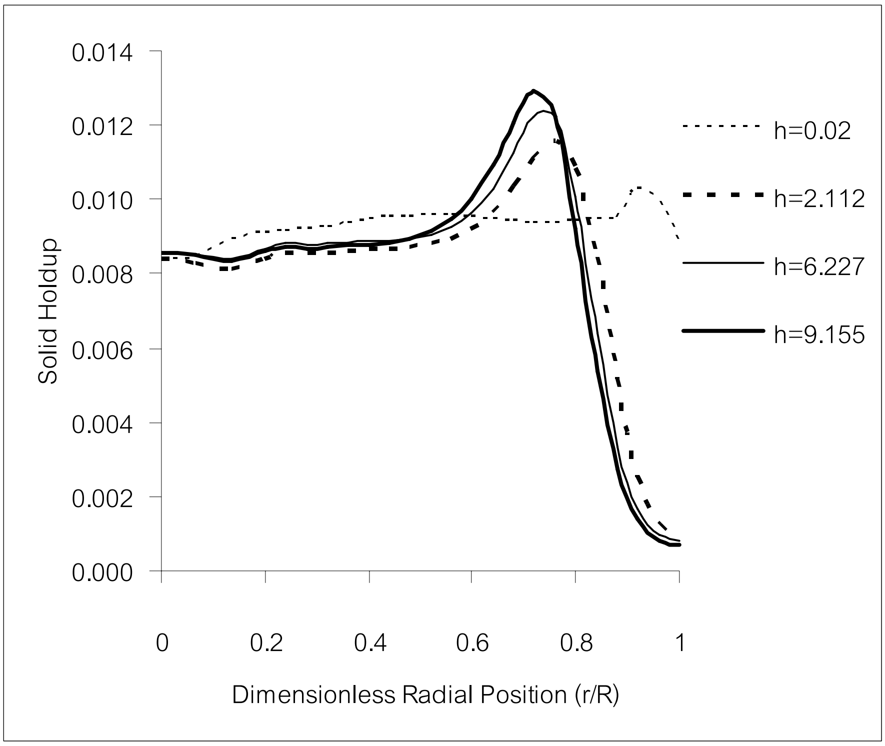

Figure 58 Radial solid holdup profile at different axial position at superficial gas velocity (U_{sg}) of 10 m/s and solid circulation rate of 130 kg/m^{2}s

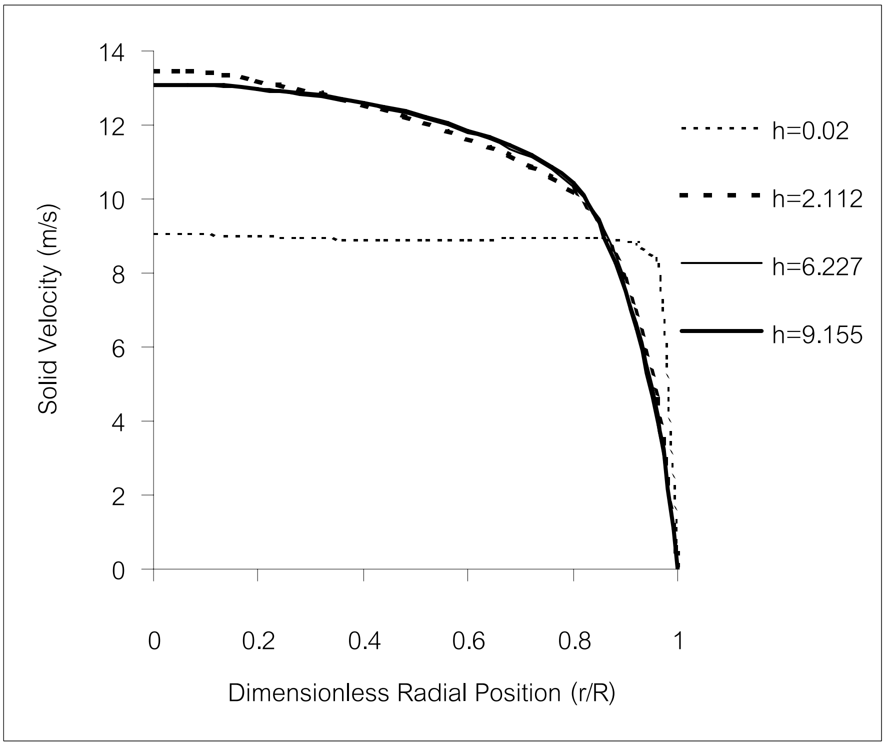

Figure 59 Radial solid velocity profile at different axial position at superficial gas velocity (U_{sg}) of 10 m/s and solid circulation rate of 130 kg/m^{2}s

Effects of Solid Circulation Rate on Hydrodynamics

The effects of solid circulation rate (G_s) on hydrodynamics are studied. The solid circulation rates of 100, 150, 200 kg/m^2s are simulated at the gas superficial velocity of 10 m/s. Figure 60 shows the effects of solid circulation rate on the axial solid holdup profiles. The ripples in the solid holdup profiles can be seen clearly from 1-4 m. The ripple is larger near the top then gets smaller until fade away after 4m. With higher solid circulation rate, the numbers of ripples is less but their sizes are larger. These ripples in axial solid holdup profiles are caused by the fluctuation of solid flow rate from the distributing tubes. Each ripple is caused by a cycle of the fluctuation in solid flow rate. With higher solid circulation rate, the fluctuations in solid flow rates are larger with longer periods for each cycle.

Solid circulation rate is an important factor to solid holdup. Solid holdup increases with higher solid circulation rate. As a matter of fact, solid holdup after reaching its fully develop state at 4 m. is almost linearly dependent with increasing solid circulation rate. Solid holdup of 0.009 for 150 kg/m^2s case is about 1.5 times higher than solid holdup of 0.006 at 100 kg/m^2s and solid holdup of 0.012 for 200 kg/m^2s case is about 2 times higher than solid holdup at 100 kg/m^2s. From these results, the cross-sectional average solid holdup could be roughly estimated by dividing solid circulation rate by superficial gas velocity and solid density.

The effects of solid circulation rate on axial solid velocity profiles of each case are shown in Figure 61. With higher solid circulation rate, solids accelerate slower at the beginning because there are more solids to be dragged by gas phase. But solid velocity with high circulation rate finally becomes higher than the solid velocity of low solid circulation rate as seen from the axial position from 1 m. to 2 m., which is in the second acceleration zone as mentioned in the section of the axial profiles of solid holdup and velocity. In the second acceleration zone, the solid velocity has already surpassed the gas velocity and is only accelerated by gravity. With higher solid content, the gas drag-back has less effect upon the solid phase; hence solids are able to move faster.

The radial solid velocity and solid holdup profiles are shown in Figure 62. The solid velocity profiles of each case are almost the same. Varying solid circulation rate has little effect on solid velocity profile but the difference in solid velocity profiles can still be seen. Solid velocity profiles in the cases with higher solid circulation rate provides flatter core than the lower ones. This is because more content of particles could induce more plug flow behavior in gas-solid flow system. The same result has also been reported by Zhang *et al*. (2000).

The flat core and the peak can be found in the radial solid holdup profile (see Figure 62). The peak radial position is between 0.6-0.8 as reported my many researchers (Yang *et al*., 1991; Bai *et al*., 1991; Wang *et al*., 1992). Solids first accumulate near the wall then moves toward center creating a peak in the radial solid holdup profile. The solid holdup peak continues moving toward the center along the downer length but at slower pace as solids move closer to the end of the downer. In

Table 7, the solid holdups in the flat core and at the peak are shown at 6.227 m. from the downer entrance, which is in fully developed zone. The peak holdup is about 50 % more than the core holdup in every case as shown in the last column of Table 7. The results from this table show that the solid holdup peak value does not depend upon solid circulation rate but is the ratio of the flat core holdup. From the results, the core holdup increases 0.003 for every 50 kg/m^2s of the solid circulation rate.

Table 7 Core and Peak Solid Holdup at 6.227 m. at 10 m/s superficial gas velocity and 1500 kg/m^3 solid density

Circulation Rate (kg/m^2s)	**Core Holdup**	**Peak Holdup**	**Peak/Core Ratio**
100	0.007	0.010	43 %
150	0.010	0.015	50 %
200	0.013	0.019	46 %

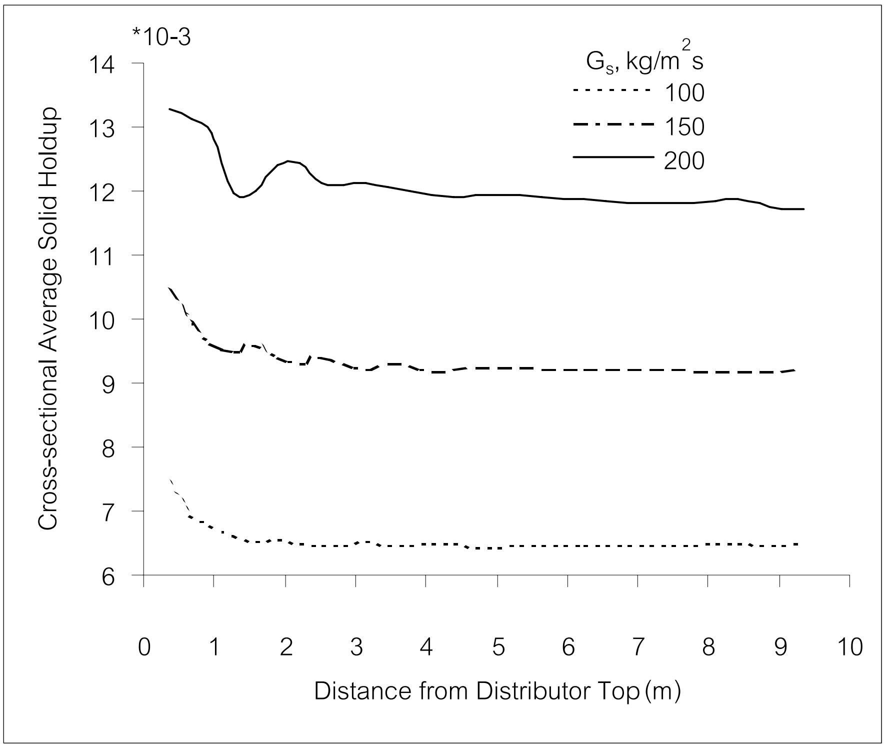

Figure 60 Axial solid holdup profiles, downer diameter = 0.1 m, downer height = 9.3 m, particle diameter = 67 μm, superficial gas velocity = 10 m/s

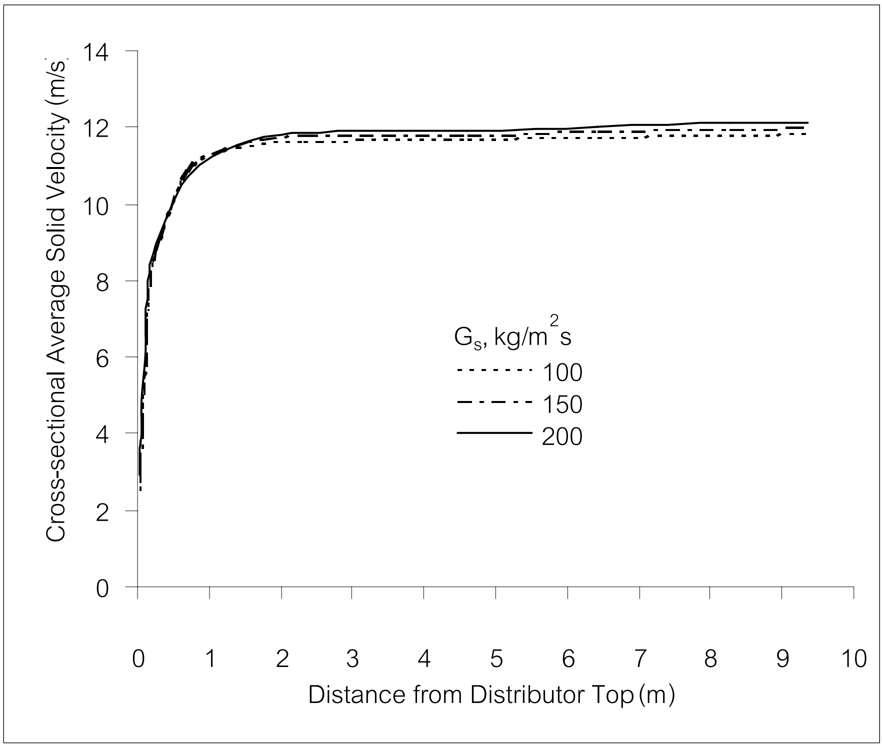

Figure 61 Axial solid velocity profiles, downer diameter = 0.1 m, downer height = 9.3 m, particle diameter = 67 μm, superficial gas velocity = 10 m/s

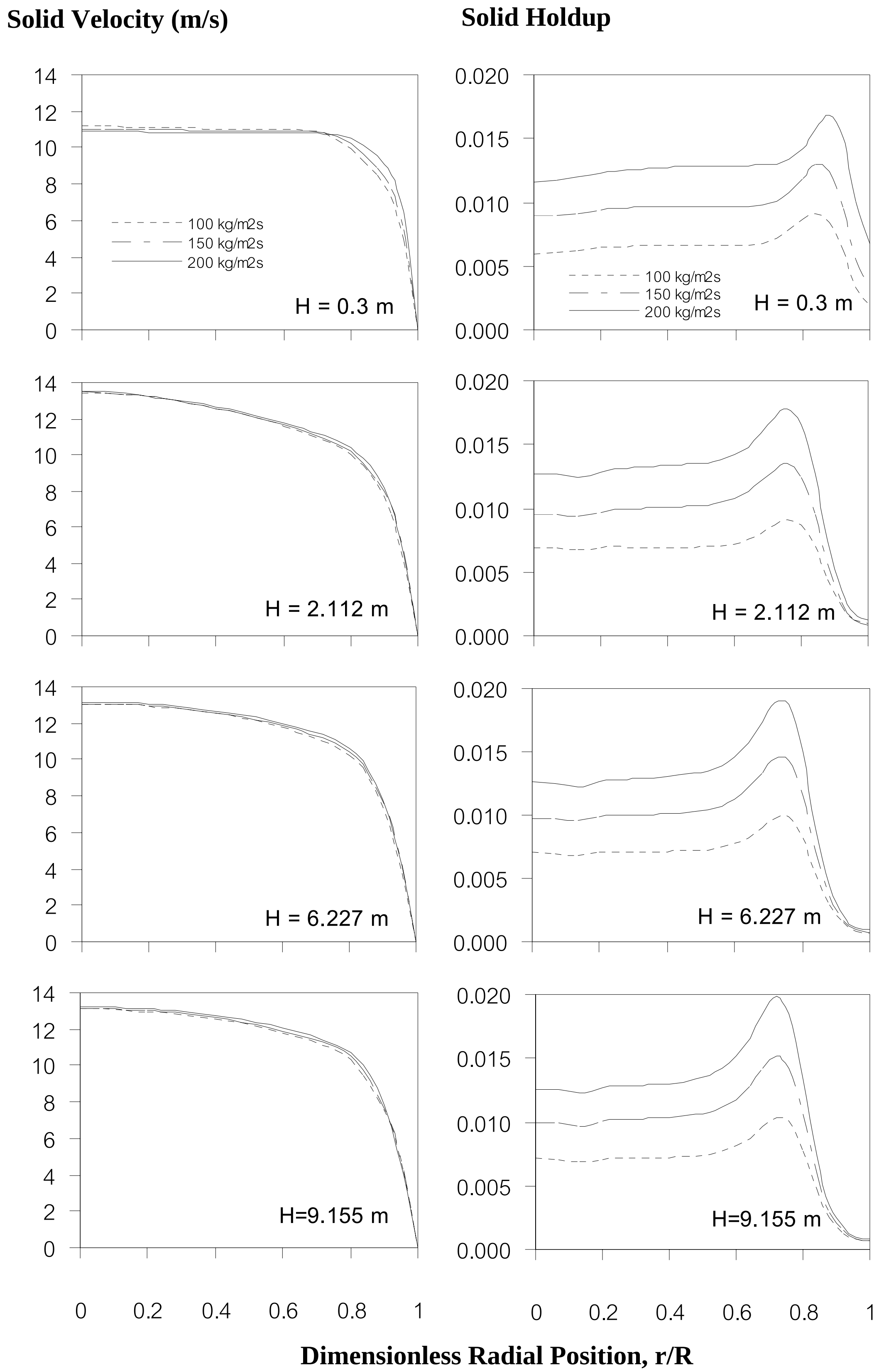

Figure 62 Radial solid velocity and solid holdup profiles, downer diameter = 0.1 m, downer height = 9.3 m, particle diameter = 67 μm, superficial gas velocity = 10 m/s

Comparisons of Simulation Results with Experimental Results

Zhang *et al*. (1999) and Yasemin *et al*. (2003) carried out experiments in a 9.3 m. high and 0.1 m. i.d. downer column and measured solid velocity and solid holdup by a fiber-optic probe.

The simulation results of this work will be compared to both experimental results of Zhang *et al*. (1999, 2000) and Yasemin *et al*. (2003). The experimental and conditions of Zhang *et al*. (1999) and Yasemin *et al*. (2003) are the same with the simulation conditions of this work, shown in Table 8.

Table 8 Experimental and Simulation Conditions

	Conditions
Particle Properties	
- Particle Density (kg/m^{2}s)	1500
- Particle Diameter (μm)	67
Operating Conditions	
- Gas Superficial Velocity (m/s)	10
- Solid Circulation Rate (kg/m^{2}s)	100, 200
Downer Sizes	
- Downer Diameter (m)	0.1
- Downer Height (m)	9.3

1. Comparison of Axial Solid Holdup and Solid Velocity Profiles

The axial solid holdup and solid velocity profiles have been compared with the experimental results of Yasemin *et al*. (2003) and shown in Figure 63 and Figure 64 respectively. The solid circulation rates of 100 and 200 kg/m^{2}s with gas superficial velocity at 10 m/s are the conditions chosen to be compared with experimental results. At the top of the downer, solid holdups of this works are lower than that from those of the experiment because they have higher velocities at downer top (see Figure 64). Solids in this works have a chance to accelerate themselves in the distributor above the downer and the acceleration rate of solids in this work is also higher than that of Yasemin's experiment. After 2 m, solid holdups of both cases from this work are similar to the experimental results.

The solid velocity profiles from this simulation are higher at the top of the downer and reach fully develop state at the axial distance before the solid velocity profiles of the experiments. The drag coefficient from this simulation might be higher than that of the experiments creating larger drag force and leading to larger acceleration rate. There is one thing in common between the simulation and the experimental results that solids in the case with higher circulation rate (200 kg/m^{2}s) accelerate slower at the downer top but become faster finally. For the simulation results, this effect can be seen from 0.7 to 2 m. from the simulation lines of Figure 64. As for the experimental results, the effect can be seen much clearer because solids accelerate slower than the simulation; hence this zone is longer. For experimental results, solids in the case of higher circulation rate move slower at 1.2 m from downer top, and then their velocities reach those of low circulation rate (100 kg/m^{2}s) at 4.4 m and become higher after this point.

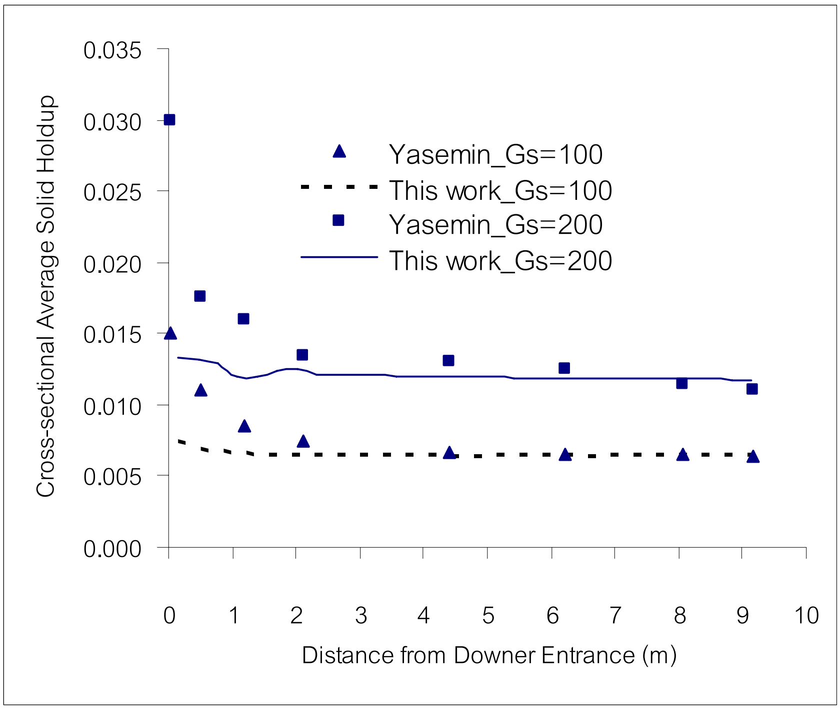

Figure 63 Axial solid holdup profiles compared with the experimental results of Yasemin *et al*. (2003), downer diameter = 0.1 m, downer height = 9.3 m, particle diameter = 67 μm, superficial gas velocity = 10 m/s

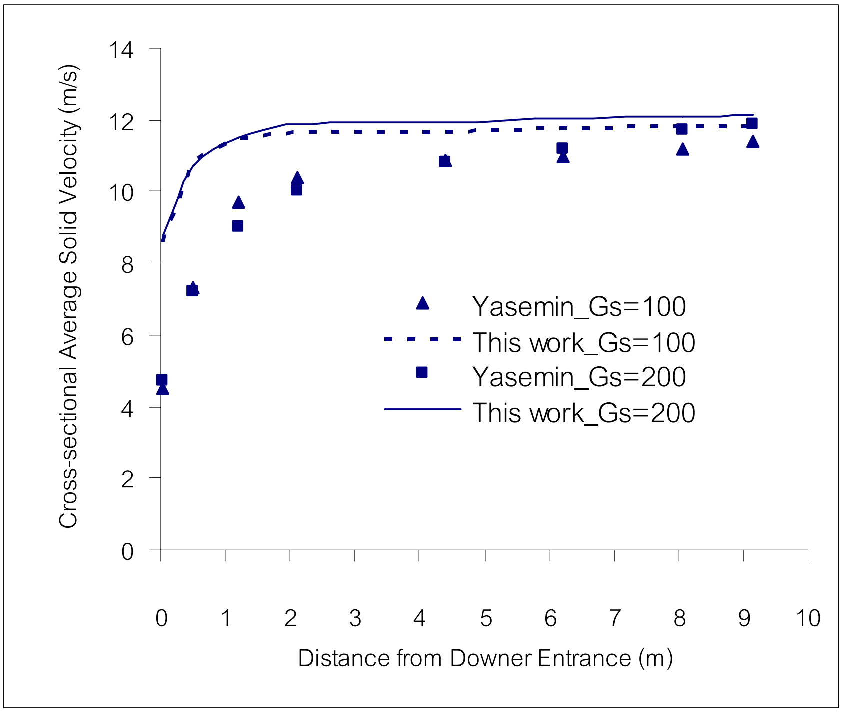

Figure 64 Axial solid velocity profiles compared with the experimental results of Yasemin *et al*. (2003), downer diameter = 0.1 m, downer height = 9.3 m, particle diameter = 67 μm, superficial gas velocity = 10 m/s

2. Comparison of Radial Solid Holdup and Solid Velocity Profiles

Radial solid holdup and solid velocity profiles with solid circulation rate of 100 kg/m^{2}s and superficial gas velocity of 10 m/s from this work have been compared with the experimental results of Zhang *et al*. (1999, 2000) in Figure 65 and Figure 66, respectively. The radial profiles of both figures are plotted at two axial positions, 4.4 and 8 m from the downer top to see the development of the radial profiles from both the simulation and the experiment. The radial solid holdup profile from this work shows the distinct peaks in the radial position range of 0.6-0.8 along the downer length, which is different from Zhang's profiles. The radial solid holdup profiles from the experiment show their peaks as well but the peak is collapsed at 8 m from downer top. The core holdup (r/R = 0 - 0.5) of the experiment increases with the downer length while the core holdup from this simulation does not change with axial position. For the experimental result, solids in the peak are collapsed into the core zone making the peak disappear and the core holdup increases. This could conclude that there is more radial movement of solids into the core zone in the experiment of Zhang than in the simulation results of this work.

After the collapse of the peak at 8 m, the core holdup at r/R = 0 - 0.6 from this work agrees well with the experimental result but the holdups in the annulus zone at r/R = 0.6 - 1 are different. For r/R = 0.6 – 0.85, the holdup of this simulation is higher than the holdup of the experiment because the peak of the simulation does not collapse into the core zone. However, for the area near the wall (r/R = 0.85 –1), the solid holdup of the experiment is higher than the holdup of this simulation. The reason for the low solid content in this zone (r/R = 0.85 – 1) is because of the low solid velocity near the wall (non-slip boundary) set in this simulation. The solids near the wall of this simulation will migrate in the direction to the core where they are able to move faster because the gas velocity is faster there.

The radial solid velocity profiles are shown in Figure 66. In the experiment of Zhang, solid velocity increases more than the solid velocity from this simulation from 4.4 to 8 m because it reaches fully develop slower than the case of simulation. At 8 m, solid velocity in the core zone (r/R = 0 - 0.6) from the experiment is equal to that of the simulation. However, in the annulus zone, solid velocity of the experiment is higher than that of the simulation due to the non-slip wall and the assumption of two-fluid model that consider the particles as a continuous phase instead of discrete elements, which might be different from the true behavior.

By comparing the radial profiles of the simulation and the experiment, the resemblances in the solid velocity and solid holdup profiles between both methods after reach their fully develop states at 8 m can be seen. The differences between the simulation and experiment profiles in the annulus zone may be occurred due to the non-slip wall and the assumptions of two-Fluid model. The radial profiles of this simulation reach their fully develop state faster than the experiment and change their shapes only little from 4.4 m to 8 m. But for the experimental result, there are big changes in the solid holdup profiles from 4.4 m to 8 m even the solid velocity profile does not change much.

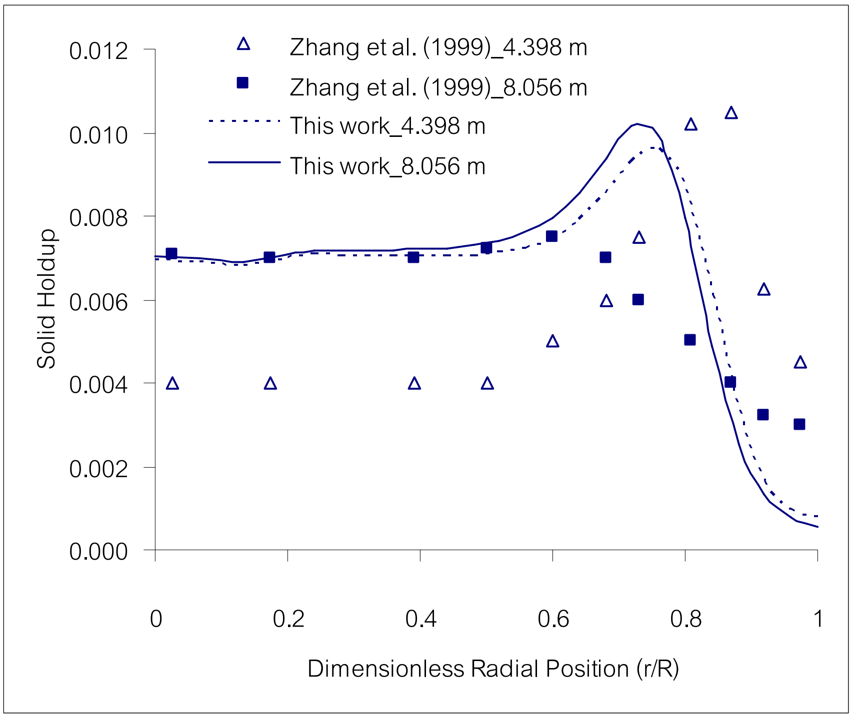

Figure 65 Radial solid holdup profiles compared with the experimental results of Zhang *et al*. (1999) at G_s=100 kg/m^{2}s, downer diameter=0.1 m, downer height=9.3 m, particle diameter=67 μm, superficial gas velocity=10 m/s

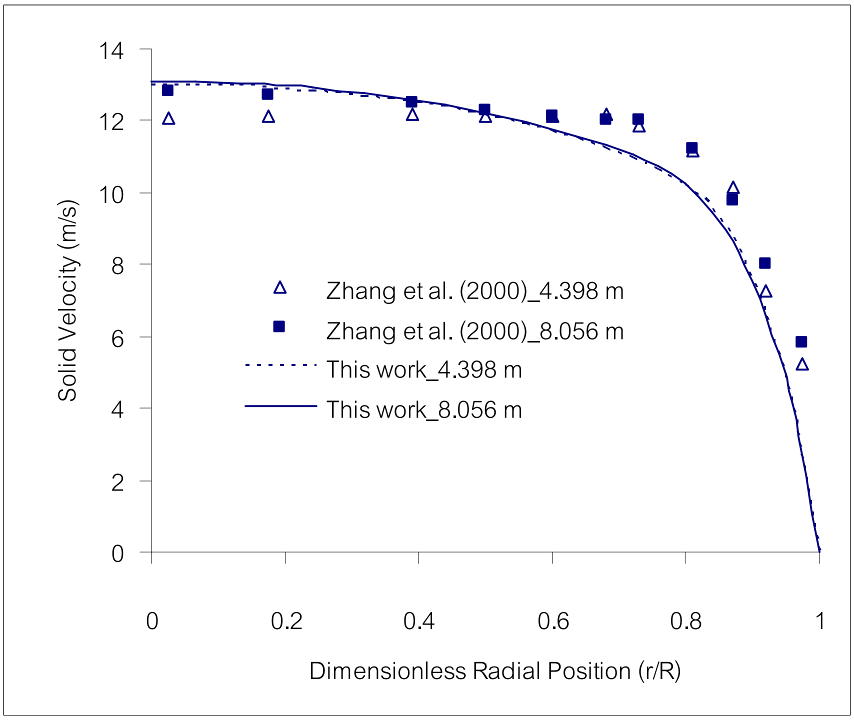

Figure 66 Radial solid velocity profiles compared with the experimental results of Zhang *et al*. (2000) at G_s=100 kg/m^{2}s, downer diameter=0.1 m, downer height=9.3 m, particle diameter=67 μm, superficial gas velocity=10 m/s

3. Comparison of Axial Pressure and Pressure Gradient Profiles

The axial pressure and pressure gradient profiles of this work are compared with those of Zhang *et al*. (1999). In Figure 67, the pressure difference between the measuring point and the downer entrance is plotted against the axial positions. In the first meter (acceleration zone), pressure drops enormously because of the drag force given to the solids. The pressure-drop of the experiment is more than that of this simulation in the first meter. The reasons are that there are more solids in this zone of the experiment than the simulation as shown in the comparison of axial solid holdup profile section, and solid velocity at the downer top of the experiment is lower resulting in more drag force (more velocity difference between gas and solids). For the experiment, the pressure-gain from solid weight surpasses the pressure-loss from the drag force and the wall friction below the first meter resulting in an increasing pressure. However, the pressure of the simulation continues decreasing after 1 m but with lower rate. Since solids already move at high velocity and do not create pressure-loss from drag force, the only reason to the decreasing pressure is the wall friction. In the two-fluid model, with non-slip wall, the force transferring from the solid phase to the wall (also from the gas phase) could be large enough to overcome the solid weight.

The axial pressure gradient is plotted in Figure 68. The axial pressure gradients from both the experiment and this simulation have the same shape. Both profiles have a linear increasing at the top section and their slopes decrease until they become constant finally. The profile of the experiment changes its slope later at 0.9 m while the profile of the simulation changes slope at 0.7 m. This fact indicates that the experimental results have longer acceleration zone. The final pressure gradient of the experiment is higher because its pressure starts increasing after 1 m from the downer entrance while that of the simulation decreases.

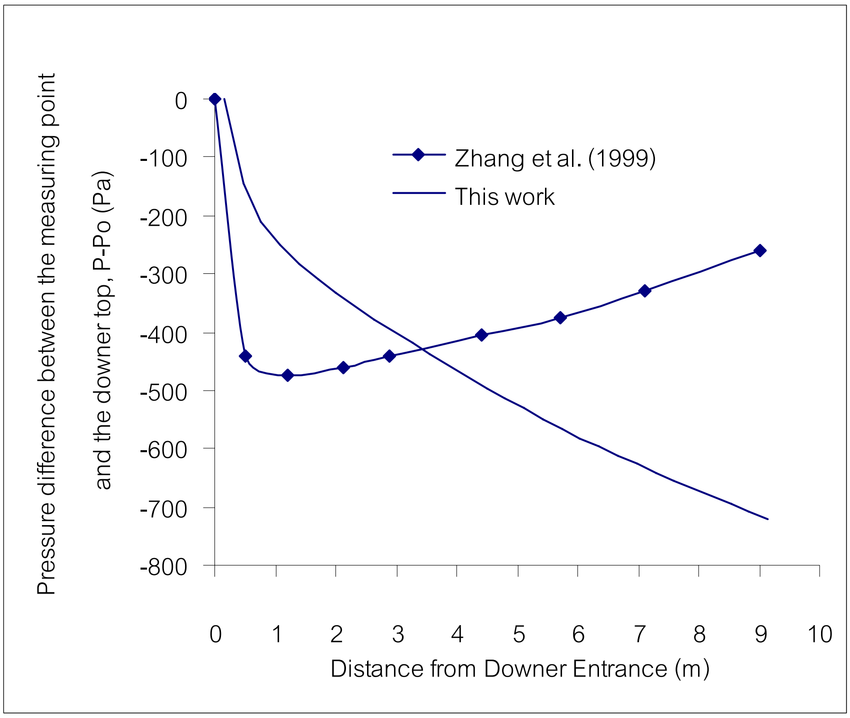

Figure 67 Axial pressure profile compared with the experimental result of Zhang *et al.* (1999) at $G_s = 100$ kg/m^{2}s, downer diameter = 0.1 m, downer height=9.3 m, d_p = 67 μm, superficial gas velocity = 10 m/s

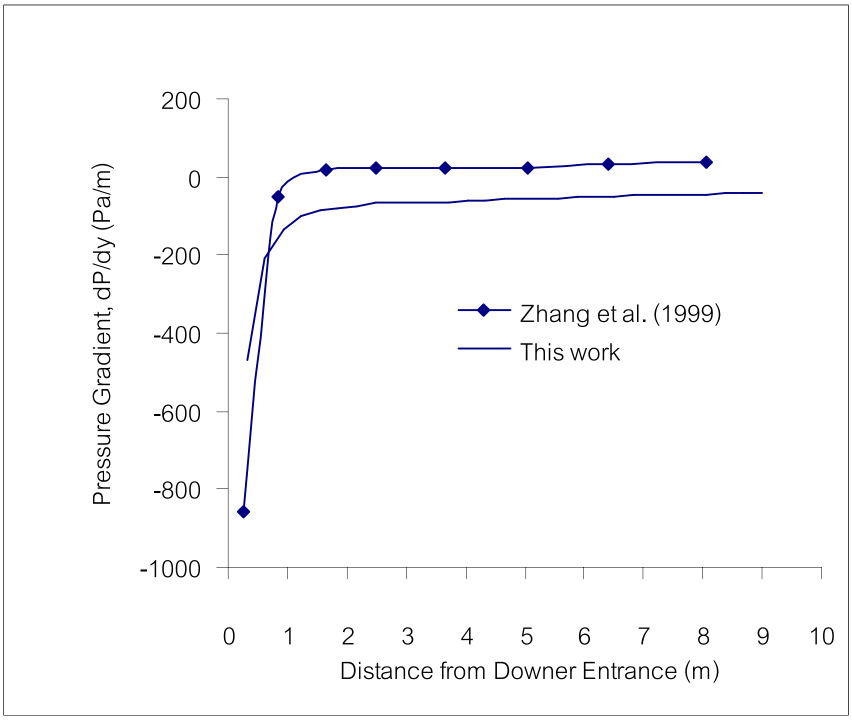

Figure 68 Axial pressure gradient profiles compared with the experimental result of Zhang *et al.* (1999) at $G_s = 100$ kg/m^{2}s, downer diameter = 0.1 m, downer height = 9.3 m, d_p = 67 μm, superficial gas velocity = 10 m/s

Comparisons of Two Fluid Model and Discrete Element Model

The simulation results of this work, which use two-fluid model (TFM), were compared with the discrete element model (DEM) simulation results of Thanomboon (2005). The axial and radial profiles of solid holdup and solid velocity are plotted together to see the difference. The simulation conditions of these two models are shown in Table 9.

Figure 69 shows the axial solid holdup profiles of both cases. The axial solid holdup profile of Thanomboon (2005) seems to decrease greatly in the first 2 meters of the downer while the axial solid holdup profile of this work decreases only little. However, after 2 meters, both axial solid holdup profiles remain constant.

Figure 70 shows the axial solid velocity profiles of both cases. The axial solid velocity profile of Thanomboon (2005) increases slower than that of this work. However, the particle velocity of Thanomboon (2005) keeps increasing throughout the downer length. On the other hand, the axial solid velocity profile of this work takes only 2 meters to reach fully development and stays constant. The reason that the particles in this work have more accelerating rate at the beginning might be their smaller size, which provides more drag force upon the particle phase. However, after the first acceleration zone, which is around 0.7 m for both cases, the particle velocity of this work increases slightly from 11 to 11.9 m/s while the particle velocity of Thanomboon (2005) increases from 6 to 11.2 m/s and seems to keep increasing if the downer is longer. The particle velocity of Thanomboon (2005) is still increasing in its second acceleration zone at the end of the downer because the drag force has less effect on these big particles.

Figure 71 shows the radial solid holdup profiles of both cases at various distances from the downer top. The solid holdup peaks of Thanomboon (2005) are smaller than this work. Both profiles do not change their shapes much. However, the holdup of Thanomboon (2005) decreases with axial distances while the holdup of this work does not change after 2 m.

Figure 72 shows the radial solid velocity profiles of both cases at various distances from the downer top. The shapes of both radial solid velocity profiles are different. The profiles of Thanomboon (2005) are flat while the profiles of this work gradually decrease in the core and decrease greatly near the wall. The main reason of the difference in the profiles shape might be the non-slip wall boundary condition in this work

In the two-fluid model, the particle phase is treated like the other fluid phase other than the gas phase. The wall boundary conditions might affect the profiles of solid holdup and solid velocity. However, the discrete element model treats each particle as individual. The wall boundary conditions have less effect upon the profiles of solid holdup and solid velocity. One of these effects that can be seen clearly is the radial solid velocity profiles. The radial solid velocity profile of this work have a slope due to the wall friction while the radial solid velocity profile of Thanomboon (2005), which uses discrete element model, is flat.

Table 9 Simulation Conditions

	This work	**Thanomboon**
Method	TFM	DEM
Particle Properties		
- Particle Density (kg/m^2s)	1,500	1,500
- Particle Diameter (μm)	67	1,400
Operating Conditions		
- Gas Superficial Velocity (m/s)	10	10
- Solid Circulation Rate (kg/m^2s)	130	142
Downer Sizes		
- Downer Diameter (m)	0.1	0.1
- Downer Height (m)	9.3	9.3

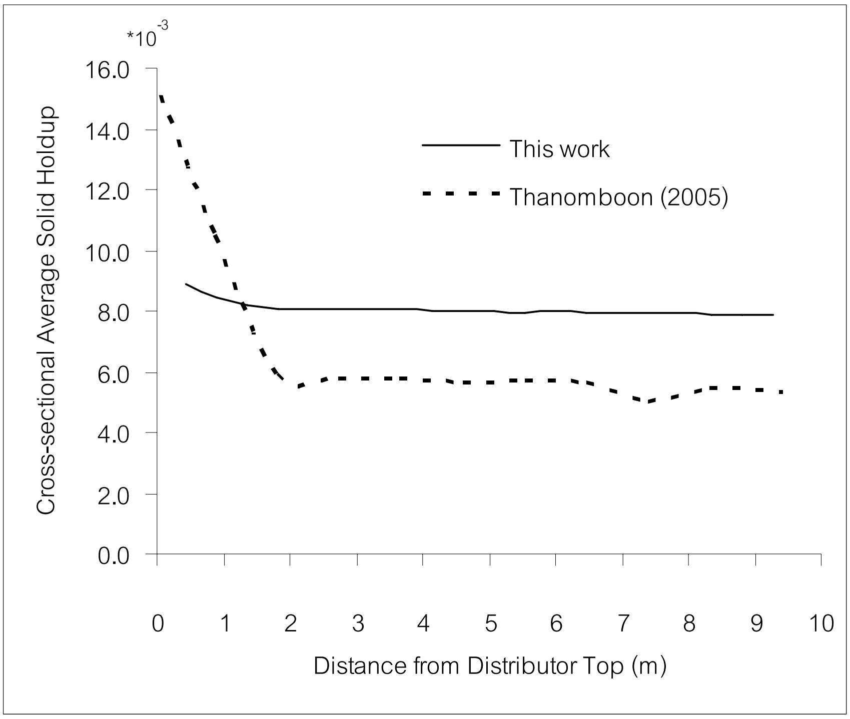

Figure 69 Axial solid holdup profiles, downer diameter = 0.1 m, downer height = 9.3 m, this work d_p = 67 μm, Thanomboon d_p = 1.4 mm, superficial gas velocity = 10 m/s

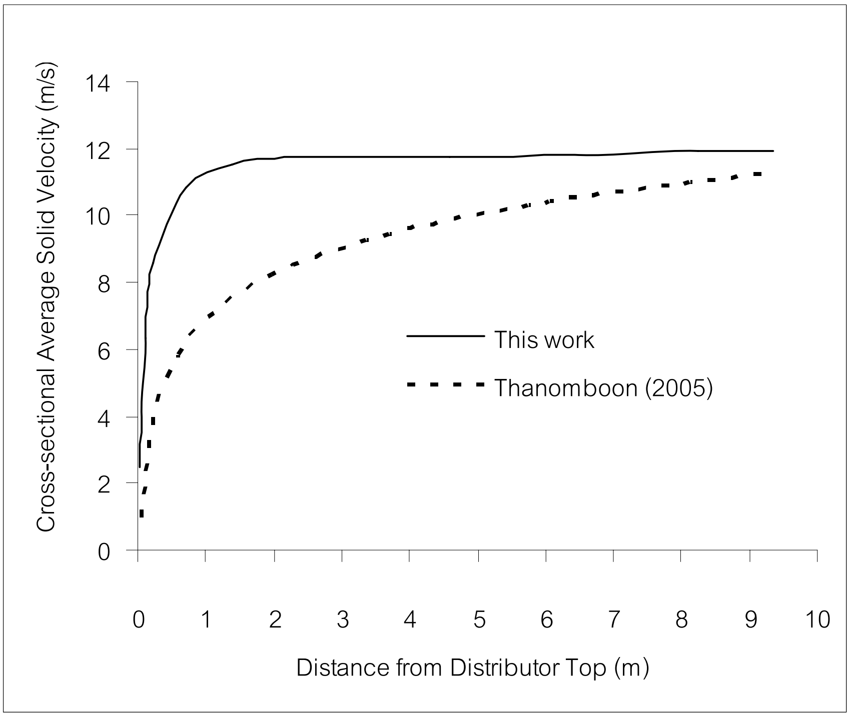

Figure 70 Axial solid velocity profiles, downer diameter = 0.1 m, downer height = 9.3 m, this work d_p = 67 μm, Thanomboon d_p = 1.4 mm, superficial gas velocity = 10 m/s

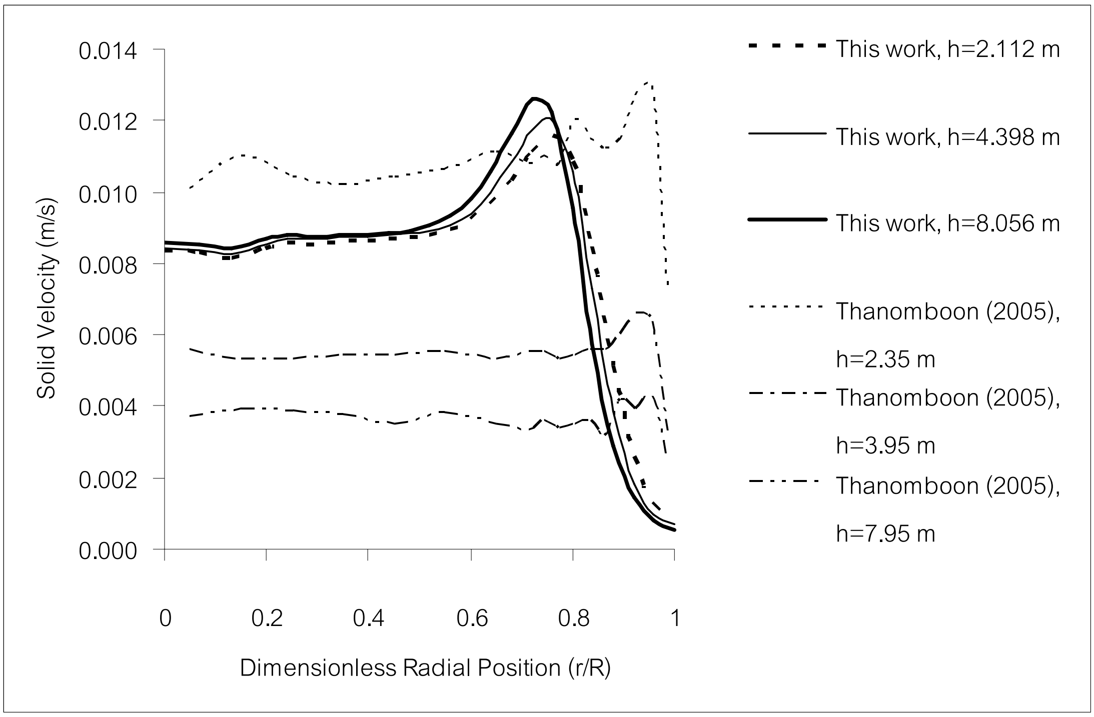

Figure 71 Radial solid holdup profiles, downer diameter = 0.1 m, downer height = 9.3 m, this work d_p = 67 μm, Thanomboon d_p = 1.4 mm, superficial gas velocity = 10 m/s

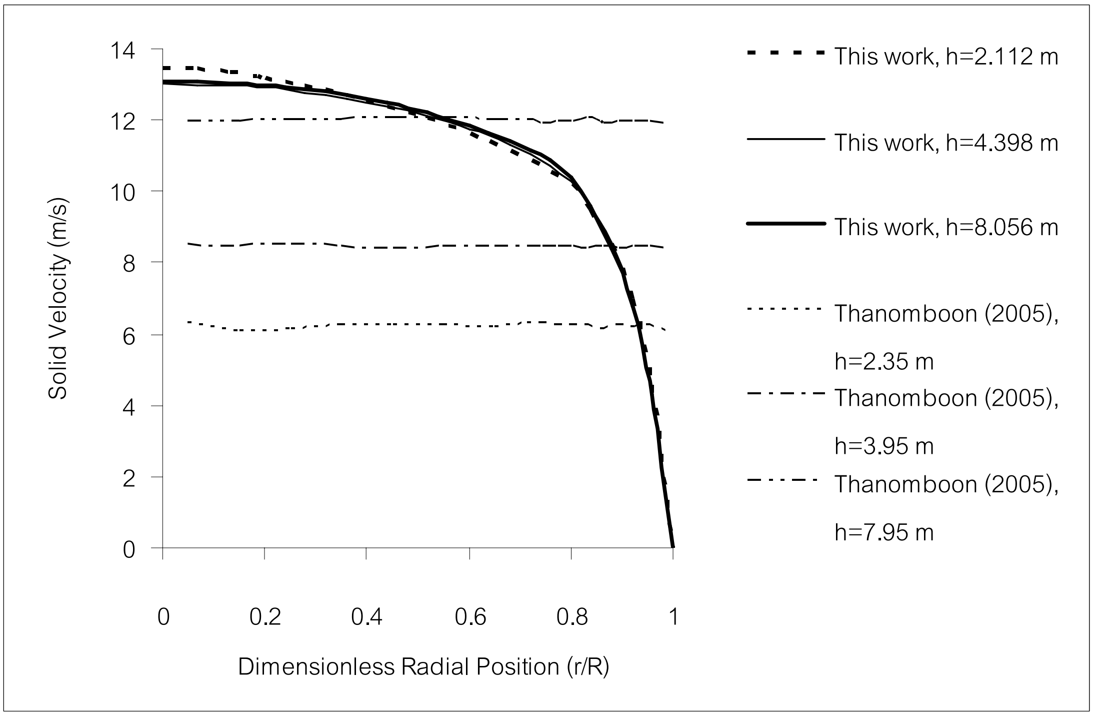

Figure 72 Radial solid velocity profiles, downer diameter = 0.1 m, downer height = 9.3 m, this work d_p = 67 μm, Thanomboon d_p = 1.4 mm, superficial gas velocity = 10 m/s

CONCLUSIONS

The 2-D circulating fluidized bed downer model is designed in this work. The model components consist of a 9.3 m in length and 0.1 m in diameter downer column, a riser, two gas-solid separators, and two storage tanks. At the wall, non-slip boundary condition is applied to both gas and solid phases. The solid distributing tubes and gas-solid separators are specially designed to enhance the downer reactor hydrodynamics. The two-fluid model is used as a mathematical model to characterize the gas-solid flow systems. This model considers the particle phase as the other fluid phase using the Eulerian approach. The pressure and viscosity of the solid phase are calculated by using the method of solid oscillating energy (granular temperature). More over, the k-ε turbulence model is used on both gas and solid phase to accurately predict the hydrodynamics in the domain.

1. Components Designs

1.1 In a real 3-D downer reactor, the cyclones are used to separate particles from the gas phase; however, the cyclone cannot be modeled in 2 dimensions. In this 2-D model, particles are separated from the gas phase using the gas-solid separator. The gas-solid separator uses the concept of centrifugal force to separate particles from the gas phase. The gas-solid separator has the advantages in separating most of the particles and is able to deal with high flow rates of both gas and particles comparing with the settling tank that uses only the gravity force.

1.2 The downer model with fewer solid distributing tubes does not have the uniform radial solid distribution as the model with more solid distributing tubes. The non-uniform of radial solid distribution in the downer model with 4 tubes can be seen clearly by the radial solid holdup profile. The solid holdup peaks are located at the same radial position of the distributing tubes. In this work, the downer model with 12 solid distributing tubes was used and shows better performance to distribute particles uniformly than the model with only 4 solid distributing tubes.

2. Hydrodynamics in a Downer

2.1 The flow in a downer is separated into core and annulus zones. There is relatively high solid concentration and velocity with uniform profiles in the core. On the contrary, there is low content of particles in the annulus zone with low velocity due to the wall friction. The model can predict the solid holdup peak in a downer reactor at r/R = 0.6-0.8 as reported by many researchers (Yang *et al*., 1991; Bai *et al*., 1991; Wang *et al*., 1992). The solid holdup peak is occurred from the migration of the particles near the wall toward the center of the downer. The radial position of solid holdup peak is closer to the center at more distance from the downer entrance. At 6 meters below the downer entrance, the solid holdup profile almost stops changing. The solid holdup at the peak is about 50 % higher than the holdup in the core of the downer.

2.2 The hydrodynamics in the downer column was formed to be 3 zones; the first acceleration zone, the second acceleration zone, and the constant solid velocity zone. In the first acceleration zone from 0-0.7 m, particles are accelerated at fast rate by both gas-drag and gravity and their velocities increases dramatically. The gas-drag plays important roles in the downer reactor because the particles are small, hence having high inter-phase drag coefficient. In the second acceleration zone from 0.7-2 m, solid velocity surpasses gas velocity and only accelerated by gravity at much slower rate. In the constant solid velocity zone after 2 m from the downer entrance, the gravity force balances with the gas-drag resulting in the constant solid velocity in this zone.

2.3 The axial pressure profile agrees well with the axial solid velocity profile. In the first acceleration zone, pressure drops enormously because of the momentum transferred to the solid phase. After the first acceleration zone, the pressure decreases slower with the downer length. Solid weight also helps in reducing the pressure-drop in the downer column. The effect of solid weight on the axial pressure-drop will be seen clearer if there are more particles in the downer column (higher solid circulation rate).

2.4 By comparing hydrodynamics in the downer at different solid circulation rate (G_s), these conclusions are found. Axial solid holdup is linearly dependent with solid circulation rate (G_s). The cross-sectional averaged solid holdup increases linearly with the increasing solid circulation rate (G_s). The drag-back force of the gas phase has less effect upon the particle phase at high solid circulation rate in the second acceleration zone. Therefore the particle velocity with higher G_s can increase more. The case with higher solid circulation rate also has a wider core in the solid velocity profile because there are more interactions among particles which induce more plug flow behavior of the solid phase. These facts agree that the hydrodynamics in a downer reactor resembles that of the ideal plug flow reactor; hence gives more uniform solid and gas residence time distribution. This reason also makes a circulating fluidized bed downer suitable for multiple reaction processes where the uniform resident time distribution (RTD) of both reactant gas and particles are important to yield high product selectivity.

2.5 The radial solid holdup and solid velocity profiles from this simulation are compared with the experimental results of Zhang *et al*. (1999). At the beginning of the downer, the radial solid holdup of the experiment has lower value than that of the simulation in the core zone. However, the solid holdup in the core zone of Zhang *et al*. (1999) increased to the same value of the simulation at the bottom section of the downer. Both radial solid holdup profiles from the experiment and the simulation have the peak near the wall of the downer but the solid holdup peak of Zhang *et al.* (1999) disappeared at the end of the downer. Solid velocity in the core zone (r/R = 0 - 0.6) from the simulation is equal to that of the experiment. However, in the annulus zone, solid velocity of the simulation is lower than that of the experiment due to the non-slip wall setting.

2.6 The axial solid holdup and solid velocity profiles from this simulation have been compared with the experimental results of Yasemin *et al*. (2003). At the beginning of the downer, solid holdup from this simulation is lower than that of the experiment because they have more velocities. However, after 2 m from downer entrance, solid holdup from this simulation is similar to the experimental result. The solid velocity profiles from this simulation are higher at the top of the downer and reach fully develop state at the axial distance before the solid velocity profiles of the experiments. The drag coefficient from this simulation might be higher than that of the experiments creating larger drag force and leading to larger acceleration rate.

2.7 By comparing the axial pressure profile of this simulation and the experiment of Zhang *et al*. (1999), the pressure-drop in the first meter section of the downer in this simulation is less than that of the experiment because there are less particles with higher velocity in this simulation. After 1 meter, the pressure of the simulation decreases while the pressure of the experiment increases indicating that the pressure-drop from the wall friction of this simulation is more. This might occurs from the non-slip boundary setting of the particle phase at the wall.

LITERATURE CITED

Anderson, T.B. and R. Jackson. 1967. A Fluid Mechanical Description of Fluidized Beds. **I&EC Fundamental.** 6: 527-539.

Bai, D.R., Y. Jin, Z.Q. Yu and N.J. Gan. 1991. Radial profiles of local solid concentration and velocity in a concurrent downflow fast fluidized bed. **Circulating fluidized bed technology III.** Pergamon Press, Toronto.

Deng, R., F. Wei, T. Liu and Y. Jin. 2002. Radial behavior in riser and downer during the FCC process**.** **Chemical Engineering and Processing.** 41: 259-266.

Ergun, S. 1952. Fluid flow through packed columns. **Chemical Engineering Progress.** 48: 89-94.

Gidaspow, D., R. Bezburuah and J. Ding. 1992. Hydrodynamics of Circulating Fluidized Beds, Kinetic Theory Approach, pp. 75-82. **Fluidization VII**, Proceedings of the 7th Engineering Foundation Conference on Fluidization.

Grace, J.R., A.A. Avidan and T.M. Knowlton. 1997. **Circulating Fluidized Beds.** Chapman & Hall.

Huilin, L., D. Gidaspow, J. Bouillard, L. Wentie. 2003. Hydrodynamic simulation of gas–solid flow in a riser using kinetic theory of granular flow. **Chemical Engineering Journal.** 95:1–13.

Herbert, P.M., T.A. Gauthier, C.L. Briens, M.A. Bergougnou. 1995. Application of fiber optic reflection probes to the measurement of local particle velocity and concentration in gas-solid flow. **Powder Technology.** 80: 243-252.

Kawaguchi, T., M. Sakamoto, T. Tanaka and Y. Tsuji. 2000. Quasi-three-dimension of spouted beds in cylinder. **Powder Technology.** 109: 3-12.

Kimm, N.K., F. Berruti and T.S. Pugsley. 1996. Modeling the hydrodynamics of downflow gas-solids reactors. **Chemical Engineering Science.** 51(11): 2661-2666.

Kunii, D. and O.Levenspiel. 1997. Circulating fluidized-bed reactors. **Chemical Engineering Science.** 52(15): 2471-2482.

Lun, C. K. K., S. B. Savage, D. J. Jeffrey and N. Chepurniy. 1984. Kinetic Theories for Granular Flow: Inelastic Particles in Couette Flow and Slightly Inelastic Particles in a General Flow Field. **J. Fluid Mech.** 140:223-256.

Miller, A. and D. Gidaspow. 1992. Dense, vertical gas–solids flow in a pipe. **AIChE J.** 38:1801–1813.

Namkung, W. and S.D. Kim. 2000. Radial gas mixing in a circulating fluidized bed. **Powder Technology.** 113: 23-29.

Ogawa S., A. Umemura, and N. Oshima. 1980. On the Equation of Fully Fluidized Granular Materials. **J. Appl. Math. Phys.** 31:483.

Thanomboon, N. 2005. **Modeling and Simulation of Particle and Gas Movement in a Down-Flow Circulating Fluidized Bed Reactor.** M.S. thesis, Kasetsart University.

Wang, Z., D. Bai and Y. Jin. 1992. Hydrodynamics of cocurrent downflow circulating fluidized bed (CDCFB). **Powder Technology.** 70: 271-275.

Yasemin, B., B. Farnco, Z. Jesse, M. Bruce. 2003. Modeling circulating fluidized bed downers. **Powder Technology.** 132: 85– 100.

Zhang, H. and J.X. Zhu. 2000. Hydrodynamics in downflow fluidized beds (2): Particle velocity and solids flux profiles. **Chemical Engineering Science.** 55: 4367-4377.

Zhang, H., J.X. Zhu and M.A. Bergougnou. 1999. Hydrodynamics in downflow fluidized beds (1): solids concentration profiles and pressure gradient distributions. **Chemical Engineering Science.** 54: 5461-5470.

Zhang, M., Z. Qian, H. Yu and F. Wei. 1999. The near wall dense ring in a large-scale down-flow circulating fluidixzed bed. **Chemical Engineering Science.** 54: 5461-5470.

Zhang, M., Z. Qian, H. Yu and F. Wei. 2003. The solid flow structure in a circulating fluidized bed riser/downer of 0.42-m. diameter. **Powder Technology.** 129: 46-52.

Zhu, J.X. and S.V. Manyele. 1998. Radial non-uniformity index (RNI) in fluidized beds and multiphase flow systems. **48th Canadian Chemical Engineering Conference.** London.

APPENDIX

Model Geometry Design in Gambit 2.2.30

1. Create geometry as shown in Appendix Figure 1. The detail geometries are shown in the "Geometry Domain" section under "Methodology".

2. Click "SPECIFY BOUNDARY TYPES COMMAND BUTTON" to specify boundary conditions. The names assigned in these tables are only for better understanding and can be changed.

2.1 Inlets

Name	Edges	Types
Main fluidizing gas	13 inlets at the bottom of solid distributing tubes	VELOCITY_INLET
Minimum fluidizing gas	24 inlets at the top of solid distributing tubes	VELOCITY_INLET
	2 inlets at the bottom of the top storage tank	
Circulating air	1 inlet at the bottom of the riser	VELOCITY_INLET

2.2 Outlets

Edges	Types
Product gas outlet	OUTLET_VENT
Circulating air outlet	OUTLET_VENT
Top storage tank vent	OUTLET_VENT
Top separator vent	OUTLET_VENT
Bottom separator vent	OUTLET_VENT

2.3 Free-slip walls

Name	Edges	Types
Solid distributing tube walls	24 solid distributing tube walls	SYMMETRY
Distributor wall	Solid distributor wall	SYMMETRY

2.4 Axisymmetric axis

Edges	Types
All edges lying on the axisymmetric axis of the model	AXIS

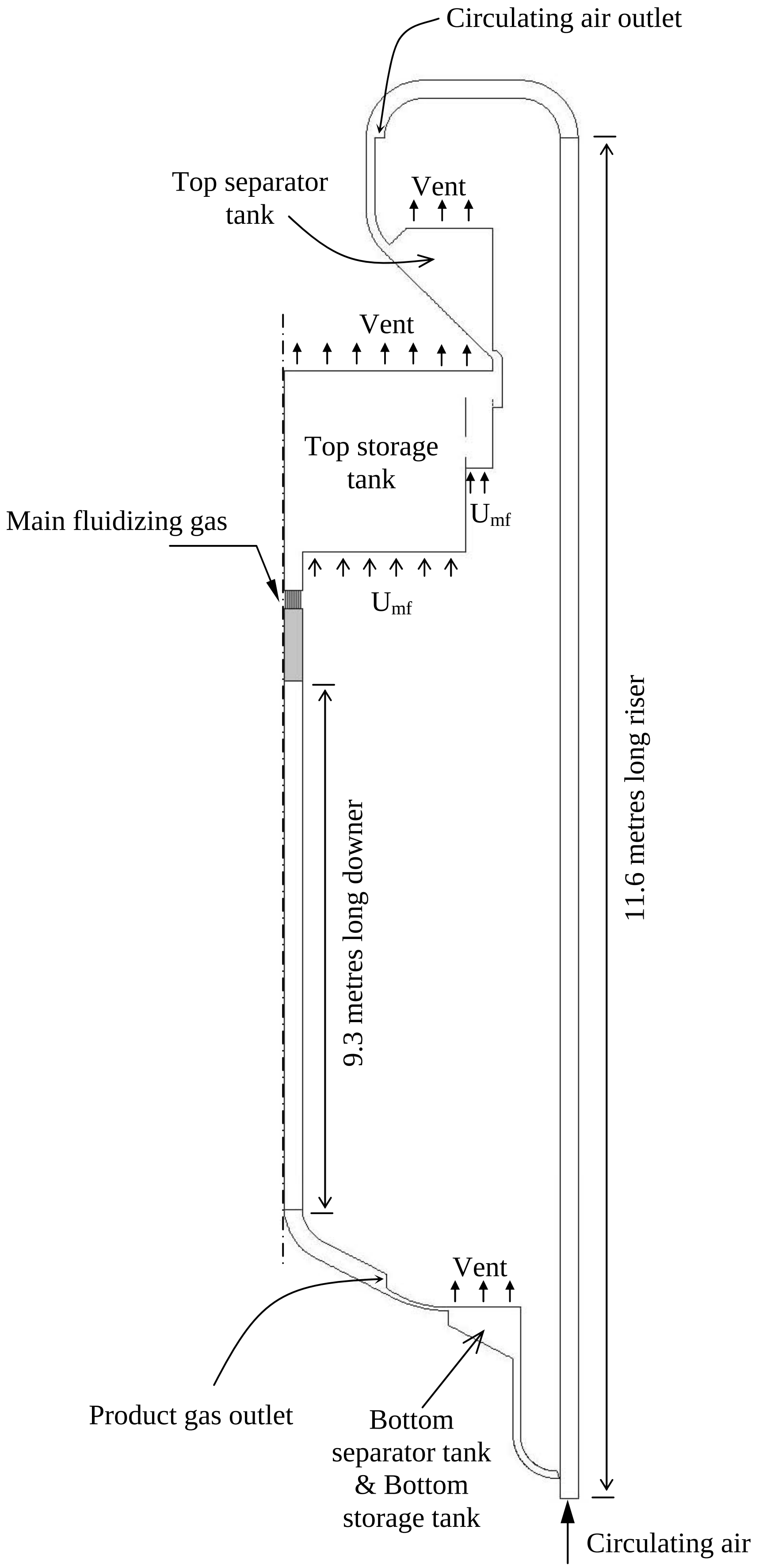

Appendix Figure 1 Model geometry

3. Click “SPECIFY CONTINUUM TYPES COMMAND BUTTON” to specify some zones that need to be assigned with the different variable values at the beginning of the calculation. These faces (Gambit calls the 2-D geometry as “face”)

3.1 The distributor

3.2 The downer column

3.3 Top storage tank

The heavy shaded area including the lower part of the top storage tank and the solid distributing tubes shown in Appendix Figure 2 is the zone that particles reside (minimum fluidized bed holdup value = 0.3) at the beginning of the calculation and need to be excluded from other areas.

Appendix Figure 2 Top storage tank zone at minimum fluidized state

3.4 Bottom storage tank

The zone in Appendix Figure 3 shows the part of the bottom storage tank that is specified at particle packing limit (solid holdup = 0.566).

Appendix Figure 3 Bottom storage tank zone with packed particles

4. Mesh all faces in the domain

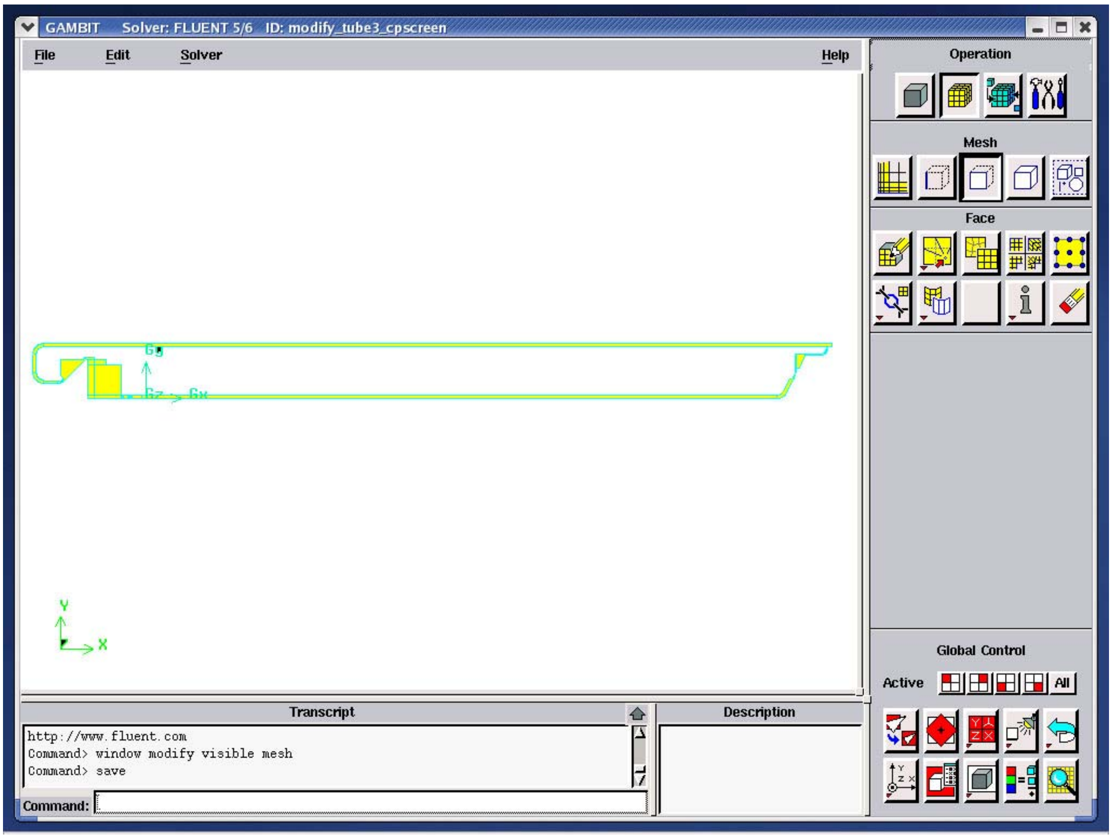

Appendix Figure 4 Domain meshing in Gambit

5. Export mesh and click the export 2-D mesh button at the pop-up window

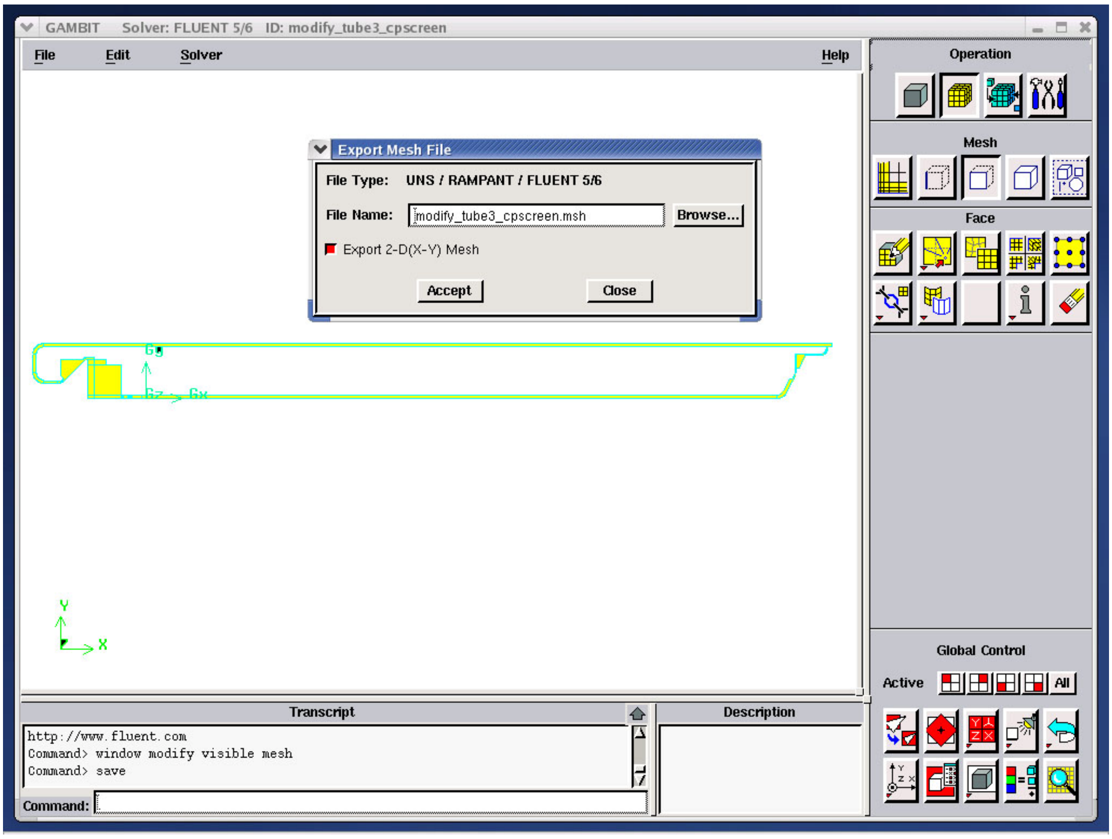

Appendix Figure 5 Mesh exported to mesh file (.msh)

Fluent 6.2 Setup Procedures

1. Read the mesh file by using the "File" menu, choosing the mesh file exported by Gambit

    1.1 File → Read → Case
    1.2 Choose the mesh file (*.msh)
    1.3 Click "OK" button

2. Define model as explained in "Mathematical Model" section under "Methodology" and define gravity. This can also be done by reading the following journal file (define_model.jou) into Fluent. The journal file can be created by the text editor program. The line starts with the semi colon ';' will be neglected by Fluent and is used to explain the options specified below.

```
;Specify axisymmetric model
/define/models/axisymmetric
yes
;Specify a time dependent calculation
/define/models/unsteady-1st-order
yes
;Specify Two-fluid model
/define/models/multiphase
eulerian
2
no
;Enable turbulent per each phase option
/define/models/viscous/ke-standard
yes
/define/models/viscous/multiphase-turbulence/ke-multiphase-models
2
;Create FCC particle material
/define/materials/change-create
air
fcc
yes
constant
1500
no
no
no
no
no
no
no
no
no
no
;Specify air as phase 1
/define/phases/phase-domain
```

```
phase-1
phase-1
yes
air
;Spedify FCC particles as phase 2
/define/phases/phase-domain
phase-2
phase-2
yes
fcc
;Specify the constitutive equations for Two-fluid model
yes
no
no
constant
67e-06
gidaspow
lun-et-al
none
gidaspow
algebraic
lun-et-al
lun-et-al
derived
0.566
/define/phases/interaction-domain
no
yes
gidaspow
no
no
0
/define/operating-conditions/gravity
yes
9.81
0
;Set under-relaxation factors
/solve/set/under-relaxation/mom
0.3
/solve/set/under-relaxation/mp
0.3
;Choose to plot the residual instead of printing in Fluent window
/solve/monitors/residual/plot
yes
/solve/monitors/residual/print
no
;Set residual of each variables
/solve/monitors/residual/convergence-criteria
1e-06
1e-06
1e-06
1e-06
```

1e-06
1e-06
1e-06
1e-06
1e-06
1e-06
;Set limits for some variables
/solve/set/limits
1
5e+10
1e-14
1e-20
1e20

3. Define boundary conditions as explained in the second topic (2. Boundary Conditions) in the "Geometry Domain" section under "Methodology" by choosing "Boundary Conditions option under the "Define" menu.

3.1 Define → Boundary Conditions
3.2 Select the boundary in the "Zone" box
3.3 Select phase in the "Phase" box
3.4 Click "Set" button
3.5 Specify values then click "OK" button

4. Create lines in the downer and the distributor for result plot by reading the journal file below (create_line.jou)

/surface/line-surface
H=0.02
0.02
0
0.02
0.05
/surface/line-surface
H=0.512
0.512
0
0.512
0.05
/surface/line-surface
H=1.198
1.198
0
1.198
0.05
/surface/line-surface
H=2.112
2.112
0

2.112
0.05
/surface/line-surface
H=4.398
4.398
0
4.398
0.05
/surface/line-surface
H=6.227
6.227
0
6.227
0.05
/surface/line-surface
H=8.056
8.056
0
8.056
0.05
/surface/line-surface
H=9.155
9.155
0
9.155
0.05
/surface/line-surface
H=-0.18
-0.18
0
-0.18
0.05
/surface/line-surface
H=-0.15
-0.15
0
-0.15
0.05
/surface/line-surface
H=-0.1
-0.1
0
-0.1
0.05
/surface/line-surface
H=-0.05
-0.05
0
-0.05
0.05
/surface/line-surface
H=0
0

0
0
0.05

5. Save the case file

   5.1 File → Write → Case
   5.2 Type the name wanted in the "Case File" box
   5.3 Click "OK" button

6. Initialize the domain.

   6.1 Solve → Initialize → Initialize
   6.2 Click "Init" button

7. Add particle to the top and button storage tanks.

   7.1 Solve → Initialize → Patch
   7.2 Choose "phase-2" in the "Phase" drop down list
   7.3 Choose "Volume Fraction" in the "Variable" box
   7.4 Choose "top storage tank" in the "Zones to patch" box
   7.5 Type "0.3" in the "Value" box
   7.6 Click "Patch" button.
   7.7 Choose "bottom storage tank" in the "Zones to patch" box (de-select the "top storage tank")
   7.8 Type "0.566" in the "Value" box
   7.9 Click "Patch" button

8. Specify gas velocity in the distributor and the downer column to help in initiating the particle flow from the top storage tank.

   8.1 Solve → Initialize → Patch
   8.2 Choose "phase-1" in the "Phase" drop down list
   8.3 Choose "Axial Velocity" in the "Variable" box
   8.4 Choose "distributor" and "downer" in the "Zones to patch" box
   8.5 Type "10" in the "Value" box
   8.6 Click "Patch" button

8. Start simulating the domain.

   8.1 Solve → Iterate
   8.2 Type "0.001" in the "Time Step Size (s)" box
   8.3 Type "3000" in the "Number of Time Steps" box (for 3 seconds of simulation)
   8.4 Type "60" in the "Max Iterations per Time Step" box instead of using the default "20"

CURRICULUM VITAE

NAME	Mr. Archwit Aimdilokwong		
BIRTH DATE	Janyuary 8, 1976		
BIRTH PLACE	Bangkok, Thailand		
EDUCATION	**YEAR**	**INSTITUTION**	**DEGREE**
	1997	Chulalongkorn University	B.Eng (ChE.)
SCHOLARSHIP	Shell Centenary Scholarship for researching		